



---

Palacký University  
Olomouc

Faculty of Science  
Department of Geoinformatics

Study programme: **P1301 Geography**  
Field of study: **Geoinformatics and cartography**

# **AIRBORNE THERMAL REMOTE SENSING IN URBAN CLIMATE RESEARCH**

Doctoral thesis

**Tomáš POUR**

Supervisor: prof. RNDr. Vít Voženílek, CSc.

Olomouc 2019

*„Per aspera ad astra.“*

## Author's Statement

I declare that this PhD thesis of P1301 Geography study program has been completed independently and under the supervision of prof. RNDr. Vít Voženílek, CSc. All the materials and resources are cited with regards to the scientific ethics, copyrights and laws protecting intellectual property. All provided and created digital data will not be published without the consent of the Department for Geoinformatics, Faculty of Science, Palacký University Olomouc.

In Olomouc, 28<sup>th</sup> May 2019

## Acknowledgement

I would like to thank my supervisor professor RNDr. Vít Voženílek, CSc. for his guidance and irreplaceable help during the writing of the thesis, during my studies and in my professional career. Many thanks to my colleagues for creating such a pleasant and creative environment within the Department of Geoinformatics and helping me whenever I needed it. Special thanks to associate professor RNDr. Jaroslav Burian, Ph.D. for support and valuable consultations throughout my studies and my office colleague Mgr. Tomáš Pohanka for his friendship and lots of support. Many valuable datasets analysed in this thesis were provided by the Institute of Urban Planning in Olomouc. Many thanks to Mgr. Lea Maňáková and Mgr. Miloslav Dvořák from the department for doing way more than was necessary.

I wouldn't be able to finish this work without the support of my wonderful girlfriend Anika and my parents providing me unconditional and everlasting support and motivation. I would also like to thank my friends for supporting me in my scientific career.

# CONTENTS

|  |           |
|--|-----------|
| <b>LIST OF ABBREVIATIONS</b> .....   | <b>7</b>  |
| <b>1 INTRODUCTION</b> .....  | <b>8</b>  |
| <b>2 OBJECTIVES</b> .....  | <b>9</b>  |
| <b>3 METHODS AND DATA</b> .....  | <b>11</b> |
| 3.1 Methods .....  | 11        |
| 3.2 Data .....   | 11        |
| 3.3 Software .....   | 12        |
| 3.4 Area of interest .....   | 12        |
| <b>4 STATE OF ART</b> .....  | <b>14</b> |
| 4.1 Thermal infrared remote sensing .....                                  | 14        |
| 4.1.1 Thermal infrared wavelength emittance.....                           | 14        |
| 4.1.2 Vignetting, atmospheric and emissivity corrections .....             | 17        |
| 4.1.3 Leading applications in TIR remote sensing .....                     | 18        |
| 4.2 Thermal imaging for urban climatology.....                             | 19        |
| 4.2.1 Surface urban heat island .....                                      | 21        |
| 4.2.2 Heat waves and health impact of heat.....                            | 21        |
| 4.3 Thermal data visualization .....                                       | 24        |
| 4.3.1 Thermal data visualization in the scientific literature .....        | 24        |
| 4.3.2 Thermal data visualization in cartography and GIS.....               | 27        |
| <b>5 OLOMOUC AIRBORNE THERMAL DATA ACQUISITION</b> .....                   | <b>29</b> |
| 5.1 Olomouc flight campaign, 10 <sup>th</sup> July 2016.....               | 29        |
| 5.2 Image processing.....  | 30        |
| 5.2.1 Radiometric correction .....   | 30        |
| 5.2.2 Atmospheric corrections .....  | 33        |
| 5.2.3 Emissivity corrections .....   | 34        |
| 5.3 Photogrammetric processing .....                                       | 36        |
| 5.4 Final product assessment.....  | 37        |
| <b>6 DESCRIPTIVE ANALYSES CARRIED OUT ON OLOMOUC THERMAL MOSAICS</b> ..... | <b>39</b> |
| 6.1 Thermal regime of materials in an urban environment .....              | 39        |
| 6.2 Investigation of microclimate using TURN method .....                  | 44        |
| 6.3 A typology based on temperature change.....                            | 48        |
| 6.3.1 Tertile-based typology .....   | 48        |
| 6.3.2 Quartile-based typology .....  | 50        |

|           |  |           |
|-----------|--|-----------|
| 6.3.3     | Quantile-based typology summary .....                                    | 51        |
| <b>7</b>  | <b>DATA FUSION ANALYSES CARRIED OUT ON OLOMOUC THERMAL MOSAICS .....</b> | <b>53</b> |
| 7.1       | Investigation of temperatures on different vertical levels .....         | 53        |
| 7.1.1     | Description of buildings dataset and its corrections .....               | 53        |
| 7.1.2     | Ground-rooftop and verticality analyses results .....                    | 55        |
| 7.2       | Local Climate Zones as the basis for zonal analysis .....                | 58        |
| 7.3       | Temperature evaluation based on open data .....                          | 64        |
| 7.3.1     | Urban Atlas 2012 .....   | 64        |
| 7.3.2     | CORINE Land Cover 2018.....  | 67        |
| <b>8</b>  | <b>RESULTS .....</b>   | <b>70</b> |
| <b>9</b>  | <b>DISCUSSION .....</b>  | <b>73</b> |
| <b>10</b> | <b>CONCLUSION .....</b>  | <b>77</b> |
|           | <b>REFERENCES.....</b>   | <b>79</b> |
|           | <b>SHRNUTÍ .....</b>   | <b>84</b> |
|           | <b>LIST OF APPENDICES.....</b>   | <b>86</b> |

## LIST OF ABBREVIATIONS

|                                   |                              |
|-----------------------------------|------------------------------|
| <b>AGL</b>                        | Above Ground Level           |
| <b>CEST</b>                       | Central-European Summer Time |
| <b>CLC</b>                        | CORINE Land Cover            |
| <b>DN</b>                         | Digital Number               |
| <b>DSM</b>                        | Digital Surface Model        |
| <b>E or <math>\epsilon</math></b> | Emissivity                   |
| <b>EM</b>                         | Electromagnetic              |
| <b>FOV</b>                        | Field of View                |
| <b>HRL</b>                        | High-Resolution Layer        |
| <b>IDW</b>                        | Inverse Distance Weighting   |
| <b>iFOV</b>                       | Instantaneous Field of View  |
| <b>LCZ</b>                        | Local Climate Zone           |
| <b>LULC</b>                       | Land-Use/Land-Cover          |
| <b>LUZ</b>                        | Large Urban Zone             |
| <b>MMU</b>                        | Minimal Mapping Unit         |
| <b>NIR</b>                        | Near Infrared                |
| <b>OBIA</b>                       | Object-Based Image Analysis  |
| <b>RS</b>                         | Remote Sensing               |
| <b>RTE</b>                        | Radiative Transfer Equation  |
| <b>SFV</b>                        | Sky View Factor              |
| <b>STL</b>                        | Street Tree Layer            |
| <b>SUHI</b>                       | Surface Urban Heat Island    |
| <b>SWIR</b>                       | Short-Wave Infrared          |
| <b>TIR</b>                        | Thermal Infrared             |
| <b>UA</b>                         | Urban Atlas                  |
| <b>UBL</b>                        | Urban Boundary Layer         |
| <b>UCL</b>                        | Urban Canopy Layer           |
| <b>UHI</b>                        | Urban Heat Island            |

# 1 INTRODUCTION

**Remote sensing** plays a strong role in both the Earth and other solar system objects observation. Both **sensors** and **carriers** have changed dramatically over the last years. What once started as a camera attached to a balloon in **1906**, capturing a black and white image of the results of the San Francisco earthquake, is now recognised as a **scientific field** with growing popularity.

**Thermal remote sensing** helps in many disciplines such as medicine, Earth Observation and machine, construction and electrical engineering. Made possible only decades ago, the ability to measure the **kinetic** or **radiant** temperature of an object from a distance is fascinating by itself because it is not possible by any living creature. The key improvements implemented over the last years vastly improved the **spatial** and **spectral resolution** and reduced the sensor's size. Even with the improvements in the scientific community, thermal remote sensing for commercial and governmental purposes remains very rare due to its **complexity**.

Nowadays, **half of the population** of our planet already lives in the cities. There are **natural phenomena** connected to the **urban environment** which were not considered as important in the past as they are today. For example, powerful **heat waves** and **heat stress** inside the cities increased in intensity due to vague city planning. The need for the **research of urban environment**, thus, becomes pivotal.

Thermal remote sensing has reached the point when the collected data become **extremely relevant** for urban environmental studies. Such possibilities enable us not only to compare the **urban environment** with its **rural** counterpart but also to differentiate the types of **thermal behaviour** within the city. The results of such research will play a **crucial role** in future **urban planning** and **population readiness** in the time of critical heat events.

The thesis is motivated by the desire to improve this field of study in terms of **technical quality** and **public enlightenment**. It follows up the previous research in bachelor's and master's theses, both regarding **urban environment** using remote sensing methods. The bachelor's thesis explored the possibilities of **inner urbanization** using very high-resolution satellite data combined with **Object-Based Image Analysis (OBIA)** method. In the diploma thesis, **five middle-European cities** with mining and/or heavy industry history were compared on their city structure basis. Following the years of experience and the current socio-political pressure in climate adaptation strategies, it is vital to explore **new possibilities of thermal remote sensing** in an urban environment to improve the quality of life of the population and ensure **sustainability** to the future.



## 2 OBJECTIVES

The objective of the thesis is to investigate and improve airborne thermal remote sensing in urban climate research. Urban climate research is benefiting from thermal remote sensing data already. However, the thermal satellite image resolution is too **coarse** to explore the structure of surface urban heat island in detail or to learn the heat conditions of **Local Climate Zones (LCZ)**. With custom-made extreme resolution thermal imagery, it is possible to research **new areas** and create **new scientific questions** inside the **urban climate** topic. Fulfilling the objective of the thesis will improve the process of data acquisition, research and analysis of the urban climate.

### SUB-OBJECTIVE 1 Olomouc Airborne Thermal Data Acquisition

The first sub-objective was to acquire and process a series of thermal datasets of Olomouc city for urban environment research. The preparation of the **flight campaign** depended on thoroughly considering various factors such as the attributes of the **carrier**, the **sensors**, the **time** of the day and the **day** of the year. This process is very important and cannot be taken lightly since the campaign cannot be repeated most of the times. The planning reflected the aim of the thesis and the thermal regime of the urban ecosystem. After that, the campaign was carried out according to the plan, along with ground sample data collection. The collected dataset contains raw signal data from the sensor. Those needed to be **corrected** to acquire the brightness and, later in the process, the **radiant surface temperature**. Digital number values were compensated for meteorological influences, the geometry of the sensor, and the emissivity of the surface. After that, they were orthorectified and georeferenced into the mosaic. The resulting mosaic is a unique dataset containing early **morning** radiant surface temperature cooled after the night and **afternoon** peak radiant surface temperature. Combination of the data acquired during these two flights is most beneficial for urban surface temperature regime studies and another urban climate research.

### SUB-OBJECTIVE 2 Descriptive Analyses Carried Out on Olomouc Thermal Mosaics

The aim of the second sub-objective was to use the thermal mosaics dataset and self-sufficient methods of **sampling**, **typology** and **classification** to characterize the area of interest. Proposed methods of quantile-based typology, material sampling and **Local Climate Zones (LCZs)** are a viable option for any kind of thermal imagery and are providing some basic information about the observed area.

**Quantile-based typology** is a method exploiting the statistical variance and the heterogeneity of the thermal image. The method focuses on objects with extreme or unique thermal behaviour. For the **sampling** of various material types, auxiliary datasets

were used. However, it would be sufficient to use a remote sensing dataset, e.g. satellite or airborne imagery in the optical part of the electromagnetic spectrum.

**Local Climate Zones** are unified basic structural segments with uniform behaviour from **urban climatology** point of view. The largest benefit of the method is that LCZs are **transferable** among cities and with some improvements also in between continents and different cultural environments. Another benefit is the ability to classify them using only the remote sensing data. The process of classification requires only **Sky View Factor** (SVF) that can be computed from the **Digital Surface Model** (DSM), buildings and vegetation data that can be acquired from **high-resolution satellite imagery**. To summarize, the goal of this sub-objective was to **introduce** and **test** the possibility to use various methods to analyse the area of interest introduced in sub-objective 1.

### **SUB-OBJECTIVE 3 Data Fusion Analyses Carried Out on Olomouc Thermal Mosaics**

The third sub-objective was to analyse the dataset and propose its fusion with other data sources to investigate the surface temperature patterns and trends among various land-cover and land-use types. The aim is to use external datasets acquired from cooperating departments such as the **Department of Urban Planning and Architecture** of the city Olomouc. **European initiatives** in land-use and land-cover mapping are another source of valuable data. These datasets provide a solid baseline for the assessment of the **thermal regime** of various city structures, material types and public spaces. Proposed analyses include the use of **CORINE Land Cover** and **Urban Atlas** datasets and the use of **building height** information for verticality analysis. The goal of this sub-objective was to use auxiliary data and Europe-wide datasets to analyse the city thermal behaviour, which may help to set up a trend and a baseline for future comparisons among multiple cities.

## 3 METHODS AND DATA

This section addresses the most important methods, software, computer languages, and data used in the thesis. Moreover, it provides basic information about the area of interest.

### 3.1 Methods

In the thesis, the self-reliant methods that are not using auxiliary and third-party data are called **descriptive**. While not all the methods used in the thesis belong to the mathematical category of **descriptive analysis**, the author wanted to emphasize that mentioned analyses are basic, simple and focus on the **elementary description** of the dataset and its basic trends. The analyses focus on sampling methods and sample comparisons of different material types and on simple statistical methods such as quantiles.

The second set of methods is described as **data fusion analyses**. By definition, data fusion is a process of integration of multiple data sources to produce more useful information than that provided by the single data source. The sub-objective 3 is based on the use of **third-party** or other **auxiliary** data that were combined with the primary dataset created in the thesis. For these analyses, a more complex approach of classification and comparison was used.

During this research, many GIS methods were used. The most commonly used were **Point Sampling** and **Zonal Statistics** (names come from QGIS); the naming convention may change in different software. These methods serve to combine the information from the raster data to vector polygon or point layers. During the microclimate analysis, an interpolation method called **Inverse Distance Weighting** was carried out. This method enables the creation of a full coverage raster of the city by using the dense point sample layer.

### 3.2 Data

Besides the self-created thermal mosaics, **several other datasets** were used in this thesis. For atmospheric corrections, a dataset from a semi-professional meteorological station **Davis** located in Olomouc was used. The data were kindly provided by their owner **Mr Robert Šišma**. Many of the auxiliary data were provided by the **Department of Urban Planning and Architecture** of Olomouc city within the framework of the cooperation with the Department of Geoinformatics, Palacký University Olomouc. The **open datasets** are described in Chapter 7.3 because their characteristics are relevant for

this specific research. The **buildings vector layer** was downloaded from the **RÚIAN system**, which is publicly available. A download plugin for Esri ArcMap software is provided in its basic licence free of charge by the company **ARCDATA Praha**. The data were updated and improved by Tuháček (2017). For the vegetation detection, satellite images from ESA satellite **Sentinel-2** were used. These data are open to the public and easily obtainable from **Copernicus Scientific Hub**.

### 3.3 Software

Many different software solutions were used during data processing and analyses. For basic data view and later export of the raw digital number (DN) values of the thermal images, **Workswell ThermoFormat** was used; an upgraded version of this software was provided along with the camera purchase by the company **Workswell**. Vignetting was performed using programming language **Python** and its basic functionality and libraries. The code was written in Microsoft's development environment called **Visual Studio Code**. Atmospheric, radiometric and emissivity corrections were performed using the equations from R package **ThermImage**, which was implemented in the Python environment. The language R and its development environment called **R Studio** are open-source solutions for statistics and mathematics. While being originally developed as a mathematical software, in recent years, its remote sensing capabilities and functionality improved dramatically. The R libraries called *packages* are available in an online repository named **CRAN**. For photogrammetric processing software, **Agisoft Photoscan Pro** and **Trimble INPHO** were used. During the PhD study, the software **Photoscan Pro** was renamed to **Metashape**. In the thesis, it is referred by its old name because the name changed in late 2018 after the images were processed. Satellite data processing was performed in **ESA SNAP Desktop**, a software developed by the **European Space Agency** specifically for Sentinel satellites and third-party cooperating missions. In the analytical part, mostly **QGIS 3.6.0 Noosa** was used. QGIS is the most popular open-source GIS software in the community. Some of the processes were computed in commercial GIS **Esri ArcMap 10.6** and **Esri ArcGIS Pro**. The graphs and tables were produced in **MS Office Excel**, and the thesis was written and formatted in **MS Office Word**. The images, maps and graphs were edited and post-processed in **Adobe Photoshop**.

### 3.4 Area of interest

**Olomouc** is the 6<sup>th</sup> largest city in the Czech Republic with a population of **100 000 residents**. The area of the city is slightly more than **100 km<sup>2</sup>**. The city is located in the

central part of the historical **Moravian region** named **Haná** on the river Morava. The history of Olomouc is an interesting combination of **military, education** and **religion**. Olomouc has always been a **fortress**, and in the 18<sup>th</sup> century, it was even more heavily fortified by forming a **bastion fortress** under the rule of **Maria Theresa**. This was very important in the city's future development as the fortress status heavily slowed down the city growth in modern times. The **green belt** surrounding the historical centre and the city walls are visible on many images in this thesis and is very important for the city structure and climate. Besides being a fortress, in 1777 Olomouc became the **seat of the archbishop**, which further increased the importance and prestige of the city. In 1573, the Olomouc university was founded, and in 1946 it was renamed to **Palacký University**. The surroundings of the city are mostly **grassland, lowlands** and **meadows**. The region Haná is also a well-known **agricultural area** with very high-quality soil.

Originally, the chosen area was only the continuously built-up area, but after calculating the flight lines, it was decided to increase the area coverage, especially in the north-south direction. The area of interest with the flight lines and ground control data locations is described later in the thesis and visualised in Figure 5.1.

## 4 STATE OF ART

**Thermal infrared (TIR) remote sensing (RS)** is a challenging field that requires interdisciplinary knowledge from **physics** and **optics**. TIR remote sensing is mainly used on two types of carriers – aeroplanes and satellite. However, the drone TIR remote sensing plays an important tactical role during fires, missing people cases, police chases, during hunting and other field applications. While satellite TIR RS is well established, the applications of airborne thermal remote sensing are rather sparse in the scientific literature. The urban applications of TIR are most commonly based on satellite imagery, which comes with many challenges and specifics that need to be considered. The last topic discussed in the following chapter is TIR data visualisation and the role of thermograms in the scientific literature.

### 4.1 Thermal infrared remote sensing

Prakash (2000) sums up the thermal remote sensing as the branch of remote sensing that deals with the acquisition, processing and interpretation of data acquired primarily in the thermal infrared (TIR) region of the electromagnetic (EM) spectrum. In the thermal remote sensing, the radiation **emitted** from the surface of the target is measured, as opposed to the optical remote sensing where we measure the radiations **reflected** by the target. Prakash (2000) further describes thermal remote sensing, in principle, as different from remote sensing in the optical and microwave region. In practice, thermal data prove to be **complementary to other remote sensing data**. Thus, though still not fully explored, thermal remote sensing reserves potentials for a variety of applications.

#### 4.1.1 Thermal infrared wavelength emittance

Every natural object reflects as well as **emits radiation** in various wavelengths. In the TIR region of the EM spectrum, the radiation emitted by the earth, due to its thermal state, is far more intense than the solar reflected radiation and, therefore, sensors operating in this wavelength region primarily detect thermal radiative properties of the ground material. As thermal remote sensing deals with the measurement of emitted radiations, for high-temperature phenomenon, the realm of thermal remote sensing broadens to encompass not only the wavelengths commonly referred to as TIR but also the short-wave infrared (SWIR), near-infrared (NIR) and in extreme cases even the visible region of the EM spectrum, Zemek et al. (2014) report.

An object, having the kinetic temperature higher than 0 °K, emits the electromagnetic (EM) radiation. The amount and the spectral distribution of the emitted energy depend on the temperature of the object and its emissivity. In the case of a pure blackbody, the spectral distribution is described in **Planck's law**. Most of the objects measured in remote sensing have the kinetic temperature between 270 and 330 °K. According to Planck's law, it means that we can measure the thermal radiation in two atmospheric windows, the first one being 3 to 5 micrometres and the second one being 8 to 14 micrometres. The first atmospheric window is not suitable for remote sensing because a part of the gathered data is also reflected in solar irradiation. The second atmospheric window is much more suitable because surface emittance is dominant in this wavelength.

An image taken in the thermal infrared part of EM spectrum can be in the form of **thermogram** or **thermal hyperspectral cube**. In the case of the thermogram, only one measured value is taken for each pixel. In the case of the hyperspectral cube, the spectral behaviour of the material over the whole range of the thermal infrared spectrum, or its subset, is measured.

Thermal data can be used for both qualitative and quantitative research. For qualitative comparison, there is no need for atmospheric corrections if interpreted correctly. For quantitative data, several **corrections** must be performed. These include (i) sensor calibrations, (ii) geometric corrections and (iii) atmospheric corrections.

According to Minkina, Dudzik (2009), the most important factor affecting the thermal characteristics of an object is the emissivity ( $\epsilon$ ). Emissivity is the ability to emit **EM radiation in thermal wavelength** compared to the radiation emitted by the black body of the same temperature. The emissivity depends on wavelength, temperature and the **direction** of emittance. If the sensor is perpendicular to the surface and the temperature is relatively stable between 270 and 330 °K, the emissivity depends only on the wavelength.

Besides emissivity, Zemek et al. (2014) describe the characteristics of the object that contribute to its temperature. These are:

- Thermal conductivity
- Thermal capacity
- Thermal inertia

Thermal conductivity describes the **speed of the heat transfer** within an object. Thermal capacity describes the **amount of heat** the material is able to contain. Thermal inertia is the ability of a material to **change its temperature** over time.

The **EM flux** of the surface consists of shortwave and longwave radiation that is either upwelling or downwelling. This system is described by the **energy budget**.

## Energy budget

The Equation 4.1 described by Zemek et al. (2014) represents the budget of energy inputs and outputs in natural systems in the form of short (lower 's' index) and long (lower 'l' index) **EM radiance**. Source of the shortwave EM radiation is the **Sun** ( $R_s^\downarrow$ ). After touching the surface, a part of the radiation is **reflected** ( $R_s^\uparrow$ ). The budget in longwave radiation in the infrared part of the EM spectrum depends according to the Stefan-Boltzmann law on radiation from the **Earth surface** ( $R_l^\uparrow$ ) and **atmosphere** ( $R_l^\downarrow$ ). The result of the radiation budget is the "overall clean radiation" ( $R_n$ ) which is then transformed into specific heat channels.

$$R_n = R_s^\downarrow - R_s^\uparrow + R_l^\downarrow - R_l^\uparrow \quad (4.1)$$

The topic can be further extended to the heat budget, which can be portrayed using:

$$R_n = J + P + G + H + LE \quad (4.2)$$

where  $J$  is energy spent on the temperature change of the surfaces,  $P$  is energy spent on **photosynthesis**,  $G$  is **heat flow** into the ground,  $H$  is a flow of the **apparent heat**, and  $LE$  is **latent heat** flux. The amount of energy used for temperature change and photosynthesis is relatively low. Therefore it is not considered when talking about energy fluxes. Most important parts of the equation are ground heat flow, apparent heat flux and latent heat flux. Updating the equation, we can calculate apparent heat flux as heat flow and latent heat flux subtracted from overall radiation:

$$H = R_n - G - LE \quad (4.3)$$

The process of EM radiation travelling through the atmosphere or any other space is described by the Radiative Transfer Equation, which includes the emission, absorption and scattering during the process.



## Radiative Transfer Equation

$$L_m = \tau \varepsilon B(T_s) + \tau(1 - \varepsilon)L_{atm}^{\downarrow} + L_{atm}^{\uparrow} \quad (4.4)$$

The signal captured by the sensor ( $L_m$ ) consists of the radiation coming from the **surface** ( $B(T_s)$ ) of a certain **temperature** ( $T_s$ ) corrected by **emissivity** ( $\varepsilon$ ) and the **penetration of the atmosphere** ( $\tau$ ), reflected radiation from the **atmosphere** ( $L_{atm}^{\downarrow}$ ) and direct emittance from the **atmosphere** ( $L_{atm}^{\uparrow}$ ). Emissivity, and thus **Radiative Transfer Equation** (RTE) equation as well, is bound to a certain wavelength.

### 4.1.2 Vignetting, atmospheric and emissivity corrections

Vignetting is a commonly known **distortion** in the visible region of the EM spectrum which affects TIR region as well. The consequence of this effect results in **uneven distribution of the signal** in a single image, where the central region is bright and regions towards the side of the image appears darker. According to Li and Zhu (2009), the effect is caused by gradually decreasing radiation illumination. The effect is stronger to the sides of the image while being strongest in the corners. Because TIR imaging works with low contrast between 1 and 2 %, compensating for vignetting effect is **crucial** for high-quality TIR image.

The atmosphere affects the measurement in three ways – it lowers the amount of emitted radiance that reaches the sensor, **emits** radiance itself and **reflects** radiance. Removal of the atmospheric effect is essential when retrieving high-quality TIR image. Atmospheric corrections differ based on sensor type. Zemek et al. (2014) define two basic categories of corrections – hyperspectral and broadband.

**Hyperspectral atmospheric corrections** rely mostly on complex models such as MODTRAN. They require accurate simulation of vertical atmospheric parameters such as CO<sub>2</sub> concentration, humidity and temperature profile aerosol model. These data are usually measured in-situ, obtained from local meteorological stations or can be simulated in the model.

**Broadband sensors**, on the other hand, do not require such a complex approach. Main variables influencing the measurements are relative humidity, object distance, above ground temperature, the temperature near the sensor and atmospheric temperature. Calibration of such sensor can be then calculated using general formulas.

### 4.1.3 Leading applications in TIR remote sensing

There are numerous **applications** of TIR remote sensing in different **geographical** topics. In physical geography, the examples are natural resources detection using thermal spectroscopy (Schlerf et al. 2012), **arctic region monitoring** (Soliman et al. 2012), **soil property research** using thermal and visible spectral region data fusion (Eisele et al. 2012) or research in **water quality** and fisheries management (Torgersen et al. 2001) using stream temperature acquired by airborne remote sensing. Due to recent droughts in Amazon forest, Jiménez-Muñoz, Mattar, Sobrino and Malhi (2016) were investigating the possibilities of using MODIS and ERA-Interim products to understand **forest response** and potential impact on carbon absorption. Sepulcre-Cantó et al. (2006) suggest **water stress detection** in non-homogeneous crop canopies as another possible application.

TIR remote sensing is also extremely beneficial in **urban studies** (Figure 4.1), especially regarding (surface) **urban heat island**, **urban modelling** and **heat comfort**. TIR remote sensing is beneficial in urban **heat budget** studies (Parlow 2003), which then overlap with urban **heat flux modelling** (Rigo, Parlow 2007). It can also help the property owners and communities regarding **urban energy efficiency** and **insulation quality** assessment (Hay et al. 2011) or help with **spatial planning**. (Jovanović et al. 2015) Most importantly, TIR remote sensing is used for detection, evaluation and monitoring of **urban heat island** (UHI) effect (Weng 2009), including assessment of surface urban heat island.

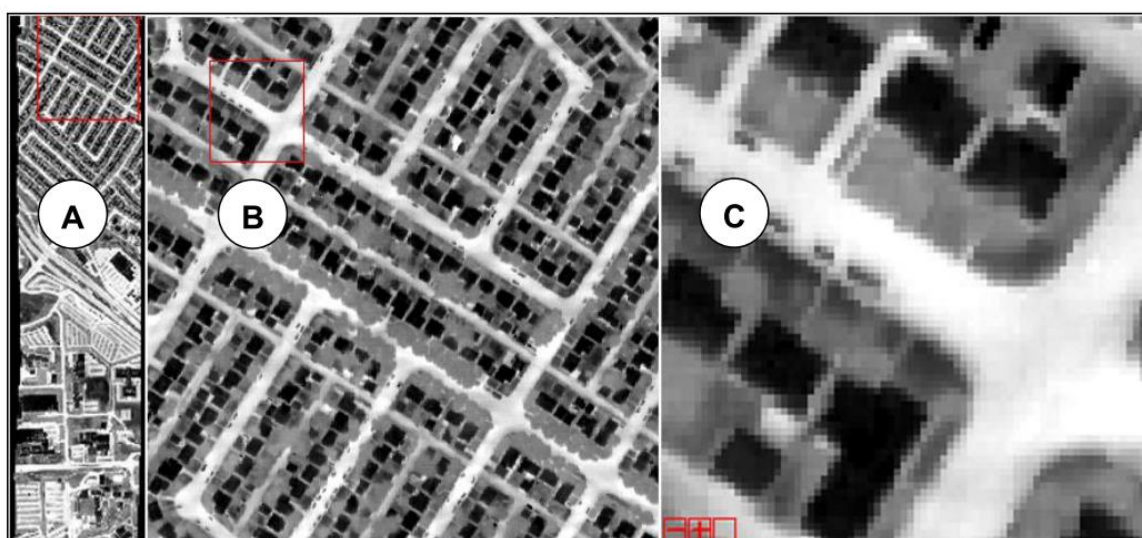


Figure 4.1 TABI 320 thermal mosaic of the Brentwood Community in Calgary, Canada.  
Source: Hay et al. (2011)

## 4.2 Thermal imaging for urban climatology

The surface temperature plays a crucial role in the research of the urban climate. Air mass above the ground is highly affected by the **surface temperature** (Figure 4.2) as well as **energy balance** and the internal climate inside buildings. Human interception and urbanization in the landscape led to a general trend of increasing temperature in the urban climate. This phenomenon is described as the **Urban Heat Island (UHI)**. UHIs are most often monitored using ground stations. Recent advances in thermal imaging and remote sensing technology allowed the use of satellite and aircraft platforms (and recently drone platforms). Nowadays, UHI studies can combine thermal remote sensing data with urban micrometeorology. This approach brings new opportunities but also new challenges. Voogt and Oke (2003) state that the emphasis on **proper and precise definitions** of various phenomena is crucial in advancements of this field.

Thermal remote sensing measures **radiation emitted** by the surface which incorporates effects of the surface such as surface moisture, thermal admittance, emissivity, sun and atmospheric irradiance and the effects of the near-surface atmosphere. The term **directional brightness temperature** is commonly used to describe the temperature calculated using the inversion of Planck's law using a certain thermal sensor that operates at a certain wavelength. Data corrected for atmospheric effects and surface emissivity are called **directional radiometric temperatures**. Roth et al. (1989) formulated the four main questions regarding satellite-derived thermal remote sensing:

- What are the characteristics of the urban surface as viewed by thermal remote sensors?
- What is the relationship between remotely observed radiometric surface temperature and the actual temperature of the urban-atmosphere interface?
- How can surface urban heat islands be related to atmospheric urban heat islands?
- How can thermal remote sensing of urban surfaces provide input into models of urban climate?

The first question can be answered using **sensor view models**. These models simulate simplified surfaces viewed by a certain model taking into account a number of variables. At a lower scale, we can model certain buildings and urban structure using **LIDAR data**; at larger scales, we work with larger areas, especially using **multispectral satellite imagery**. Understanding the characteristics of surfaces is important for further work with local variability. Spatial phenomena such as **roof or vegetation geometry**, **building height** and others affect remotely sensed data in a major way.

According to Zemek et al. (2014), thermal remote sensing measurements are affected by two main sources: **the atmosphere** and **the measured surface**. While atmospheric corrections are rather well established due to other remote sensing applications, we cannot say the same about the **thermodynamic properties** and **geometry of the surface**. Emissivity corrections can be applied easily when the surface material is known to the researcher. On the other hand, the geometry of the object and the effect of **thermal anisotropy** are not easily removable. Various models are trying to predict this phenomenon and improve thermal images.

Oke et al. (2017) described the correlation between surface temperature and air temperature at Urban Canopy Layer (UCL) as a possible result of micro-advection caused by increased surface temperature. For the night-time case of the UHI, **surface–air temperature** differences are expected to be minimized as winds increase, due to mixing and disruption of any surface-based inversion layer. Under calm winds and clear skies, when the UHI has its best expression, micro-scale processes dependent on surface thermal properties, sky view factor and microscale advection will be most apparent thereby increasing differences between the UHI and **Surface Urban Heat Island (SUHI)**.

As the main disadvantage of using thermal remote sensing data in urban climate models is according to Voogt and Oke (2003) the difference between **surface temperature** and the **aerodynamic temperature** needed for the calculation of the surface sensible heat flux.

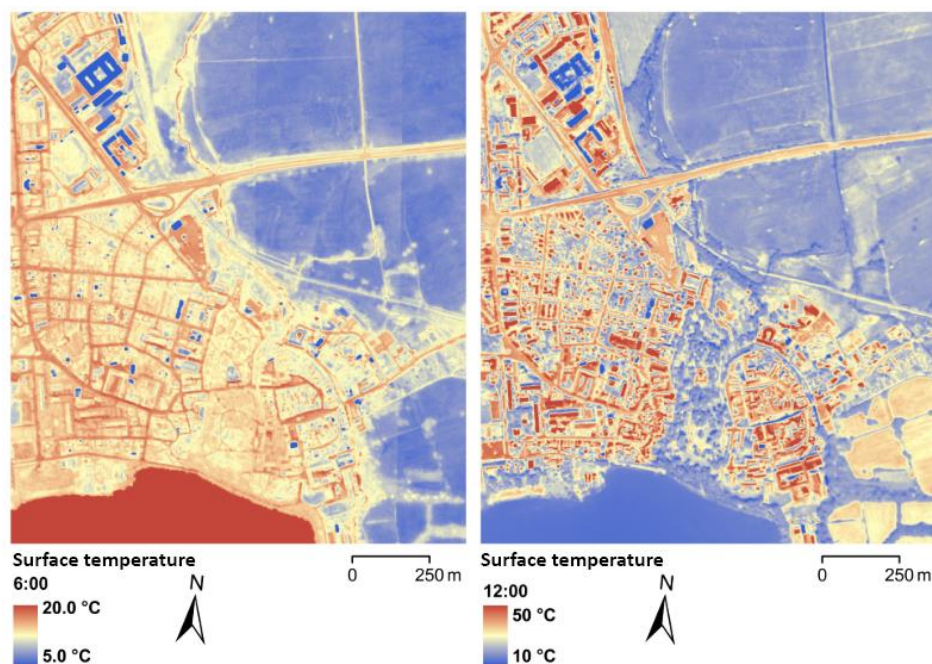


Figure 4.2 Thermal image of city Třeboň, the Czech Republic on 27<sup>th</sup> July 2008.  
Source: edited from Zemek (2014)

### 4.2.1 Surface urban heat island

Urban heat island and its uniqueness for the urban environment is known since Sundborg (1952) articulated the theory about **urban energy balance** based on the **incoming** and **outgoing** energy flux balance. He further elaborated, that the energy absorbed by the urban surface system from solar radiation and generated by anthropogenic activity is physically balanced by warming the air above the surface, the evaporation of moisture, and storage of heat in surface materials.

Oke (2002) pointed out that UHI can be observed on **two different levels**. **Urban Canopy Layer** (UCL) describes the air mass between the surface and approximate mean building height, while **Urban Boundary Level** (UBL) lays above the canopy layer and is affected by the upward urban effect. For UCL measuring, regular measurement in meteorological height or vehicle-mounted sensors is sufficient to model this phenomenon. However, Chrysoulakis et al. (2016) suggest UBL specialized sensor platforms for proper measurements at UBL. A special case of UHI called **Surface Urban Heat Island** (SUHI) is observed by remote sensing platforms. However, analysis of this phenomenon must be carried out with caution because of the properties of various materials.

Because anthropogenic heat flux contributes the most to the urban heat island effect, Gunawardena et al. (2017) suggest **greenspaces** and **bluespaces** as the natural countermeasure. In their meta-analysis, they suggest careful urban planning heavily based on **urban modelling** to mitigate the UHI effect.

### 4.2.2 Heat waves and health impact of heat

Heat waves are undeniably a very serious danger to our society. According to the United Nations report (United Nations 2016), **54.5 %** of the world population lived in cities in 2016. By 2030, the **urban environment** will be the home of 60 % of the global population. A third of the people living in the urban environment will live in cities with a population of over **half a million** inhabitants. “In 28 countries or areas, more than 40 per cent of the urban population is concentrated in a single city of more than one million inhabitants”, the report further elaborates. In central Europe, up to 85 % of the population lives in cities or urban agglomerations. Cities are not only **vulnerable** to natural disasters such as hurricanes, typhoons, flooding and earthquakes but also directly impact the **severity** of events such as heat waves.

Hayhoe et al. (2010) report that in the year 1995, a single **heat wave** event resulted in nearly **800 deaths** in Chicago, US. Robine et al. (2008) observed the summer of 2003, summarizing that the **death toll** in 16 European countries caused by heat waves

**exceeded 70 000**. This event was specifically described in Paris (Dhainaut et al. 2004) where there were 2600 emergency department visits, 1900 hospitalizations and 475 deaths exceeding regular statistics for the time period. During 2006 California, US heat wave and 2011 Texas heat waves, there was a significant increase in **hospitalizations** and **emergency department** visits, reported by Zhang et al. (2015) and Knowlton et al. (2009).

According to Urban et al. (2016), **cardiovascular disease mortality** is tied to the occurrence of **high-temperature events**. These results are based on data from the Czech Republic between the years 1994 and 2009. The study also highlights the relationship to geographical conditions, the **density of the population, age structure** and **socio-economic status**, which is discussed later in this chapter. Similar results were also published by Åström, Bertil and Joacim (2011), focusing on the **elderly population**. This article, reviewing 24 studies between 2008 and 2010, also adds **respiratory mortality** to the list of diseases tied to heat wave events. Moreover, the authors raised a concern about collecting information about non-lethal impacts of such events – **morbidity**. These include **damage to internal organs, heat discomfort, dizziness** and others.

### Definition of a heat wave

The definition of a **heat wave** or high-temperature event varies. In general, this phenomenon can be described as a series of days when the temperature exceeds extreme values for a certain region. Many studies combine day-time maximum and night-time minimum when defining heat waves.

**Local geographical conditions** and the **sensitivity** of the population must be taken into consideration as well. For the southern part of the United States of America, the heat wave threshold was set by Robinson (2001) to **day-time maximum** over 40 °C, **night-time minimum** of 26 °C and **48 hours of duration**. For the southern part of the Czech Republic, Kyselý et al. (2000) were studying heat waves of **72 hours** minimum duration with day-time maximum exceeding 30 °C and day-time minimum not dropping below 25 °C. Austrian Heat Protection Plan, described by Reischl et al. (2017), sets the threshold to 72 hours with a day-time maximum over 27 °C.

### Heatwave vulnerability

According to the European Climate Adaptation Platform of the European Environment Agency (Heat waves – Climate-ADAPT, 2018), the factors defining vulnerability to heat waves can be divided into three categories:

- Exposure
- Sensitivity
- Response capacity

**Exposure** to heat waves refers to the contact with the stressor itself. In heat wave studies, this reflects the time spent outside in a **harmful location**. In other words, it refers to the **city structure**, the amount of **green** and **blue** space and **spatial planning** of the city, which can reduce the number and effect of areas dangerous to humans.

**Sensitivity** to heat waves reflects the **state of the population** and is a threshold at which the phenomenon becomes dangerous to human health. This includes the portion of **very young** (0-4 years of age) or **very old** (above 65 years of age) population, **socio-economic status**, the **quality of living** etc.

**Response** or **adaptive capacity** to heat waves regards the ability of the population to cope with such extreme event when it appears. According to Voelkel et al. (2018), **high income**, **social cohesion** and **knowledge of the surroundings** help people to survive heat waves (Figure 4.3) without harm.

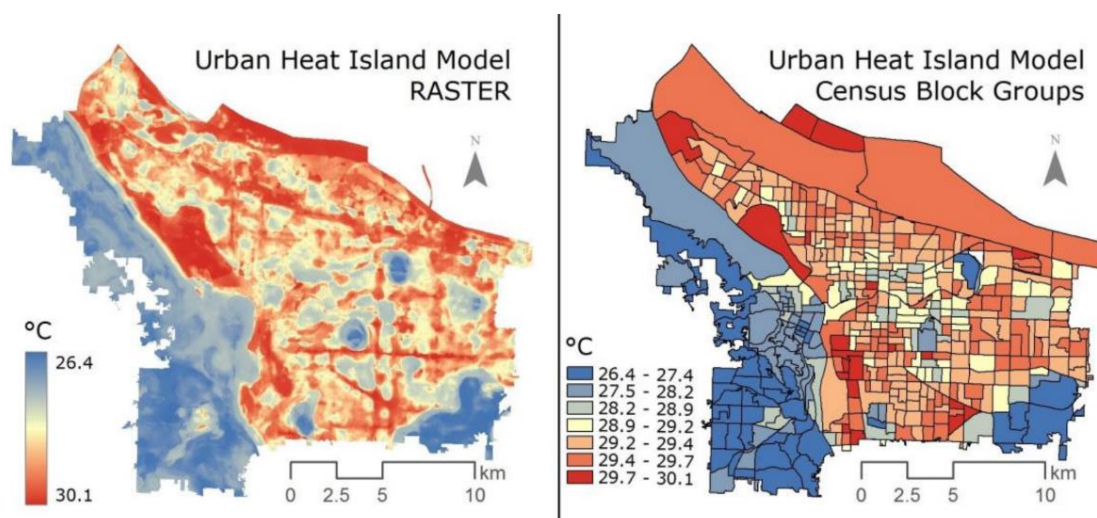


Figure 4.3 Modelling of the urban heat island on the census block level in Portland, Oregon. Original data (left) were recalculated to census blocks (right). Source: Voelkel et al. (2018)

## 4.3 Thermal data visualization

The topic of thermal data visualization is very important because of **thermogram reading**. Thermal imaging has **no unified colour scheme**, nor any **technique of visualisation** has been used as standard. One of the largest challenges is the visualisation of multiple images. Keeping the **same colour scheme** and its range often results in **worse contrast** and detail. Thus, the author must choose between **easy reading and interpretation** at the cost of contrast in the image and possibly important detail, especially in the heterogeneous image.

### 4.3.1 Thermal data visualization in the scientific literature

Thermal data are widely used in many applications. In scientific papers, they are usually visualized **without any special care**, most of the time using default settings of the used software. One of the largest companies producing professional thermal cameras, FLIR, uses a set of colour schemes and offers some customisation settings in their software. The problem is that the field is **rapidly evolving** and the number and specific colour coding of the colour schemes may differ from product to product. In video *Which is the Best Color Palette for Thermal Imaging? - YouTube* (2015), there was a short interview with a FLIR employee, **Dave Lee**, about choosing the right colour palette. In the video, Mr Lee says: “Try one, if it works better for you, use it, if it doesn’t, try something else.” This basically summarizes the **general consensus** within the field of thermal visualisation. In follow-up video *Thermal Color Palettes | FLIR Delta - Episode 4 - YouTube* (2018) which is part of the company FLIR series of tutorials featuring Mr Lee again describing various topics regarding thermal imaging, including the thermal colour palettes. In the video, some features of different colour palettes are described. In general, it is recommended to use **Whitehot** (Figure 4.4) or **Blackhot** for real-time applications while coloured palettes are beneficial for post-processing visualisation.

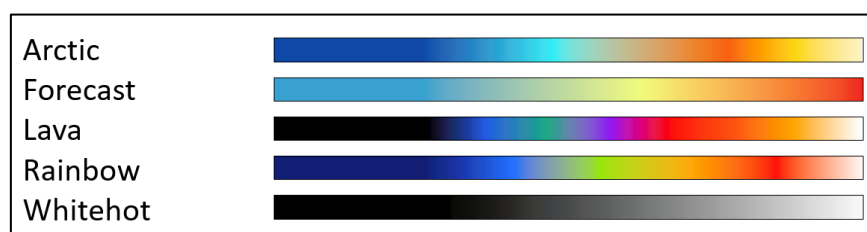


Figure 4.4 Example of the most common colour schemes from FLIR software. Another often used colour schemes are *Iron*, which is similar to *Lava* in the choice of colours, and *Blackhot*, which is inverted *Whitehot*.



In Figure 4.5, a part of **botanical research** regarding leaf temperature is shown. It is presented as a series of images, but the colour schemes are not unified, making the interpretation and temperature reading very difficult even for an experienced individual.

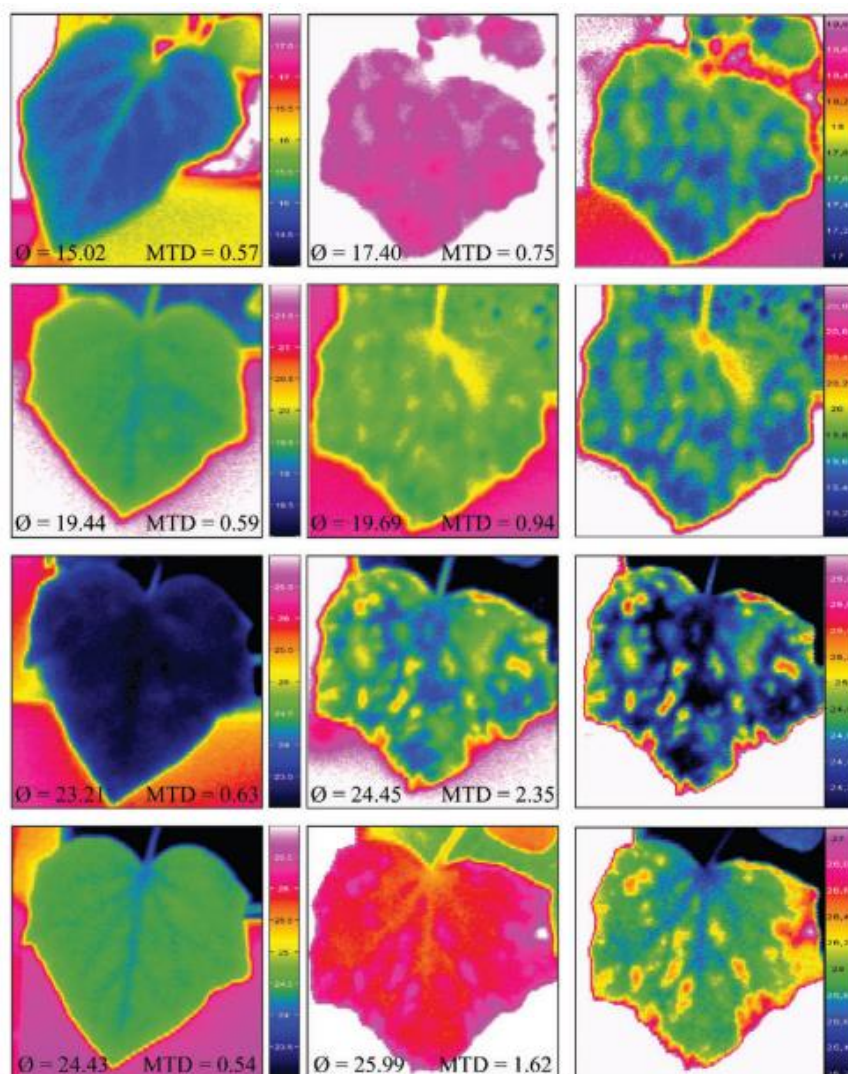
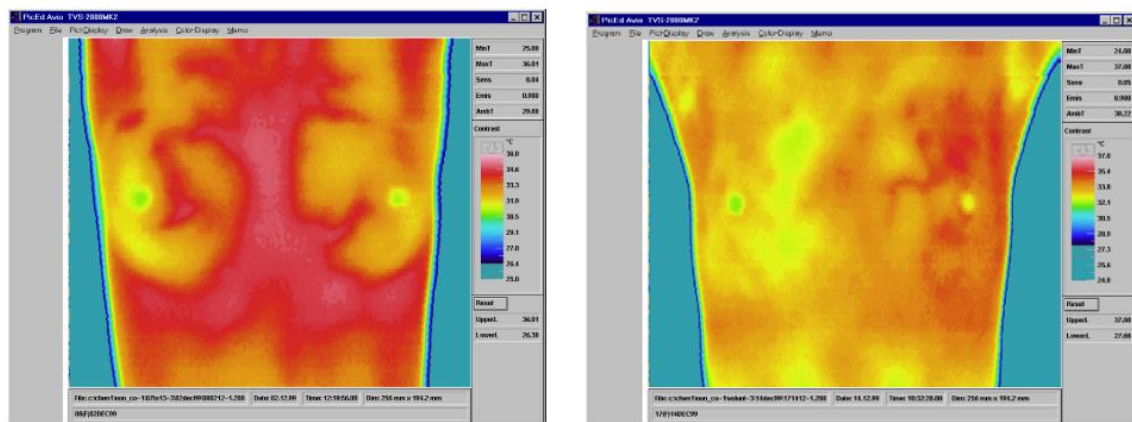


Figure 4.5 The effect of environmental conditions on temperature distribution.  
Source: Oerke et al. (2006)

In another study performed by Fok et al. (2002), representing the **medical application field**, there are thermograms showing the temperature of the human body. These thermograms are used for investigating early cases of breast cancer, e.g. Figure 4.6. The authors have used a professional **medical software** creating a **data filtering**, where the **background** is visualized in cyan, while the important part of the image is visualized using a **colour scheme**. Moreover, the colour scheme is not unified in this case as well. Thus, yellow colour in the left image represents about 31.7 °C, while in the

right image, yellow colour stands for about 33 °C. These **inconsistencies** are striking and **negatively impact** the readability and interpretation of the thermogram.



(a) Temperature variation of a typical healthy patient.

(b) Temperature variation of a typical unhealthy patient.

Figure 4.6 Typical thermography results in medicine. Source: Fok et al. (2002)

There are only a few studies regarding thermal data visualization as the main topic. Very valuable is the work of Tan and Acharya (2015) showed in Figure 4.7, where they investigate the possibilities of using pseudo-colours for **thermal visualization**. They also incorporate methods that can be described as **data filtering**, using dark colours to separate image background and highlight a certain part of the histogram using a single colour or colour scheme. A very interesting concept is written by Cimbalista (2014). He proposes a **retina adapted colour algorithm** for better visualization. This concept is patented and focuses only on high-temperature values for industrial use.

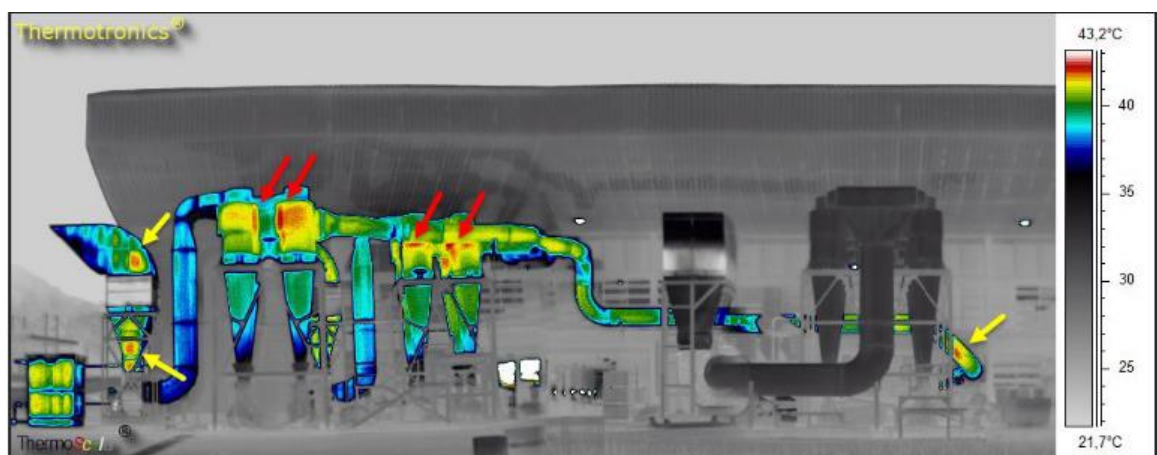


Figure 4.7 Retina adapted colour algorithm. Source: Cimbalista (2014)

### 4.3.2 Thermal data visualization in cartography and GIS

The thermal visualisation of maps in scientific literature is very rare and sparse. This is most probably caused by the very limited or non-existent space in scientific journals that could be used for larger appendices and maps. Therefore, most of the articles show only thumbnails or examples or no actual thermal maps at all; e.g. Leng et al. (2019). The largest issue with thermal imagery is that it needs to be investigated in detail, which requires a lot of space, large format printing or software tools.

Cartographic representation of thermograms has **no strict rules**, and there is **no standardized colour scheme**. There also seems to be no agreement on what data should be used to help the user with **orientation** within the map. The thermogram usually covers the whole area of the image. Therefore, it is crucial to **navigate** the user on the map effectively.

From recent studies, one of the illustrative examples can be the work of O'Sullivan et al. (2019). Figure 4.8 from their work shows how **complicated** it is to visualise only one river streams. Moreover, the colour scheme is very **badly readable**, and the user is not able to clearly tell the temperature of various parts of the rivers. To further improve the readability, two zooms were created (*a* and *b* in Picture 4.8).

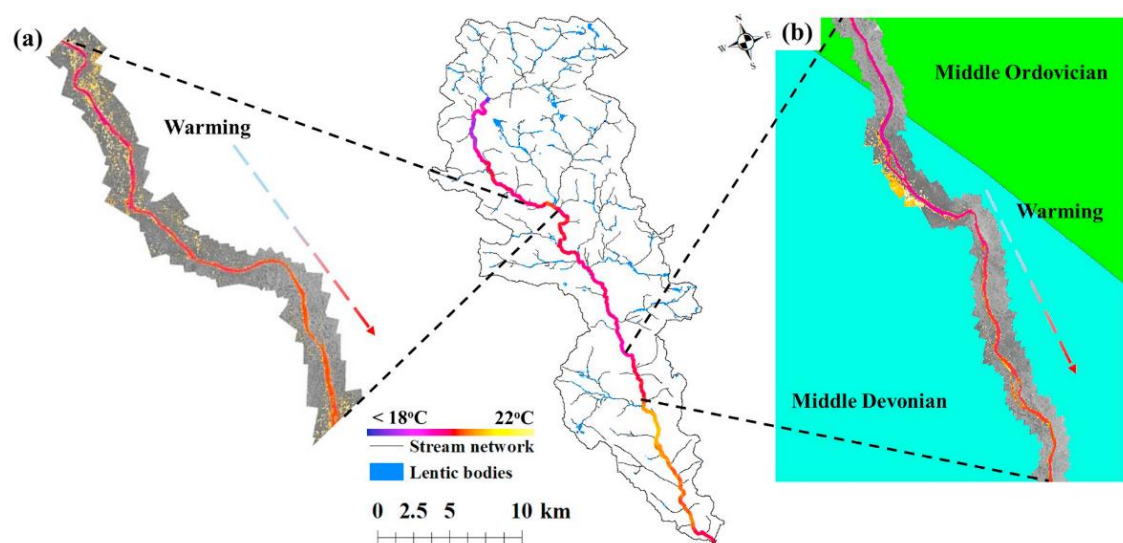


Figure 4.8 Clearwater Brook main stem temperature gradient. Source: O'Sullivan et al. (2019)

Another example of a thermal map is Figure 4.9, where Irani Rahaghi et al. (2019) visualise the measurement of **lake surface water temperature**. In the image, there are linear objects that are barely recognisable, and the user cannot really tell if it is water surface or alien object. Thus, it is very important to provide **additional information** to the users, so they can properly interpret the information from the image.

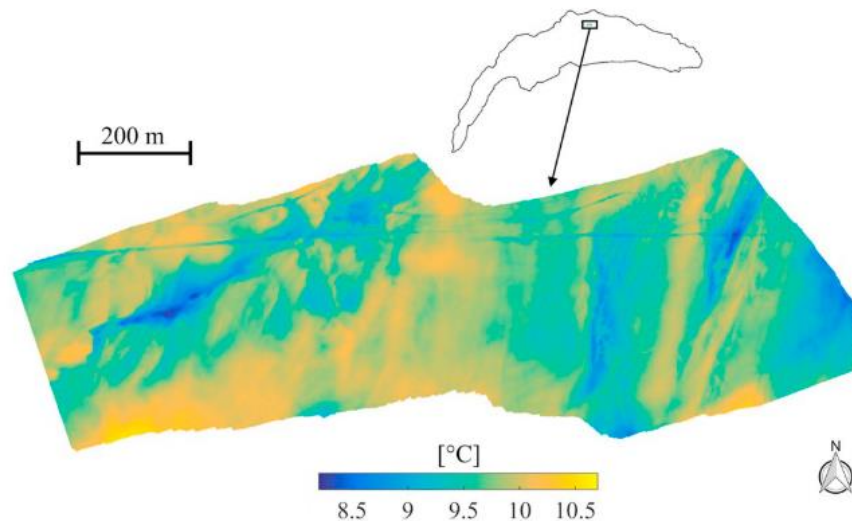


Figure 4.9 Lake Surface Water Temperature (LSWT) over a section of Lake Geneva obtained from aerial remote sensing on 18th March 2016 at 15:30. Source: Irani Rahaghi et al. (2019)

The thermal map, especially of a **heterogeneous urban environment**, is probably best suited for web-maps. A very good example of such data dissemination is **UrbanAdapt** project (*Thermal map of surfaces, Brno 2015*). The web-map (Figure 4.10) allows users to zoom and turn on some auxiliary layers such as **building outlines**, city districts and street names that help with the **orientation**. Moreover, the web-map allows users to switch between **summer and winter campaign**, which allows further comparison.



Figure 4.10 Overview of a web-map visualising thermal map of city Brno, Czech Republic.

## 5 OLOMOUC AIRBORNE THERMAL DATA ACQUISITION

The process of the production of a **high-quality extreme resolution thermal mosaic** of Olomouc city is described in the following chapter. The mosaic contains the radiometric temperature of the surface at **two different times** during the day. The process includes flight planning, data acquisition, data correction, and photogrammetry processing.

### 5.1 Olomouc flight campaign, 10<sup>th</sup> July 2016

The aeroplane Cessna 172 was mounted with a photogrammetric sensor **Phase One iXA-R 180** and a thermal camera **Workswell Thermal Vision Pro** (based on a **FLIR Tau2** core). This version of Tau2 is mounted with 13 mm, f/1,25 optics which allows a **field of view** (FoV) of  $45^\circ \times 37^\circ$  with an **iFoV** of 1,308 mrad. The flight campaign consisted of thermal and visible spectrum imaging. The flight height and spectral resolution were chosen primarily considering the thermal sensor because of its smaller iFoV. **Different scenarios** were created to satisfy the need for overlap and fine spatial resolution. After spatial resolutions from 30 cm to 130 cm were considered, the final decision was to aim for a **100 cm spatial resolution** per pixel edge. Based on this decision, the rest of the variables were calculated, as shown in Table 5.1. The size of the scene was 512 m  $\times$  640 m, and the average flight height was set to 769 m above sea level.

Table 5.1 Basic parameters of the flight campaign

| Parameters                    | Value              |
|-------------------------------|--------------------|
| Average flight height         | 769 m AGL          |
| Map scale                     | 1 : 58824          |
| Scene size                    | 512 $\times$ 640 m |
| Distance between images       | 307 m              |
| Distance between flight lines | 384 m              |

The area of interest is about **10 km  $\times$  8 km** in size, which required 22 flight lines; visualized in Figure 5.1. The flight was carried out on July 10, 2016. Because the closest airport does not allow night take-offs and landings, the **early flight** started as soon as possible; that is, right after civil dawn, which was at 4:55 CEST for that day. The second flight time was aimed at the **highest** possible stored temperature; the flight started at 15:00 CEST. Both flights took about 180 minutes and consisted of approximately 2135 thermal images.



Figure 5.1 Flight lines and ground control locations over the Olomouc city. The flight was carried out from the west towards the east. In red, the planned flight lines are visualised. Blue dots symbolise the ground truth data locations.

## 5.2 Image processing

Thermal imaging requires similar **corrections** as other conventional remote sensing methods do. According to Zemek (2014), the corrections can be divided into **four main groups**: geometric, radiometric, atmospheric, and emissivity corrections.

### 5.2.1 Radiometric correction

Radiometric correction originates from a **camera calibration** based on imaging a black body object of **known temperature**. In our case, this calibration was performed by the manufacturer with results shown in Table 5.2. The camera is always calibrated to

specific measured **surface temperature**, and the error increases farther away from this point. The **FLIR Tau2** sensor used for the campaign was calibrated to temperatures between 40° C and 50° C. As seen in Table 5.2, the error increases approximately by 0.5° C every 20° C of the measured temperature.

Table 5.2 - Accuracy protocol after the calibration for the thermal sensor FLIR Tau2

| Radiation temperature (°C) | Sensor measurement (°C) | Difference (°C) |
|----------------------------|-------------------------|-----------------|
| 0                          | 1,5                     | 1.5             |
| 20                         | 21                      | 1               |
| 40                         | 40,4                    | 0.4             |
| 70                         | 68,9                    | -1.1            |
| 120                        | 118,4                   | -1.6            |

**Off-axis vignetting** compensation had to be performed, which is, according to Li and Zhu (2009), a phenomenon commonly present in thermal imaging. **Vignetting** appears on all images, be it optical or from a near-infrared sensor. In thermal imaging, this effect is usually very strong due to the **low contrast** of imaging systems. The further the object is away from the system's axis and the larger the field of view, the more serious the vignetting becomes, as seen in Figure 5.2.

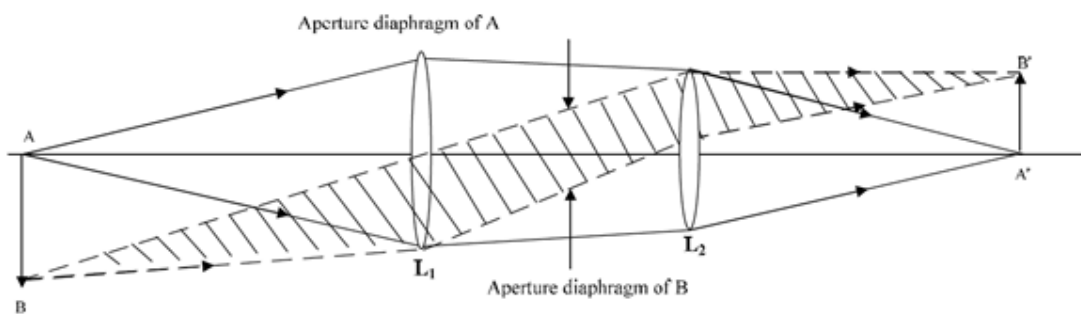


Figure 5.2. The off-axis vignetting principle shown in the two-lens system. The signal originating in nadir (A) is captured as A' with full strength. On the contrary, the signal originating further from nadir (B) is mitigated (B') while passing through the lens system (lenses L<sub>1</sub> and L<sub>2</sub>). Source: Li and Zhu (2009)

The off-axis vignetting effect not only **distorts** the real kinetic temperature data but also **corrupts** the images for mosaicking. The digital values towards the sides of the images suffer from heavy error, not allowing the **mosaicking algorithm** proper tying of neighbouring images. In general, the off-axis vignetting results in a **gradient of declining temperature** from the image nadir to the image sides.

Four images were acquired to compensate for the **vignetting effect**. An object with a **smooth, unpolished** surface with **constant emissivity** and temperature was used. The

images were taken from a strictly orthogonal position from approximately **40 cm** away. However, in this thermal measurement, the off-axis vignetting effect does not seem to increase with distance from the emitting object (Figure 5.3); it maintains the **same pattern** and same difference on airborne images as on close-range images. Another fact is that it does not represent a **linear gradient** from the nadir to the sides but rather shows an **irregular pattern**. Although the temperature appears lower especially in corners in what corresponds to the off-axis effect described previously, in the lower-right corner, the effect is much stronger than in the rest of the corners, and the effect is stronger in the lower part of the picture, in general. Another **inconsistency** appears in the **upper-central area**. According to the theory, there is no possibility that the digital values near the upper edge of the image are like those in nadir, due to the conditions mentioned above. The true reason for the **vignetting-like** effect in these images was not identified. However, the error was **treated and solved** the same way as the casual vignetting without any problems.

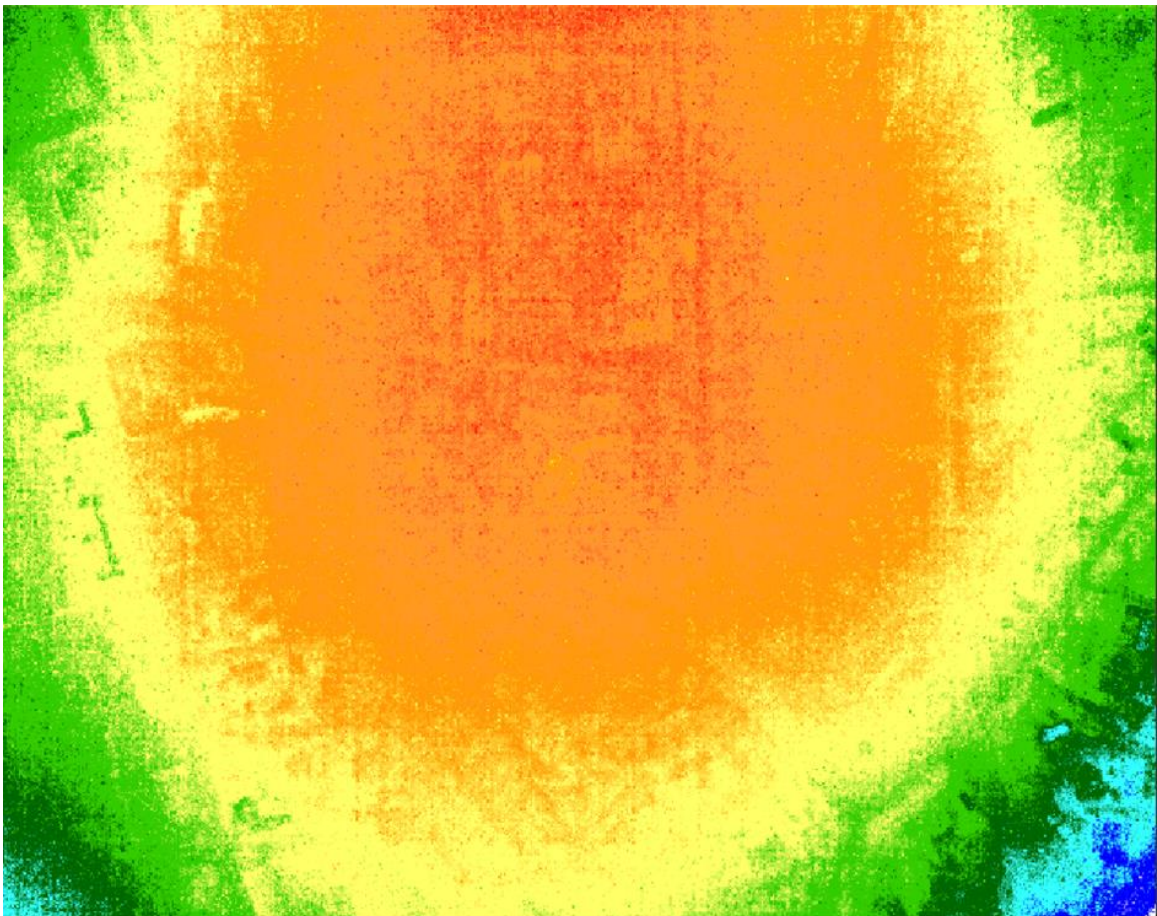


Figure 5.3 Off-axis vignetting pattern based on mean from 4 images of homogeneous objects from a short distance. Red colour means no difference from the highest value while blue colour means about 5° K difference from the highest value.



Images were to be exported to **raw numbers** because the camera produces images already recalculated to temperatures. At the raw number level, the largest pixel value was **subtracted** from each pixel value in the entire image to obtain the **vignetting mask**. This was performed on four images. A **low-pass filter** was applied afterwards to smoothen the **differences** in the mask. In the next step, the masks of the four images were averaged to secure the most suitable outcome; the result is shown in Figure 5.3. The final mask was added to all images.

The results are satisfactory, regarding visual comparison and value comparison. After applying the vignetting mask, the same objects show **highly similar values** as many other images in different parts of the image, as shown in Table 5.3.

Table 5.3 Comparison of the same materials in different parts of the image before and after correction

|                        | Image centre temperature (°C) | Image corner temperature (before correction, °C) | Image corner temperature (after correction, °C) | Temperature difference (°C) |
|------------------------|-------------------------------|--|---|-----------------------------|
| <b>Metal roof tile</b> | 42.84                         | 38.00  | 42.59   | 0.25                        |
| <b>Cobblestone</b>     | 38.29                         | 33.39  | 38.26   | 0.02                        |

### 5.2.2 Atmospheric corrections

Atmospheric corrections are based on modelling the atmospheric **signal loss** and **atmospheric emission**. Main atmospheric characteristics affecting thermal imaging are **air temperature** and **air humidity**.

Two meteorological data sources were available as the auxiliary data source. One is a **GNSS reference station** operated by the Department of Geoinformatics, Palacký University Olomouc. The station provides reference GNSS data for VESOG and CzechGeo projects. Moreover, it provides **basic information** about the atmosphere every five minutes. The basic variables are air **temperature**, air **pressure**, and air **humidity**. The other source comes from a **semi-professional meteorological station** located near the city borders. The station provides information about air temperature, air pressure, and air humidity as well as solar irradiation.

In the study, we used an algorithm developed specifically for **FLIR cameras** integrated as an R package called **Thermimage** (Glenn J. Tattersall 2018). This package recalculates data from raw values to temperature based on calibration constants acquired during the calibration, applies corrections for atmospheric **transmission loss** based on distance from the object, compensates for radiance emitted from surrounding objects (**reflected temperature**), and compensates for **emissivity**.

The algorithm uses equations from Minkina and Dudzik (2009) to simulate the **signal passing** through the atmosphere using atmospheric constants and humidity recalculated to water vapour pressure. **Water vapour pressure** ( $WVP$ ) is calculated from atmospheric temperature ( $AT$ ) and humidity ( $RH$ ) based on Equation 5.1.

$$WVP = \left(\frac{RH}{100}\right) \cdot \exp(1.5587 + 0.06939 \cdot AT - 0.00027816 \cdot AT^2 + 0.00000068455 \cdot AT^3) \quad (5.1)$$

The algorithm uses atmospheric constants  $ATA1$ ,  $ATA2$ ,  $ATB1$ ,  $ATB2$ , and  $ATX$ , as seen in Equation 5.2, which generates the  $TAU$  value later used in the calculation. The values of atmospheric constants can be found in the package documentation (Glenn J. Tattersall, 2018).

$$TAU = ATX \cdot \exp\left(\left(\frac{OD}{2}\right)^{-\frac{1}{2}} \cdot (ATA1 + ATB1 \cdot \sqrt{WVP})\right) + (1 - ATX) \cdot \exp\left(\left(\frac{OD}{2}\right)^{-\frac{1}{2}} \cdot (ATA2 + ATB2 \cdot \sqrt{WVP})\right) \quad (5.2)$$

For brightness temperature ( $BT$ ), the algorithm uses the following equation

$$BT = \frac{B}{\ln\left(\frac{R1}{R2(S+O)+F}\right)} \quad (5.3)$$

where  $BT$  is brightness temperature in degrees Kelvin,  $S$  is original raw data in 16-bit form, and  $R1$ ,  $R2$ ,  $B$ ,  $F$ , and  $O$  are constants acquired during the calibration of the camera.

### 5.2.3 Emissivity corrections

Emissivity is a characteristic of the viewed object which affects the resulting temperature in a major way. Emissivity is defined as the ratio of **emitted thermal radiation** of the object to the thermal radiation of a **blackbody**. Emissivity is unique for each material and **wavelength**.

Emissivity corrections are of special importance in thermal remote sensing because they may cause the **highest amount of error** in the data (Minkina and Dudzik 2009). Low

emissivity objects such as **metal rooftops** appear as very low-temperature objects, which is not the case in reality. Even though most objects have a similar emissivity of about 0.95, the remaining objects must be corrected to analyse the data further.

The emissivity of every object in the image for a certain wavelength must be known for proper emissivity corrections. At the satellite image level, this issue is solved by **estimating emissivity from NDVI** with which it correlates. At the fine scale level, however, low emissivity objects are very significant, especially for analysis following the imaging, and are not recognised in the NDVI image. Therefore, at a finer scale, emissivity must be compensated for each object separately. This problem has no easy solution and is still quite new because there were not many thermal campaigns solving this issue.

The proposed approach combines the use of **auxiliary GIS and satellite imaging data** to access the land cover. The national system RÚIAN which manages certain land cover classes was used. After some minor corrections, it shows **buildings, roads, and sidewalks** accurately. A simple threshold for NDVI based on **QuickBird** satellite imagery was created to separate vegetation and non-vegetation classes. When combining the data, we created an easy hierarchy rule saying that vegetation can overlap roads, pavements, and buildings and that buildings can overlap roads and pavements. After this mash-up was created, we semi-manually tied these objects with their respective material emissivity number. This approach allowed us to **partially eliminate** the cold spots that might corrupt further analysis results.

When calculating kinetic temperature, the radiance reflected from surrounding objects must be calculated first. The same equation is used except that the raw value ( $S$ ) is replaced with the reflected temperature ( $RT$ ). Thus

$$RAW_{refl} = \frac{B}{\ln\left(\frac{R1}{R2(RT+O)}+F\right)} \quad (5.4)$$

and emissivity of the object is applied

$$RAW_{em} = \frac{S-RAW_{refl}(1-E)}{E} \quad (5.5)$$

where  $E$  is emissivity of the imaged object. Now, the kinetic temperature can be concluded using the original equation while replacing raw data with the new value corrected for reflected radiance and emissivity.

$$KT = \frac{B}{\ln\left(\frac{R1}{R2(RAW_{em}+O)}+F\right)} \quad (5.6)$$

### 5.3 Photogrammetric processing

The biggest challenge of the **mosaicking** part of the study was the fact that plenty of images were corrupted due to blurring caused by the slow shutter speed of the camera and high aeroplane speed. Moreover, the aeroplane was considerably light. Therefore, it suffered from **heavy wind** and was unsteady in general.

AgiSoft Photoscan Professional (currently called **Metashape**) and **Trimble INPHO** software were used for the photogrammetric process. The entire process is shown in Figure 5.4. The basic method for image orientation and calculation of the exterior orientation parameters is **Structure from Motion (SfM)**. This approach includes a few methods like “Stereo matching” or “Multi-view stereo – MVS”. Stereo methods can be global or local. Semi-global matching methods are implemented in Agisoft Photoscan Pro. The main fundamental difference between SfM and classic photogrammetry is the use of a **new generation** of image matching algorithms, which allow for unstructured image acquisition. While classic photogrammetric methods typically rely on strips of overlapping images acquired in parallel flight lines, MVS was designed to reconstitute the **three-dimensional geometry** of buildings and objects from randomly acquired images (Fonstad et al. 2013). The multi-view matching method performs very well for oblique images as well as for classic aerial images with forward-overlap and side-overlap.

Moreover, different settings and **digital elevation models** were tried. Namely, we used an automatically generated elevation model created by Agisoft with the semi-global matching method (SGM), digital surface model, and digital elevation model. The low overlap of the images in combination with **corrupted images** caused serious damage to the mosaic. The algorithm could not identify a large number of images and created gaps in the mosaic or, in the worst case, tried to distort images to fill the gaps. This process was **unsatisfying**, but most of the corrupted images were located outside the city or in the suburbs. Therefore, it was decided to reduce the area of interest to only the city centre, which was of high quality in the images in general. The final mosaic was created from only **117 images** in the case of the morning flight and **115** in the case of the afternoon flight.

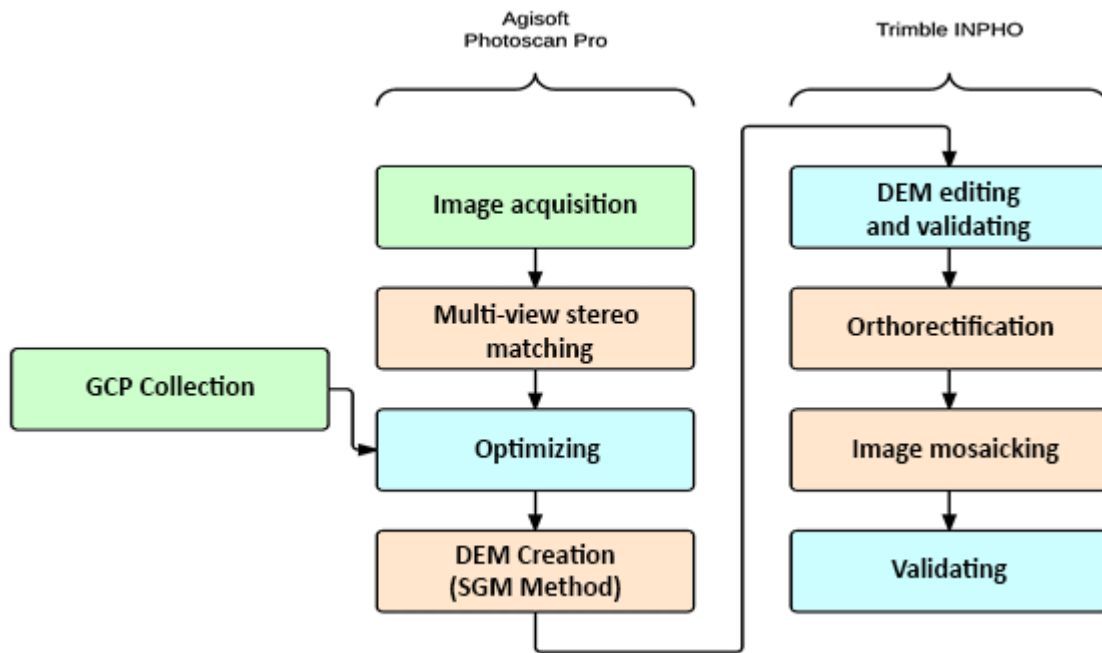


Figure 5.4 Workflow of photogrammetric image processing for the flight campaign over Olomouc city. Green colour shows data inputs, in light brown, are the main methods described in the text, and the light blue steps are auxiliary processes in the workflow.

## 5.4 Final product assessment

This work resulted in two raster datasets representing **two flight campaigns** (morning and afternoon). The final mosaic covers approximately **75 % of the area** due to bad overlaps in the corner regions. Along with the flight campaign, a ground survey using a hand-held thermal camera **FLIR E60** was performed. From this measurement, a control dataset was created with **six locations** gathering data for **four materials**. The locations were manually chosen, so they are evenly distributed over the area of interest. The presence of a water body and the feasibility of data acquisition at the same time as the aerial sensor was desirable. The location of ground measurement was recorded using a **GPS receiver**. As illustrated in Table 5.4, the final error after corrections is around one degree Celsius, which is very satisfactory, given the base error of the camera. The classes with the **largest error** are **water** and **asphalt**. This phenomenon might have been caused by the **heterogeneity** of the material and the **difficulty of measuring** water temperature due to physical unavailability of the river stream.

Table 5.4 The comparison of the ground truth data and the data acquired from the airborne campaign. The data are sorted by location and material type. In the rightest column, the average values for each material are shown for both the ground and the airborne dataset as well as their average difference (error).

|          |            | Cemetery | Residential | Shopping mall | Monastery | Suburbs | Industrial | Average |
|----------|------------|----------|-------------|---------------|-----------|---------|------------|---------|
| Asphalt  | Ground     | 18.9     | 20.2        | 21            | 22.2      | 23.2    |            | 21.1    |
|          | Airborne   | 17.1     | 20.6        | 20.5          | 19.5      | 20.9    |            | 19.7    |
|          | Difference | 1.8      | 0.4         | 0.5           | 2.7       | 2.3     |            | 1.5     |
| Grass    | Ground     | 12.5     | 16.3        | 16.3          | 16.8      | 17.6    | 18         | 16.3    |
|          | Airborne   | 14.9     | 16          | 15.9          | 15.7      | 18.2    | 17.8       | 16.4    |
|          | Difference | 2.4      | 0.3         | 0.4           | 1.1       | 0.6     | 0.2        | 0.8     |
| Concrete | Ground     | 16.1     |             | 21.0          |           |         | 23.2       | 20.1    |
|          | Airborne   | 15.1     |             | 20.0          |           |         | 22.4       | 19.2    |
|          | Difference | 1.0      |             | 1.0           |           |         | 0.8        | 0.9     |
| Water    | Ground     |          | 23.2        | 16.2          | 18.4      | 17.3    |            | 18.8    |
|          | Airborne   |          | 22.2        | 18.8          | 18.2      | 17.9    |            | 19.3    |
|          | Difference |          | 1.0         | 2.6           | 0.2       | 0.6     |            | 1.1     |

## 6 DESCRIPTIVE ANALYSES CARRIED OUT ON OLOMOUC THERMAL MOSAICS

The first group of analyses is based on **self-reliant** methods requiring no or **minimal auxiliary data** to perform. The first method consists of **manual sampling** from optical imagery and then analysis performed on the collected values. The second method exploits the sample dataset as it is based on the **spatial distribution** of **asphalt-concrete** material temperature. The third method is based on a **statistical analysis** of the datasets investigating extreme values in the thermograms.

### 6.1 Thermal regime of materials in an urban environment

For the first analysis, a simple **data sampling** approach was carried out. More than any functional class, land-cover or land-use type, the temperature regime depends on the specific **material type**. Meaning that asphalt rooftop is very similar on TIR imagery as the asphalt road, although it is completely different land-use and functional class.

At first, a **preliminary dataset** was gathered. The material samples were chosen manually with ten samples for each class, totalling **100 samples**. As the source of information, the photomosaic created alongside the thermal mosaic was used. For the preliminary investigation, a mixture of land-use and land-cover classes was selected. For example, the high-rise buildings were apartment buildings typical for the socialist era. Sun inclined and declined buildings were chosen based on their south-north orientation with approximately 45° tolerance.

The resulting diagram is visualised in Figure 6.1. The high-rise buildings show the **largest difference** in temperature in between datasets. The low morning temperature is most probably caused by **very good ventilation** and lower air temperature at the rooftop level. Highest day-time temperature is, on the other hand, caused by low-quality materials used for the rooftop, usually asphalt paint. Very interesting is the difference between cobblestone and asphalt. **Cobblestone** is used mostly in the city centre in the pedestrian zone and as the street material in the surroundings. The diagram shows **15 % increased temperature** of the asphalt in comparison to the cobblestone.

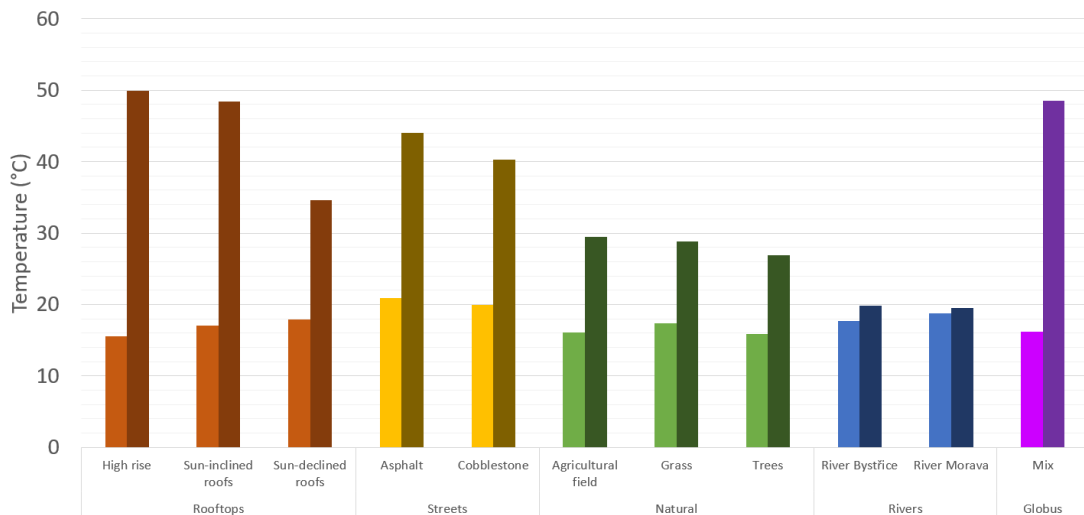


Figure 6.1 Thermal regime of materials in the urban environment of the city of Olomouc. The light colours are visualising morning temperature. Darker colours stand for the afternoon temperature. The last class 'Globus' covers the area surrounding the largest shopping area in the city and contains all the buildings, parking lots and sparse ornamental vegetation.

The difference between the two rivers is caused by their characteristics. The Morava river is a wide, slow and relatively deeper water body while the Bystřice river is **shallow** and much **faster** with many **rocky** areas. The difference in thermal behaviour is apparent as the Morava river has larger thermal inertia and is not so prone to temperature changes.

The natural materials also show some very specific behaviour. The difference between grass and tree classes is particularly interesting. There are two possible reasons for trees to have lower temperature morning and afternoon temperature. It might be caused either by the general wind in higher vertical level or by the fact that the grass patches are often mixed with some bare soil that is generally heating up more than just grass as a plant.



### The second sampling

After the first sampling and evaluation, a more sophisticated approach was performed. The **second sampling** was based on auxiliary data from the city's municipality. The data contained information about specific road material type, so a more accurate typology and sampling could have been performed.

The road material class was further divided into the five most common material types. Road material classes are:

- Asphalt concrete
- Macadam
- Cobblestone
- Gravel
- Concrete

The **asphalt concrete** class is covering the majority of the roads in Olomouc and represents more than 90 % of the area. **Macadam** is used mainly for parking lots, **cobblestone** in the historical centre of the city, **gravel** was found in the suburbs used for utility roads, and pure **concrete** was identified in several industrial areas.

The class of natural materials was divided into several subclasses as well. These are:

- Grass
- Bare soil
- Tree crowns
- Agricultural crops

The **grass** material was sampled based on another auxiliary dataset containing information for Technical Services of the city of Olomouc, helping them with effective watering. **Tree crowns** class was identified based on the optical imagery combined with the **Digital Surface Model (DSM)**. **Agricultural crops** were differentiated from **bare soil** class based on the **Normalized Difference Vegetation Index (NDVI)**.

Water bodies were distinguished on topographic maps of the area and in **OpenStreetMap** data. There are two small lakes close to the city, **Hamrys** and **Morava's oxbow lake**. Two main rivers, **Morava** and **Bystřice**, were identified, and more samples than in the preliminary study were gathered. The **Trusovický brook** is a very small stream flowing into the Morava river before reaching the city. **Morava arm** is a part of the river that separates from the main river before it reaches the city and reconnects with it in the city.

The number of samples for each class is shown in Table 6.1. A large number of samples taken for **asphalt concrete** material is due to its use in the next analysis as the main input. The other numbers of samples were chosen based on the sampled material

type with respect to their appearance in the image. For example, the Hamrys lake has only a few hundreds of square meters. Therefore, it is not helpful to gather more than a handful of samples.

Table 6.1 The number of samples digitised for each material in each class.

|                          |                  |                   |                |                   |              |            |
|--------------------------|------------------|-------------------|----------------|-------------------|--------------|------------|
| <b>Road Materials</b>    | Asphalt concrete | Macadam           | Cobblestone    | Gravel            | Concrete     |            |
|                          | 1796             | 46                | 49             | 24                | 19           |            |
| <b>Natural materials</b> | Bare soil        | Grass             | Tree crowns    | Agricultural crop |              |            |
|                          | 77               | 51                | 47             | 83                |              |            |
| <b>Water bodies</b>      | Hamrys lake      | Morava oxbow lake | Bystřice river | Trusovický brook  | Morava river | Morava arm |
|                          | 14               | 11                | 24             | 17                | 76           | 32         |

The results of the analysis are visualized in Figure 6.2. The materials within their respective groups are **sorted descending** based on their afternoon temperature for better orientation. The asphalt concrete material is easily recognized as the one with the largest afternoon temperature as well as the temperature difference between the morning and the afternoon. It heats about **10 % more** than the other road materials. The difference between asphalt concrete and cobblestone is even more striking than in the preliminary dataset due to the larger number of samples.

All the natural materials have very low morning temperature and tend not to heat up as much as the artificial ones. For example, in the afternoon, the grass material class is about **40 % cooler** than the asphalt concrete. Within the natural materials, the bare soil is approximately **5° C hotter** than the other materials due to bare soil absorbing a large portion of the incoming EM radiation while plants use the energy for photosynthesis.

The water bodies group shows some very interesting information as well. The most significant is the **Hamrys lake**, which is a **still water body** prone to incoming EM radiation. The difference between the rivers **Morava** and **Bystřice** is the same as described in the **preliminary results** section. **Morava's oxbow lake** is a very interesting phenomenon as it does not change its temperature at all throughout the day. The **Trusovický brook** is a very shallow and fast stream, and its **thermal behaviour** is similar to the **Bystřice river**.

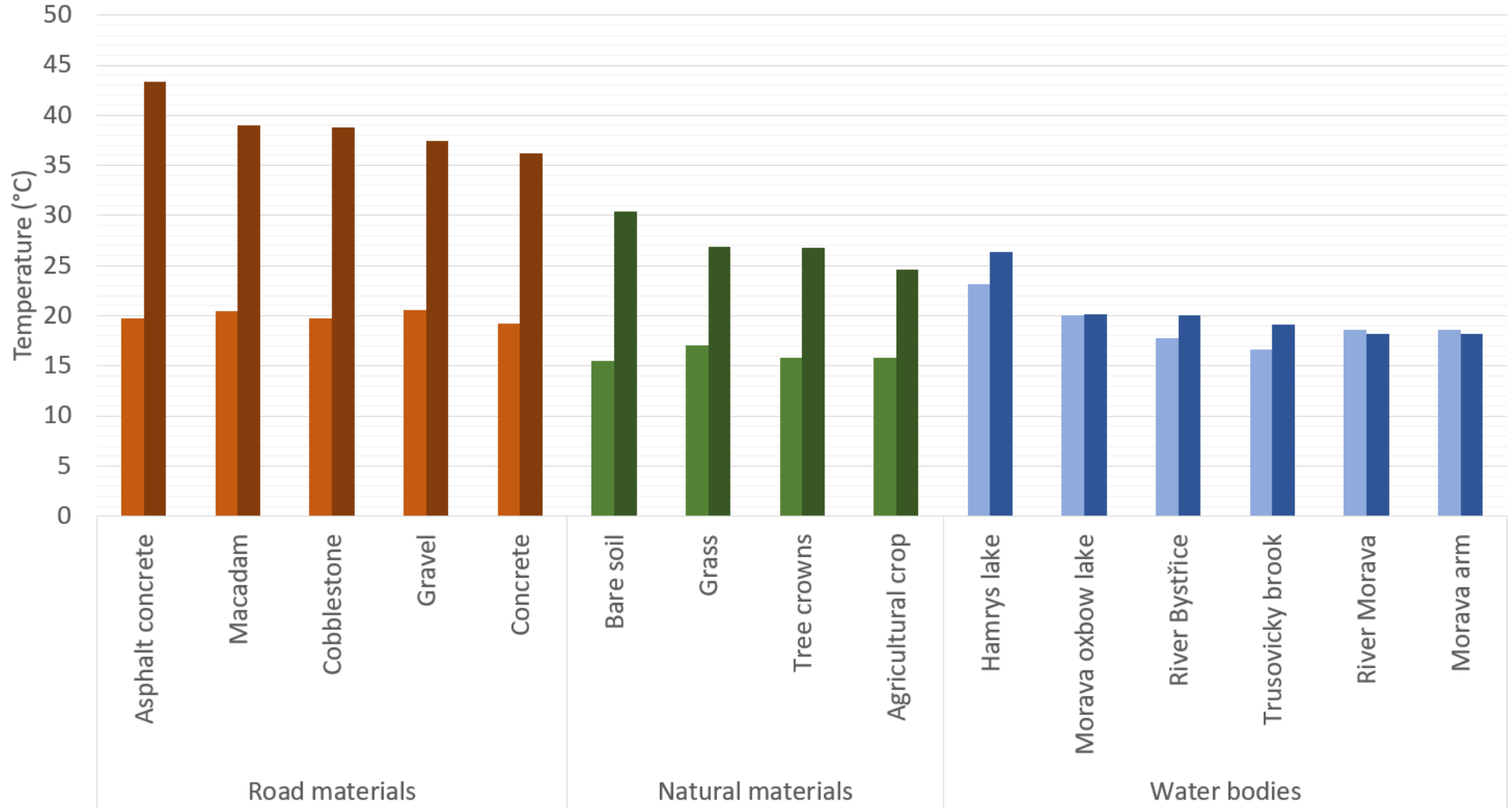


Figure 6.2 Thermal material regime in the city of Olomouc. Light colours are the morning temperature; darker colours are the afternoon temperature.

## 6.2 Investigation of microclimate using TURN method

This analysis was heavily inspired by **Thermal Urban Road Normalization (TURN)** method published by Rahman et al. (2014). TURN is based on the premise that roads as objects are pseudo-invariant features and can be used to model the **microclimatic variability**. The main reasons supporting this approach are:

- Roads distribution and frequency in the modern urban environment
- Same material type for most of the major roads
- The strong correlation between night-time air temperature and road temperature

Based on these fundamentals, all differences from the mean road temperature can be considered as the effect of the microclimate. In the mentioned paper, Rahman et al. (2014) subtracted the resulting **microclimatic influence** from the image to correct the thermal imagery for it. However, quantifying the microclimatic effect over the whole city area is very interesting as is and thus it is calculated and described in this thesis.

In the original paper, Rahman et al. (2014) identified the roads based on local GIS data, specifically, from **linear objects**. For this study, the polygon layer with road material types was available. Therefore, more accurate sampling based on the actual material type, could have been performed.

The process of sample generation is very problematic. The original TURN study performed simply took **auxiliary linear GIS road data** and created point geometry along the lines. After that, some postprocessing was performed to, for example, remove points covered by vegetation. While this approach is practically true GIS and very correct, in Olomouc dataset, there were issues forbidding this approach. The basic layer that was used for this study was road material polygon layer provided by the Institute of Urban Planning of the city Olomouc. The dataset is **very detailed**, includes the tram lines, tram stations, distinguishes more than **30 types of road materials** and contains a layer of **sidewalks**. One downside of the dataset is that some of the roads are not owned and operated by the municipality and thus do not have all the attributes, and their material type is **'unknown'** or **'unspecified'**, even though it was apparently asphalt concrete or something very similar. These roads were kept out of the sampling dataset to keep the analysis intact.

One of the largest issues using an automated approach for the city of Olomouc is tram lines that are usually from a different material than **asphalt-concrete**. The second issue comes from various **pedestrian safety islands**, **green lines** in between the lanes and other **anomalies**. A large portion of the points is affected by **building shadows**. Many streets are completely covered by **vegetation**. For these reasons, the sample

dataset was created manually, considering only *asphalt-concrete* road material type, which is the most common throughout the city.

### Visualisation and description of the microclimate

The dataset from the previous method was used, having almost **1800 samples** of asphalt concrete road material. The samples were **hand-picked** trying to avoid tram lines, pedestrian safety islands, grass patches, shadows and other anomalies. In the original study, Rahman et al. (2014) used **Inverse Distance Weighting (IDW)** as the interpolation method after trying several others. Therefore, in this study, only IDW was applied, and no other methods were tested. The resolution of the final interpolated surface was downscaled to **10 × 10 m** for computational and practical reasons. The mean temperature of the asphalt concrete was **subtracted** from both morning and afternoon dataset creating relative temperature change in the area, which can be attributed to the **microclimatic influence**. This change is visualised in Figure 6.3 and has a range of  $\pm 9.5$  degrees from the mean temperature. The morning (A) and the afternoon (B) maps are visualised in the same figure for easier comparison and better orientation. In the morning dataset, the temperature difference is lower, and the values are much more accumulated around the mean. The standard deviation of the morning (A) data is 1.5, while for the afternoon data, it is 2.5. Therefore, the morning part of the image (A) is visualised as only part of the colour scale.

In the **morning microclimatic map** of Olomouc (Figure 6.3, part **A**), there is a visible trend of hotter areas surrounding the city centre from west and north. In the northern and western part, this gradient seems to stop at the green belt extended towards the north by the football stadium and the surrounding area. However, in the southern part, there are no apparent buildings or objects that could act in a similar way. The only part that is slightly hotter in the city centre are the surroundings of Saint Wenceslas Cathedral and the area of Palacký University rectorate and archbishop's palace. The whole area is slightly elevated than the other parts of the city, which looks like an easy explanation. On the other hand, nearby Olomouc hill (also called Michael's hillock) is even higher and does not show similar behaviour.

The **afternoon microclimatic map** of Olomouc is shown in the right part of the image (**B**). The spatial distribution of the difference changes dramatically from the morning dataset. The cold spots moved towards the area of **Olomouc airport** in the western part of the city while hot spots appear in the industrial zone. Very interesting is that some areas in the south-central part of the image remain relatively **hot in both pictures**. The area around the cathedral and the rectorate is significantly **above average** while the Olomouc hill remains **close to the average** temperature. Very interesting are **various hotspots** appearing in the western part of the image.

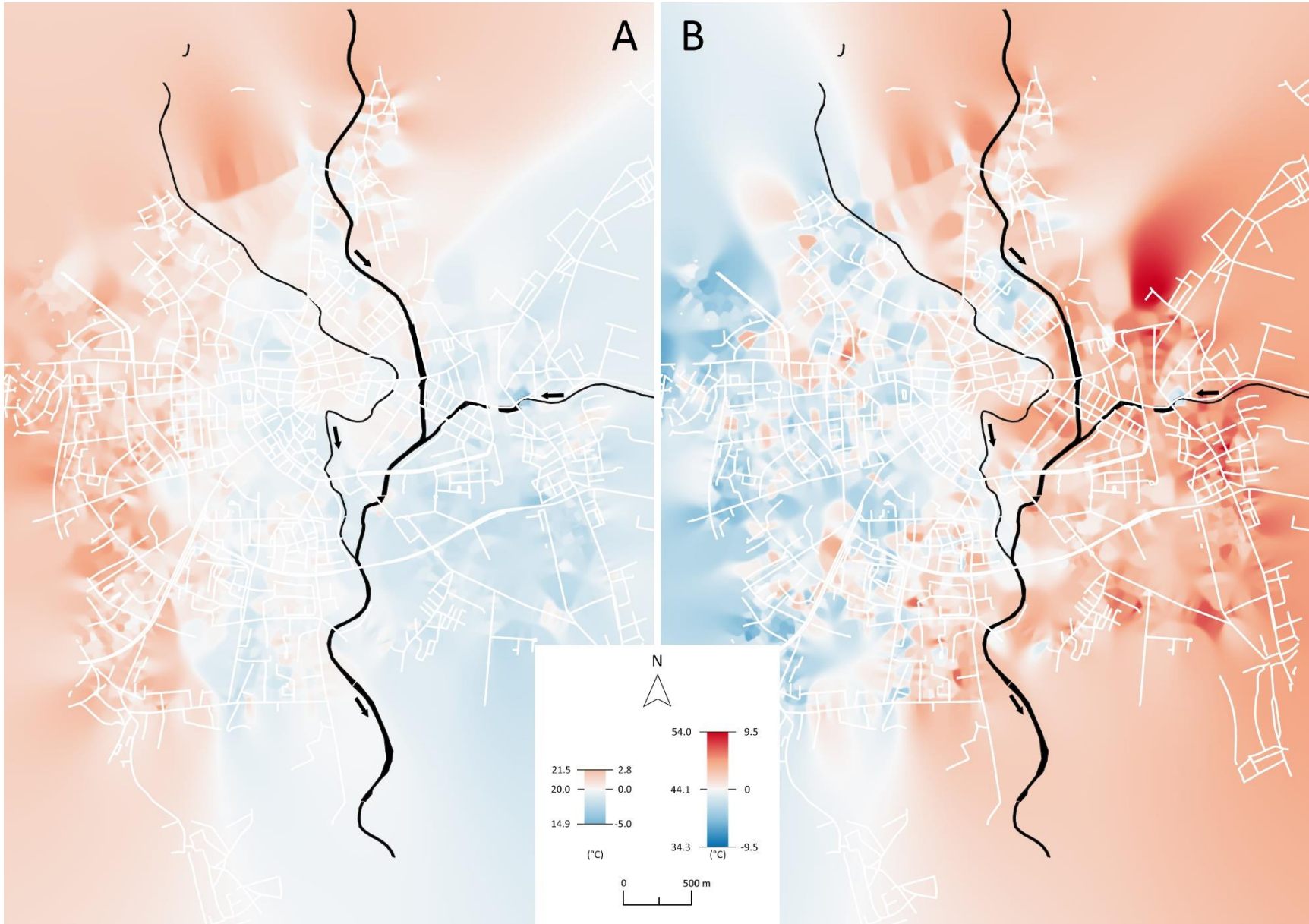


Figure 6.3 Microclimatic map of Olomouc in the morning (A) and in the afternoon (B). Auxiliary data used are street network (white) and water bodies (black). The Legend shows relative differences of temperature from the mean as well as their absolute values.

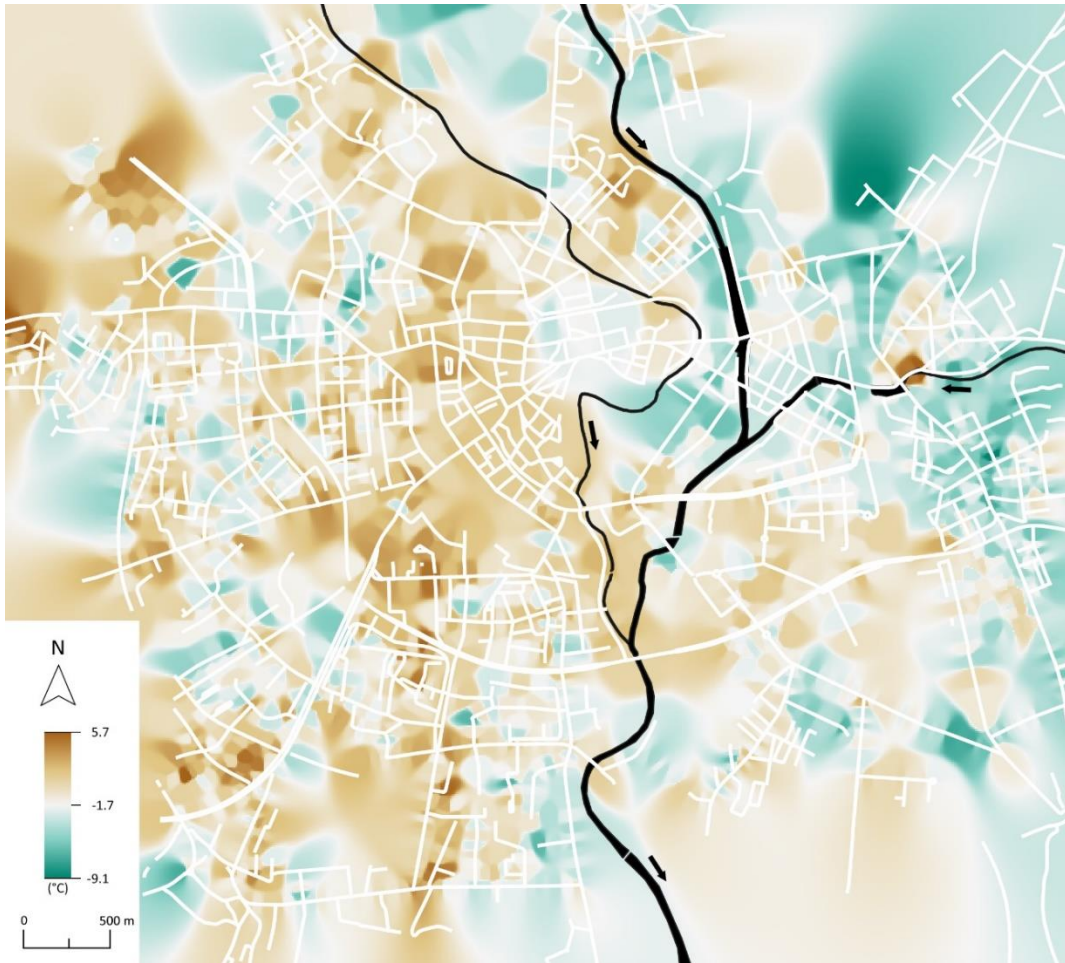


Figure 6.4 The microclimatic effect from the morning and the afternoon added together

In the next step, both microclimatic maps were summed up. This means that if an area was for example 3 °C **colder** than the mean and in the after it was 3° C **hotter**, it would have 0 °C difference in the summed-up image, visualised in Figure 6.4. On the other hand, if the are was slightly hotter in the morning and much hotter in the afternoon, it would gain positive value in this image. To summarize this method, it shows the **cumulative difference** of the area temperature from the respective **mean values**.

While in the previous comparison, a visible gradient was present, using this method, we can see a trend of scattered islands. One of the apparent trends is the overall low temperature in the north-eastern part of the city. That means that in this area, it is on average below the mean temperature compared to the rest of the city. In the city centre and even in the green belt towards the south-west, the overall balance is above average value. However, the most heated areas in the image are two shopping mall areas and the Olomouc airport. The shopping areas are located in the south-west and north-west parts of the city. The Olomouc airport is on the western edge of the image.

### 6.3 A typology based on temperature change

For **immediate classification** of the thermal data, an approach based on **relative change** was carried out. The method exploits an easy principle that most of the objects can be identified based on their **typical behaviour**, i.e. the change in temperature between the two times of the day. The typology always has 4 unspecified classes. The first class consists of objects having a relatively low temperature in the morning and relatively low temperature in the afternoon (*LL*). The second class are objects with a relatively low temperature in the morning and relatively high in the afternoon (*LH*). Third and fourth classes are created similarly (*HL*, *HH*). Having relatively low temperature means having a temperature below a specific **threshold**. These thresholds were calculated based on tertiles in the first case and based on quartiles in the second. This means that the first class in the first study contains objects that were **among 33 % coldest** objects in the morning as well as among **33% coldest objects** in the afternoon. Other classes are defined in a similar way. The second study works with quartiles, meaning that it considers **25% coldest and hottest objects**. It is also possible to use this method for different types of quantiles. However, having fewer quantiles (**medians**) results in very chaotic image and having more quantiles (**quintiles**) on the other hand, results in an empty image, which is hard to interpret.

This method has many **limits** and **inaccuracies** as it depends on the **distribution** of values within the dataset. However, it is not meant as a classification method that provides a perfect delineation of given phenomena. It is quite the opposite, a rather **quick and universal tool** for investigation of unknown territory. As described in the following chapter, it is a suitable tool for pinpointing areas of interest and **quickly recognizing** the situation in the image.

#### 6.3.1 Tertile-based typology

The first typology is very dense and might appear chaotic because of that. The legend is shown in Table 6.1 and remains consistent also for the second typology. The colours were chosen to represent the land cover that the group typically represents. **Vegetation** stays in the lowest tertile throughout the day. Thus, the first class is coloured **green**. The second class is coloured **blue** as **water** surfaces are among the hottest in the morning and the coldest in the afternoon. Remaining classes are hot in the afternoon and either cold or hot in the morning. As seen in Figure 5.5, these are typically **artificial materials** such as rooftops, roads and pavements.



Table 6.1 Tertile typology. Combinations of extreme (lowest or highest) tertiles are highlighted in colours. Empty areas are not used in the analysis.

| Tertiles<br>Typology |              | Afternoon Tertiles |    |              |
|----------------------|--------------|--------------------|----|--------------|
|                      |              | T1<br>(Low)        | T2 | T3<br>(High) |
| Morning<br>Tertiles  | T1<br>(Low)  | <b>tLL</b>         |    | <b>tLH</b>   |
|                      | T2           |                    |    |              |
|                      | T3<br>(High) | <b>tHL</b>         |    | <b>tHH</b>   |

The result (Figure 6.5) of the method is surprisingly helpful in the **general description** of the area of interest. The *tHL* class accurately outlines **the Morava river** in the central part of the image. On the other hand, most of **the Bystřice river** was not classified at all. This caused by different characteristics of this water body. In the southern part of the image, one can recognize that some fields were also classified because of the **soil moisture**. In detail, it can also be recognized that a **small pond** in one of the parks and outside part of the city's **swimming pool** was assigned to the *tHL* class.

The *tLL* class pinpoints the largest areas of **vegetation**. The south-eastern part of the inner-city green belt is not classified most probably because the northern forests and meadows took a big portion of the 33 % coldest objects; showing one of the **weaknesses** of this method.

*tHH* and *tLH* classes mostly do stand for **buildings** and **roads**. It is apparent that the *tLH* class is much more visible in the western part of the area; in the most western part, even covering a few fields. The *tHH* class fills the eastern industrial area and a portion of the city centre. This effect might be partly caused by the temperature gradient in the morning dataset related to **long flight campaign duration**. However, the western part of the city contains also red classes which are usually roads. This leads to an explanation that the western part of the city is much better ventilated, which results in **lower morning temperature**. This interpretation is supported by the fact that the western part of the city has higher elevation and thus is more exposed to **general wind** above the building canopy layer.

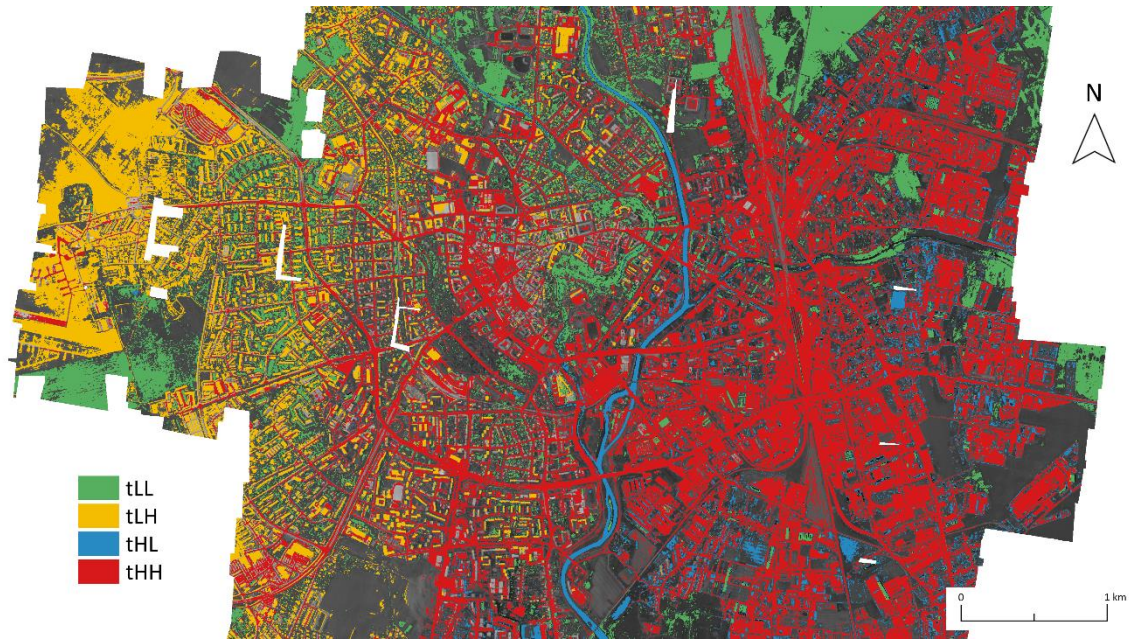


Fig. 6.5 Tertile typology visualized over afternoon thermal mosaic of Olomouc.

### 6.3.2 Quartile-based typology

Quartile-based typology is very similar to the one based on tertiles. In this case, the data threshold is placed at **25 %** of the temperature values distribution. Colour legend remains the same as in the previous example. In Table 6.2., there is the visualisation of the **coloured classes**.

Table 6.2 Quartile typology. Combinations of extreme (lowest or highest) tertiles are highlighted in colours. Empty areas are not used in the analysis.

| Quantiles<br>Typology |              | Afternoon Quartiles |    |    |              |
|-----------------------|--------------|---------------------|----|----|--------------|
|                       |              | Q1<br>(Low)         | Q2 | Q3 | Q4<br>(High) |
| Morning<br>Quartiles  | Q1<br>(Low)  | <b>qLL</b>          |    |    | <b>qLH</b>   |
|                       | Q2           |                     |    |    |              |
|                       | Q3           |                     |    |    |              |
|                       | Q4<br>(High) | <b>qHL</b>          |    |    | <b>qHH</b>   |

In many aspects, the **quartile-based typology** is like the **tertile-based** one. The image looks **clearer**, and it pinpoints only **extreme** values regarding the thermal regime types. Increasing the number of quantiles to quintiles, the number of coloured objects would further decrease.

The map of Quartile typology is shown in Figure 6.6. Regarding the *qLL* class, the classified areas of the **green belt** further decreased in favour of the **meadows** in the northern part of the area. The *qHL* class was also slightly decreased in size. The fields in the southern part are less visible now, and the Bystřice river to the east has almost vanished. *qLH* and *qHH* classes suffered a significant area loss, but their overall dominance is still present. The **west-east gradient** is still easily identifiable.

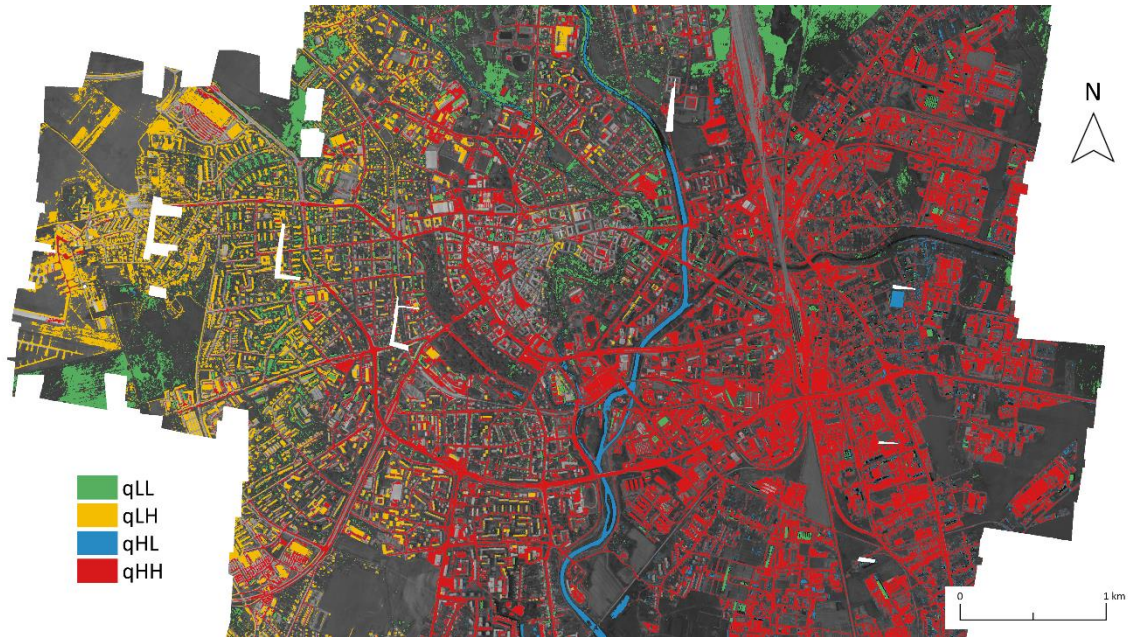


Figure 6.6 Quartile typology over afternoon thermal mosaic of Olomouc.

### 6.3.3 Quantile-based typology summary

To conclude, the typology based on quantiles shows **promising results** that can be interpreted as a **general trend**. For this area of interest, the quartile-based typology looked more promising as the image was more easily readable while still maintaining the information value. The method exploits the **heterogeneity** of the surface and the variability of the materials to explore extreme cases in temperature change throughout the day. For future studies, it is **highly recommended** to perform this analysis as it is not computation heavy or time demanding. It is also possible that for certain areas, other types of quantiles will prove useful, e.g. quintiles.

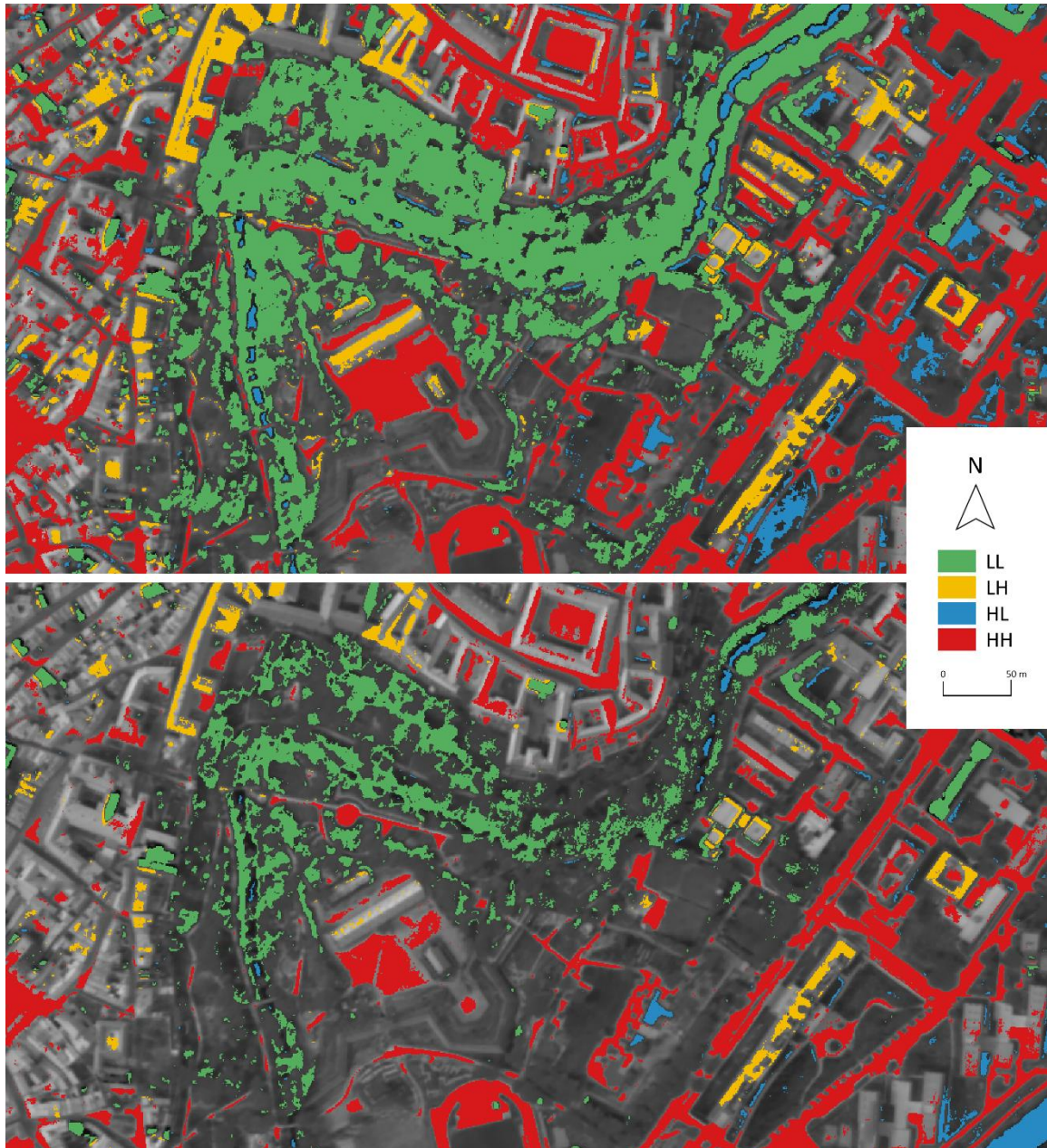


Figure 6.7 Visual comparison of Tertile typology (top) and Quartile typology (bottom).

In Figure 6.7, the **difference** between Tertile and Quartile typologies is shown. The key is to understand that these typologies are not supposed to serve as precise classifications but merely as an indicator of **interesting phenomena** in the city. Therefore, dense or sparse classification is not necessarily a downside. The user needs to choose what is better for a certain application. For **visualisation**, the sparse Quartile typology may be easy to read and thus better. On the other hand, if the image is read by an operator or analyst **in detail**, the dense Tertile typology will serve the purpose better.

## 7 DATA FUSION ANALYSES CARRIED OUT ON OLOMOUC THERMAL MOSAICS

The second chapter regarding analyses is focusing on the **external data source**. In this section, data from municipal government and open Europe-wide initiatives data are used to evaluate the surface temperature and the **thermal regime**. Moreover, Local Climate Zones are tested as a concept of comparison in both inter-city and intra-city approaches.

### 7.1 Investigation of temperatures on different vertical levels

Verticality is a very important factor in **urban climate research**. One of the crucial paradigms regarding the quality of life within the city and the effect of long-wave irradiation on **humans** is that people live in the streets, not on the rooftops. Having a small to medium resolution **thermal satellite images** provides us with information about the temperature of the city surface. However, these data tell us only a little about the inner structure of the city. In fact, the denser the city is, the stronger the UHI effect might appear in comparison to a **rural area**. This is caused mainly by materials used for rooftops. Another example of factors contributing to the temperature difference between the rooftop and ground level are **shadows** and **vegetation**. On the contrary, the rooftop level should not be affected by city canyons, upwelling radiation and should be ventilated much more effectively. In this chapter, **GIS tools** are used to investigate the various possible hypothesis.

#### 7.1.1 Description of buildings dataset and its corrections

The building dataset comes from the governmental **Registry of Territorial Identification, Addresses and Real Estate** (*ČÚZK - RÚIAN*, 2019). The system was fully established on 1<sup>st</sup> July 2012 and is since then serviced by **State Administration of Land Surveying and Cadastre** (*ČÚZK*). It is a Czech **national system** collecting data originally stored in multiple systems. The initial data that filled the system came from **Information System of the Cadastre of Real Estate** (ISKN), **Register of Census Districts and Buildings** (RSO), **Territorial Identification Registry of Addresses** (UIR-ADR), Database of Deliver Sites of Czech Post (DDM) and Registry of Municipal Symbols (REKOS). The system is freely accessible through various means such as **Public Remote Access** (VDP), Information System of Territorial Identification (ISÚI) or service *Atom* operated by ČÚZK. In this thesis, data were downloaded using ArcGIS plugin named VFR Import. The plugin was created by company **ARCDATA PRAHA**, and its basic version is available **free of charge**. The RÚIAN dataset consists of many different layers in many vector types. For

example, the layer of **built-up** objects used in this thesis is available as both point and multi-polygon layer. The dataset was significantly enhanced by Tuháček (2017). The database was corrected for some errors and filled with missing features resulting in a total of **18 627 building objects**. The height of the buildings was calculated based on the 5<sup>th</sup> Generation Digital Terrain Model of the Czech Republic (DMR 5G) and 1<sup>st</sup> Generation Digital Surface Model of the Czech Republic (DMP 1G). The **difference** of the models was added to the polygon layer **attribute table**.

There were multiple errors that forbid the immediate use of the data. These obstacles come from the specifics of the **airborne campaign** and the **RÚIAN data**. The RÚIAN data contain information only about the building **footprint**; therefore, in some cases, it does not precisely represent the **rooftop** layer. Another problem was the quality of the mosaic. The spatial accuracy of the mosaicking process was very bad in certain parts of the image due to multiple issues within the processing chain. This caused **significant offset**, especially in the western part of the image. Furthermore, the image suffers heavily from the **skewing effect of tall buildings**, which creates **offset** (Figure 7.1) increasing with building height. For these reasons, the dataset was **manually edited**, and the offset was adjusted to the afternoon thermal mosaic. Some buildings had to be **manually added** because they were either still missing from RÚIAN dataset due to **outdated information** or are not supposed to be part of it all.

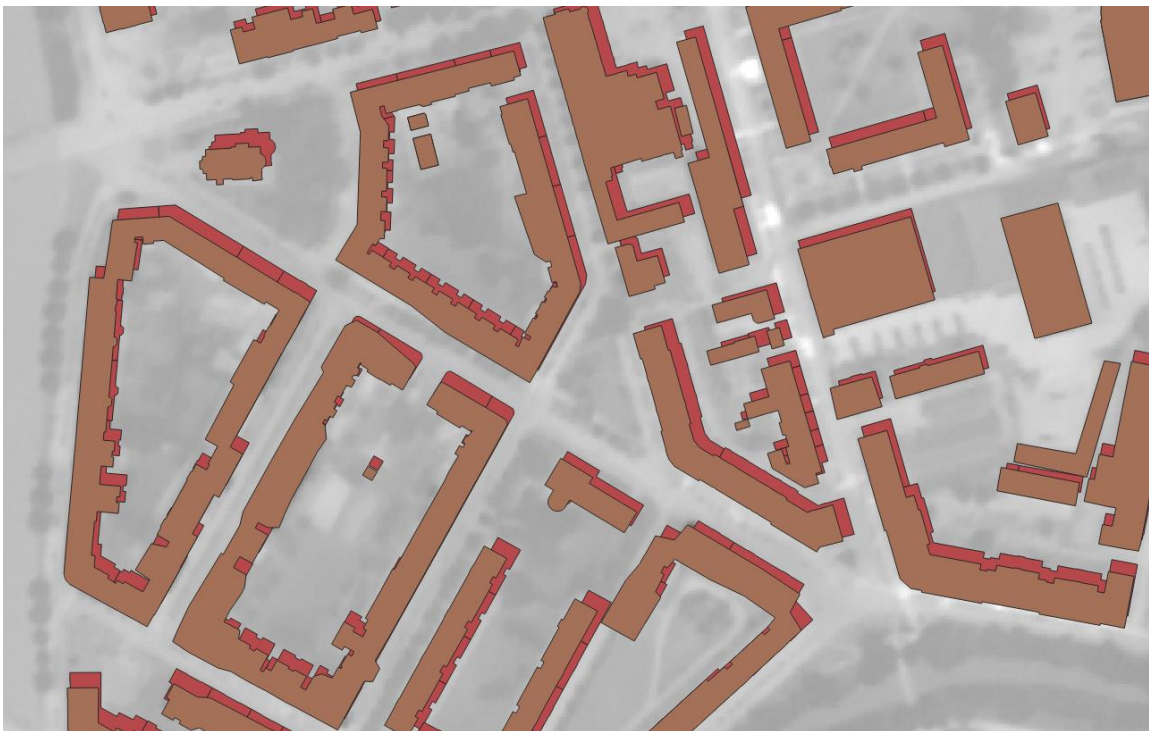


Figure 7.1 The difference before and after the manual location adjustment. The original dataset is visualized in red, the corrected data in brown.

### 7.1.2 Ground-rooftop and verticality analyses results

Regarding the difference between ground and rooftop height levels, the results show a very significant difference (Figure 7.2). In the morning, most of the materials share similar temperature around 17.5 °C because of the night cooling effect. In the afternoon, however, the rooftop level shows a drastic increase of 18.44 °C in comparison to ground level 12.62 °C. To summarize, within the observed timeframe, rooftop materials heated up on average 46 % more than ground level materials. These results prove the high importance of very high-resolution or down-scaled data providing context for city surface temperature.

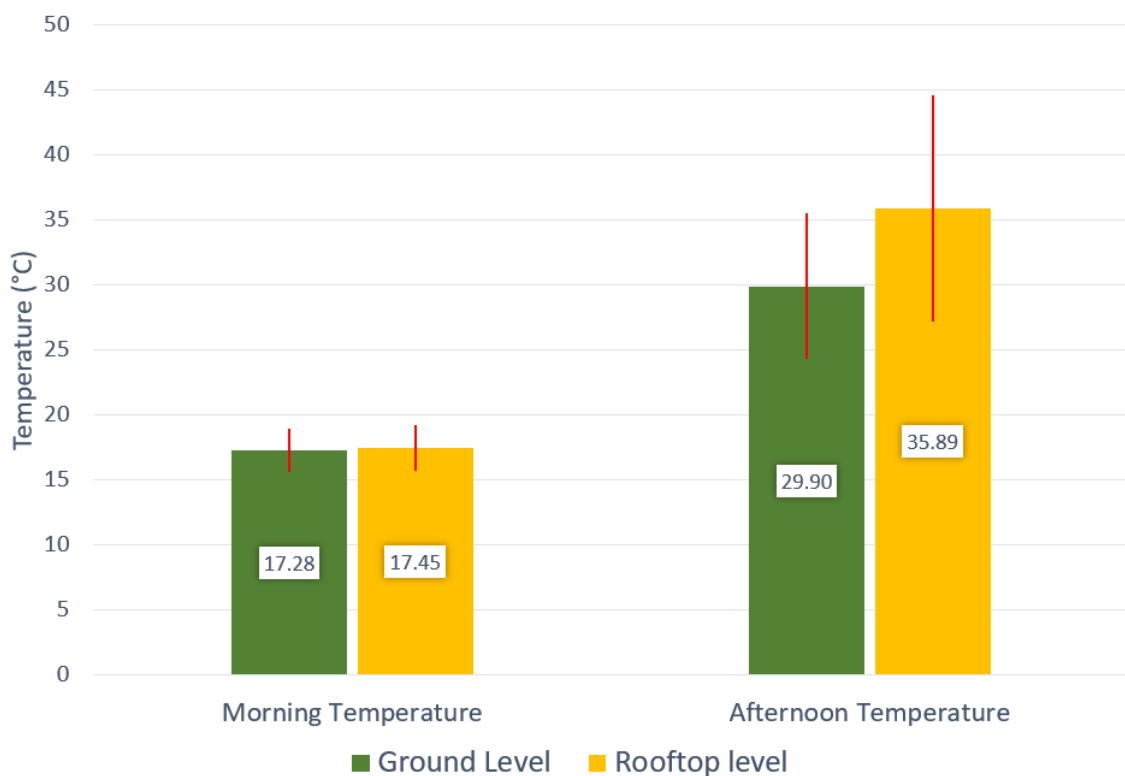


Figure 7.2 Comparison of temperature means on different vertical levels. Red line shows the standard deviation of the datasets.

The second hypothesis regarded the connection between roof temperature and the building height. There are multiple characteristics that affect the air temperature in higher urban levels and the actual temperature of the material. In general, the temperature should be lower due to better ventilation and lower air temperature tied to a higher altitude. There are many other factors tied to the measured material. Besides the material type, the temperature is also affected by the age of the material, corrosion or kind of other damage, temporal cover such as moss or other vegetation, and so on. The question asked was whether the correlation between the material

temperature and the height is significant. The original dataset of more than 15 000 building objects was filtered to be more easily visualized. The outliers were removed first, especially buildings errors such as with negative height. After that, the buildings with missing temperature or height parameter were removed. In the last step, all buildings below 10 m of height were removed. Most of these buildings were outdoor garages, various shacks, temporary buildings and others. The remaining approximately 5000 buildings were analysed and visualized (Figures 7.3 and 7.4).

In both graphs, the values for tallest buildings are cut off for better visibility. However, those values were included in the calculation. In the afternoon dataset (Figure 7.3), where there is a larger contrast between various materials, the correlation coefficient of 0.06 has been calculated. Most of the buildings are between 10 and 15 m height at around 35° C radiometric surface temperature. There is also a cluster around 27 m height with a similar distribution of temperature. Moreover, linear regression (visualised as red line) shows no visible trend in the data. Even from visual comparison, the elevated rooftops in the right part of the graph have no visible increase or decrease in temperature.

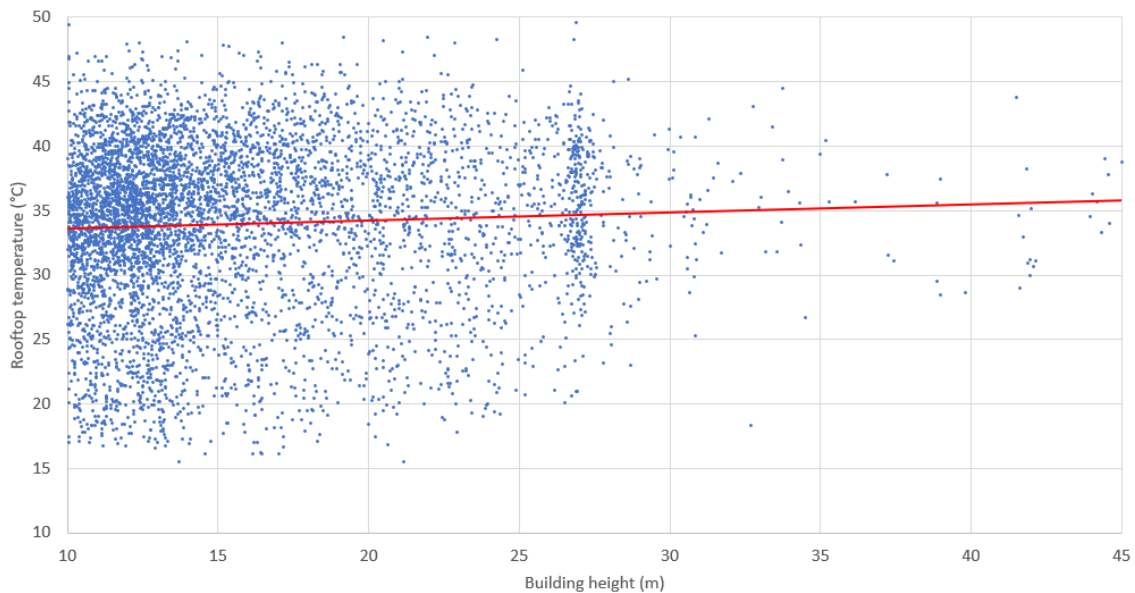


Figure 7.3 Afternoon rooftop surface temperature at different building height levels. Each blue dot represents a rooftop and its mean afternoon temperature. Regression (trend) is visualized as a red line.

The morning dataset shows much larger **consistency** (and less contrast) of temperatures due to **night-time cooling** effect, and thus it was less probable to find any clear trend in the dataset. The correlation coefficient of the two variables equals -0.05. The distribution of building heights is the same as in the previous figure. It is apparent,



however, that most of the temperature values are in the lower part of the graph. It is also worth noting that the y-axis of the graph has **spacing** 1° C while in Figure 7.3, it was 5° C per division. In combination with the **linear regression**, there is no clear connection between the building height and the rooftop temperature.

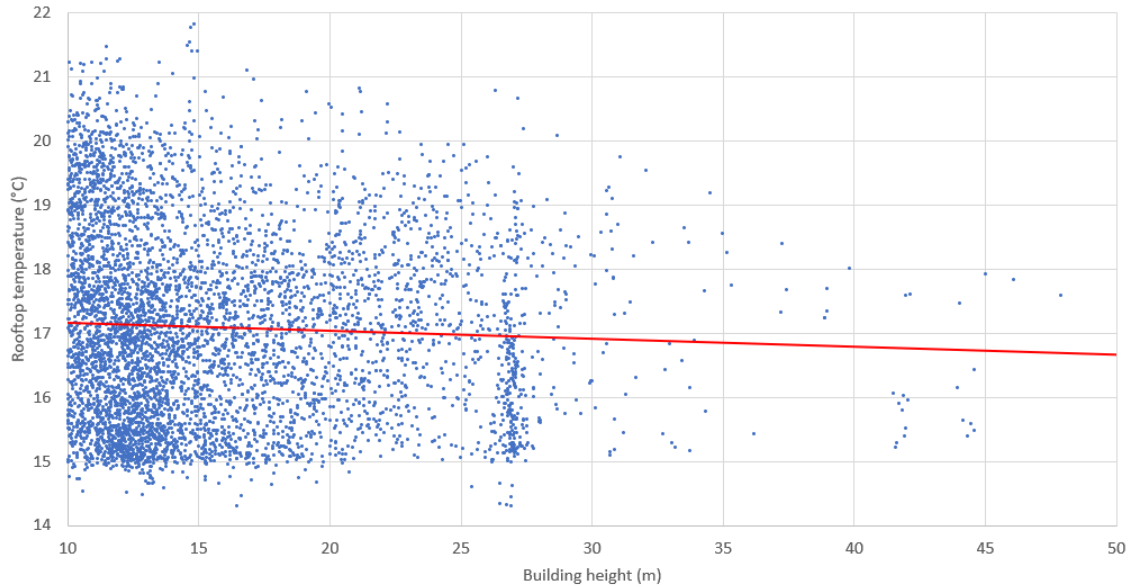


Figure 7.4 Morning rooftop surface temperature at different building height levels. Each blue dot represents a rooftop and its mean morning temperature. Regression (trend) is visualized as a red line.

In conclusion, the height attribute does **not** have any clear **impact** on the rooftop material temperature using this data and method. While there possibly is some impact, the **other attributes** affecting the temperature are probably much more significant for the measurement. For further investigation, it would be beneficial to use **auxiliary data** regarding rooftop material, its age, rooftop inclination and shape and other characteristics.

## 7.2 Local Climate Zones as the basis for zonal analysis

The principle of **Local Climate Zones** (LCZ) was firstly presented by Stewart, Oke (2012). LCZs are supposed to be the answer for **urban statistical analysis** as they set a **basic unit of comparison**. From the point of climatology, LCZs are relatively **homogeneous areas** (neighbourhoods) about 4 km<sup>2</sup> large. They are classified based on their structural characteristics, which are discussed later in this section. The main strength of LCZs is the possibility of comparing similar data from different regions and creating metadata information for climate data.

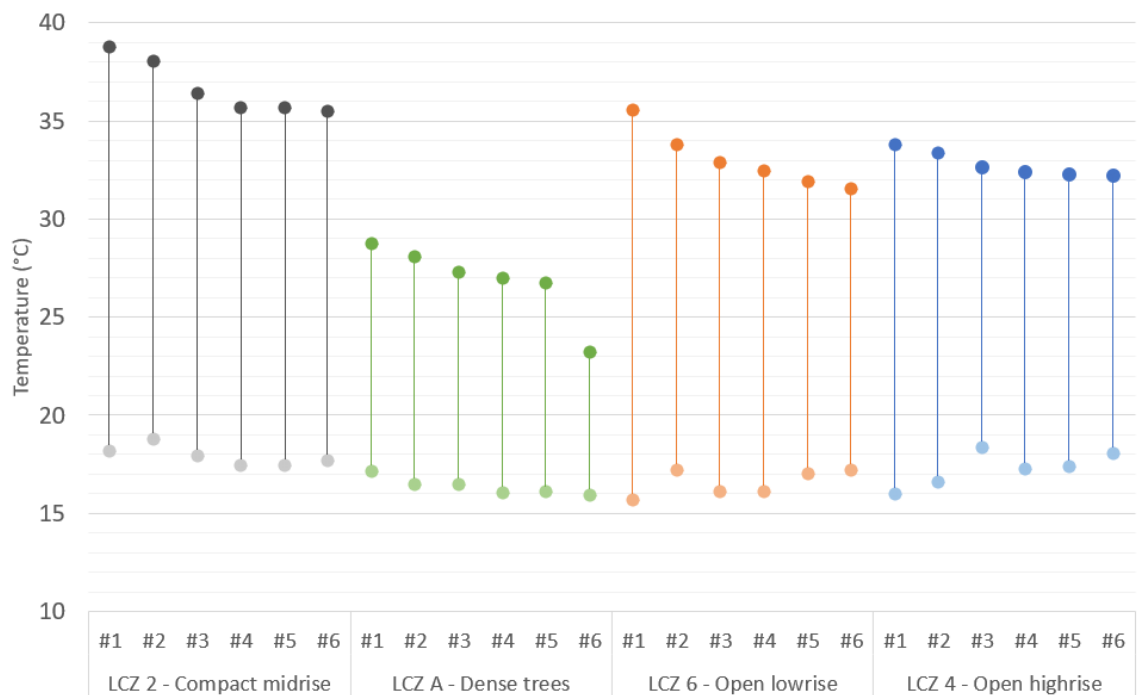


Figure 7.5 Preliminary results of LCZ analysis. Brighter colours stand for the morning temperature; darker colours stand for the afternoon temperature. The samples within the class are sorted ascending by the afternoon temperature.

As a **pilot study** (Figure 7.5), four types of LCZs were manually digitised within the city of Olomouc. Compact midrise LCZ2 is represented by city centre with **narrow streets** and low sky view factor. **City parks** and surrounding forest patches were classified as LCZA – dense (or close-set) trees. **Early 20th century villas** with a high amount of vegetation in between the buildings were classified as open low-rise (LCZ6), and **socialist-era apartment buildings** were classified as open high-rise (LCZ4). **Six neighbourhoods** were chosen for each class to compare not only their sole characteristics but also intra-city behaviour.

LCZ4 is showing very similar behaviour in different parts of the city because of the unified structure of unified construction pattern. LCZ2 is showing some difference, which is probably caused by street and **rooftop orientation**. The samples for LCZA were city parks as well as a forest in the surrounding of the city, showing the largest difference in temperature. LCZ6 showed some differences, especially in morning temperatures. Within this class, the actual share of **vegetation** plays a crucial role, and the class itself shows the largest variation in **vegetation type, structure and building type**.

### The second sampling

Classification of LCZs is based on **several characteristics** as described by Stewart, Oke (2012). The key characteristics are:

- Sky View Factor (SVF)
- Built-up area fraction
- Vegetation fraction
- Impervious surface fraction

The original plan of this thesis was to create a **semi-automatic classification** based on these characteristics similar to Geletič, Lehnert (2016) and Lehnert et al. (2015). The problem was with the data sources. **Sky View Factor** is best calculated from Digital Surface Model (DSM), and while the LiDAR-based DSM 1G (1<sup>st</sup> generation) for the Czech Republic was available, the **spatial resolution** turned out to be problematic. Specifically, the narrow streets in the city centre were **not recognisable**. It would also be needed to distinguish between ground and rooftop/tree canopy layers.

On the other hand, the **built-up area fraction** was easily and precisely calculated from existing data. **Vegetation** was calculated based on **NDVI** from **Sentinel-2** satellite, which turned out to be rather inaccurate. The impervious surfaces could have been calculated as a combination of pavements layer, built-up area and polygon street network.

To conclude, it was decided that also the **second sampling** is to be collected **manually**. Much larger patches of the surface were digitised covering nearly the entire area of the city. **47 LCZs** were identified; eight were not classified as they had very specific land-use/land-cover mixture and could not be classified easily. One of the examples is the area around **football stadium** which contains an outdoor swimming pool, three football fields with tribunes, several tennis courts, some low-rise and mid-rise buildings as well as multiple high-rise hotels. Following the LCZ methodology, the climatic characteristic of this area is unclear.

After the LCZs were identified, some **basic characteristics** were calculated. At first, the **vegetation fraction** calculated from **Sentinel-2 NDVI** index is shown in Figure 7.6. The most obvious feature of the diagram is more than 60 % vegetation fraction for LCZA, which stands for the *Dense trees* class. Some vegetation is also along the rivers (class LCZG). There is a lack of vegetation in industrial areas (LCZ8) and dense mid-rise class (LCZ2) in the historical city centre. Among the residential LCZs, the LCZ6 (open low-rise) has the highest vegetation fraction while LCZ4 (open high-rise) and LCZ5 (open mid-rise) have on average lower values. It is also valuable to point out that the vegetation fraction is more tied towards a certain location than to an LCZ type with only the LCZ6 being an exception.

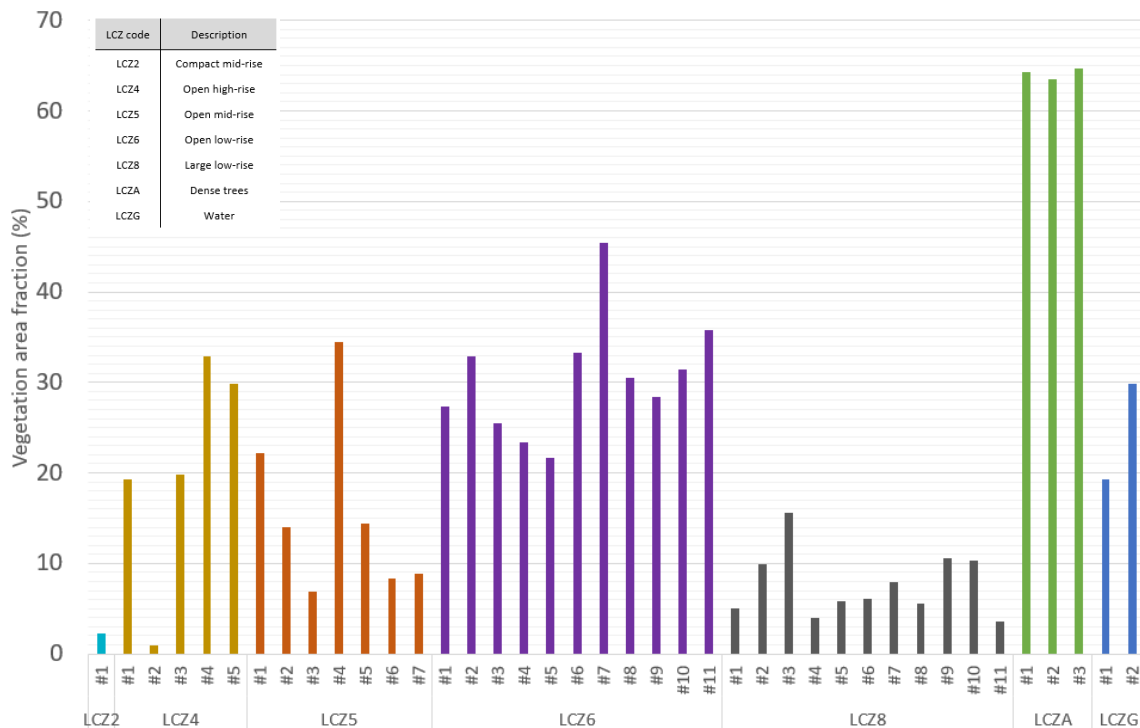


Figure 7.6 Vegetation fraction in various Local Climate Zones in Olomouc. LCZs within the class type are sorted by a built-up fraction (see Figure 6.7).

The second characteristic measured on LCZ level was **built-up area fraction** visualised in Figure 7.7. The highest built-up area fraction has the most compact class (LCZ2). It is interesting that open mid-rise (LCZ5) has on average higher building fraction than open high-rise (LCZ4). Towards LCZ6 (open low-rise) the trend of decreasing building fraction is visible. Industrial areas (LCZ8) have surprisingly high building density while dense trees (LCZA) and water bodies (LCZG) have almost no buildings in their area.

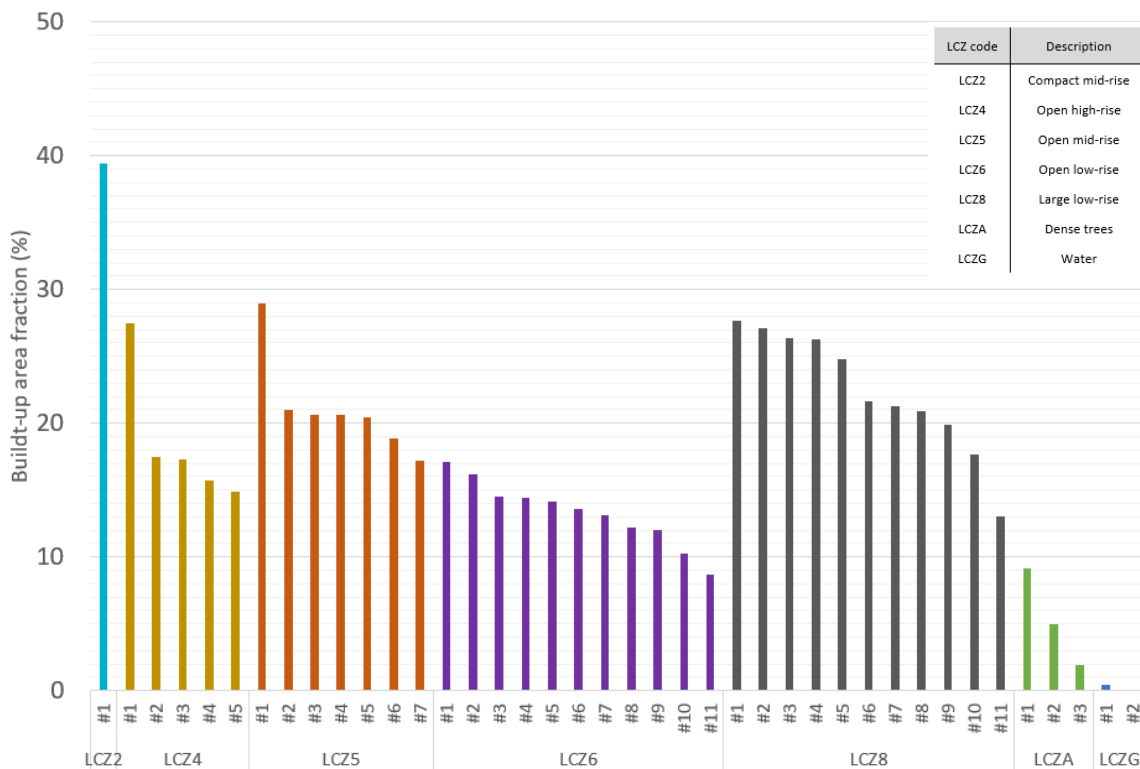


Figure 7.7 Built-up area fraction in LCZs in Olomouc. LCZs within the class type are sorted by built-up area fraction.

The final Figure 7.8 regarding **vegetation** and **building** fractions combines these two characteristics and complements them with the *other* category, which is calculated only for **visualisation** purposes. The main purpose of this diagram is to put emphasis on the **relationship** between vegetation and built-up areas. For example, in LCZ6 (open low-rise) it is clearly identifiable that most of the areas do have **twice** as much vegetation as buildings. Even though the large open high-rise areas from the socialist area do usually have a **playground** for kids and smaller patches of **grass** or **parks**, in the statistics, these are clearly **underrepresented** within the class. Only LCZ4 areas #4 and #5 show better **vegetation to building ratio**.

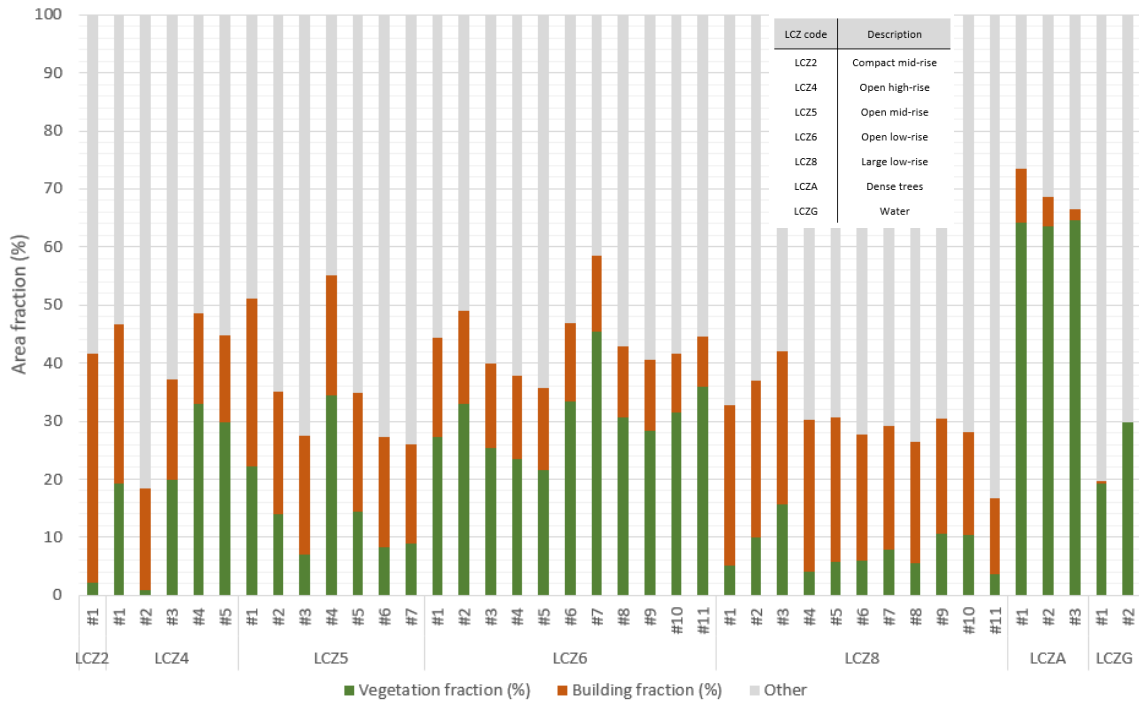


Figure 7.8 LCZs characteristics based on the vegetation and building fractions complemented to 100 % by the class *other*.

The most important part of this analysis is its relation to the **surface temperature**. In Figure 7.9, the temperature of different LCZs is shown. For easier interpretation, vertical lines visualising **temperature change** between the morning and the afternoon temperatures are used. Moreover, horizontal blue dashed lines are representing the **mean** morning (light blue) and afternoon (dark blue) temperature within certain LCZ type for easier visual comparison of the LCZ types as they have large variability. Open low-rise (LCZ6) seems to be the best area in terms of temperature regime among residential areas. It is important to emphasise that the **average surface temperature** of the other residential zones (LC22, LC24, and LC25) is the same or higher than the temperature of industrial areas (LC28).

To summarise, the LCZ methodology is a **viable and interesting** option in urban climatology research. It is important to improve semi-automatic and automatic approaches of their **classification** as well as carefully choosing the input data. It might be beneficial to connect the methodology with **object-based image analysis (OBIA)**, **segmentation** and other technologies.

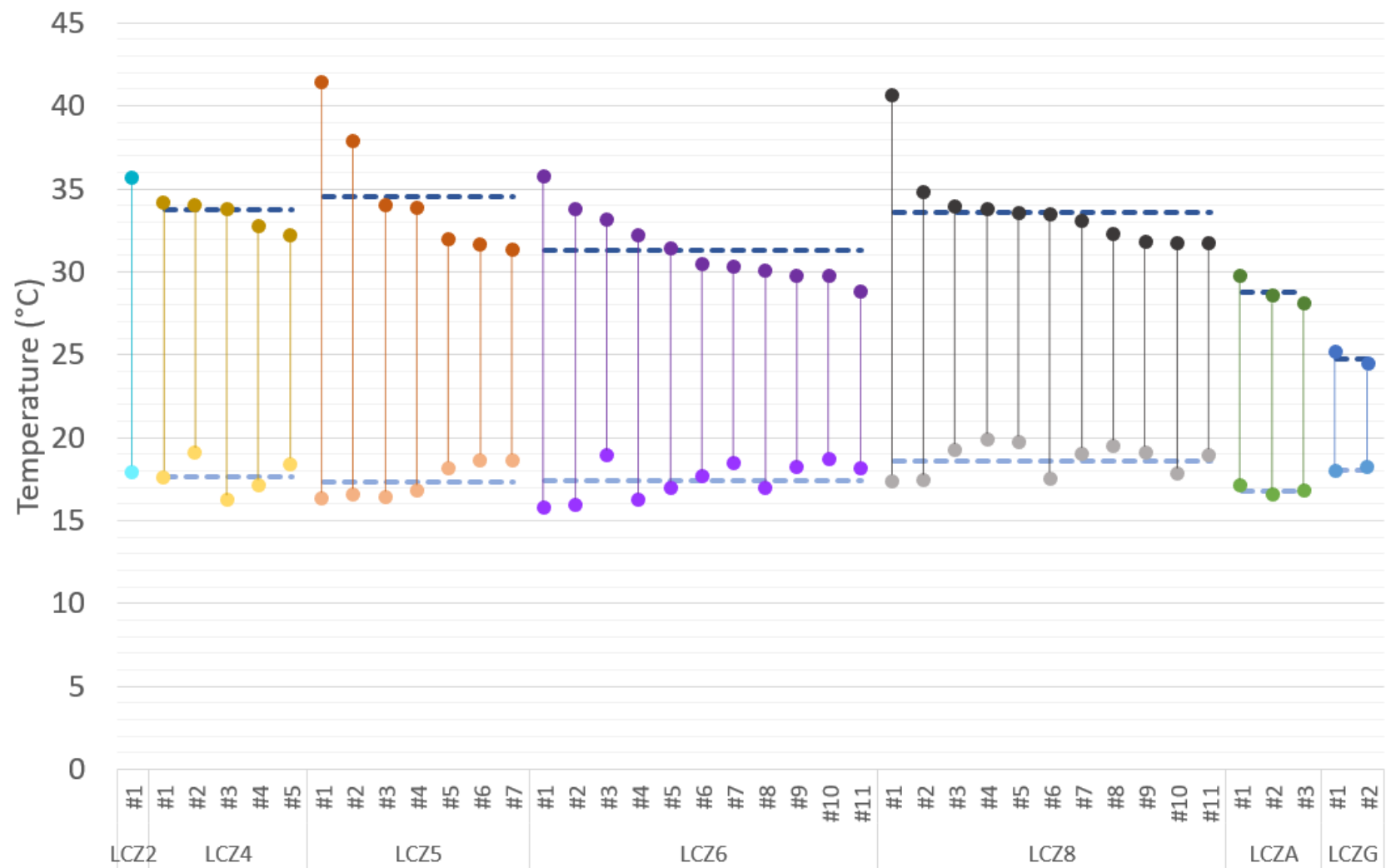


Figure 7.9 Temperature regime of various LCZs. The lighter colours implicate the morning temperature; the darker colours stand for the afternoon temperature. The dashed line shows averages of the LCZ classes for both morning and afternoon temperatures.

## 7.3 Temperature evaluation based on open data

European programme **Copernicus** offers several products that are very valuable to urban research. **Copernicus services** can be divided into three categories. These are **global datasets**, **pan-European datasets** and **local datasets**. Global datasets are mostly focused on observation of the whole system of the **Earth**. These datasets are aiming at the **monitoring of energy** and water cycles, vegetation or cryosphere. All these products are tied to Copernicus' main goal – the monitoring of global **climate change**. Because the global datasets focus on the global scale, their resolution is very coarse, and these datasets are not suitable for city-scale analysis.

Another group of products cover **pan-European datasets**. There is a total of three products: CORINE Land Cover (CLC), High-Resolution Layers (HRL) and European Settlement Map (ESM). ESM 2012 is a **percentage built-up area** coverage layer that is based on a machine learning algorithm. It has a decent resolution of 2.5 m per pixel, but it wouldn't be used in this study because there are more accurate and precise data provided from the **local authority**, and the ESM 2012 was not up to date. The similar dataset is HRL, which contains the imperviousness of the surface over the whole of Europe. The HRL dataset does have a slightly better **time resolution**, but the significantly worse **spatial resolution** of 20 m. Other product families included in HRL are regarding forests, grassland and water bodies. From these datasets, **CORINE Land Cover** was chosen for further analysis. CLC has a very good temporal resolution, decent spatial resolution and is very well produced and documented. Its characteristics are described in detail in Chapter 4.5.2.

The final group of datasets called 'local' consists of three projects. **Natura 2000** and **Riparian Zones** are focused on vegetation and biological activity and therefore not suitable for analysis of a city. However, the final dataset, called **Urban Atlas**, is very valuable and will be further analysed. For a dataset covering all European cities, UA 2012 is very detailed, accurate and precise. Its history and structure are further described in the following chapter.

### 7.3.1 Urban Atlas 2012

Urban Atlas (UA; *Urban Atlas — Copernicus Land Monitoring Service*, 2019) is a tremendously unique dataset. It is a Europe-wide mapping service under European Space Agency **Copernicus programme** monitoring the land-use and land-cover changes over Large Urban Zones (LUZ). For the year 2006, there were 319 LUZs defined for the analysis, including cities with **more than 100 000 inhabitants**. In the year 2012, the number grew to 785 cities including EU28, EFTA and West Balkan countries and Turkey.



The dataset is limited by minimal mapping unit (MMU). The MMU for 17 urban classes is 0.25 ha, while for 10 rural classes the **MMU is 1 ha**. The methodology consists of Earth Observation (EO) data interpretation enhanced by topographic maps and auxiliary information, including local expertise.

Moreover, the dataset also contains several **sub-products**; namely change detection between 2006 and 2012 (*Copernicus Land Monitoring Service - Urban Atlas — European Environment Agency 2018*), Street Tree Layer (STL), building heights (2012 dataset only) and population estimates. However, these **auxiliary data** are provided only for some cities as the coverage changed between the years. All these datasets are accessible after free registration at **Copernicus Land Monitoring Service** webpage ([land.copernicus.eu](http://land.copernicus.eu)). Currently, UA 2012 covers **15 Czech cities** with almost a third of the total country population (Table 7.1).

Table 7.1 Czech cities included in 2012 UA dataset. All cities except those highlighted in orange are also accessible in 2006 UA dataset.

| City             | Population<br>(in thousands) | Download size<br>(in MB) |
|------------------|------------------------------|--------------------------|
| Praha            | 1295                         | 159.9                    |
| Brno             | 379                          | 61.4                     |
| Ostrava          | 290                          | 58.2                     |
| Plzeň            | 170                          | 52.3                     |
| Liberec          | 104                          | 26.7                     |
| Olomouc          | 100                          | 28.1                     |
| České Budějovice | 94                           | 40.2                     |
| Ústí nad Labem   | 93                           | 19.6                     |
| Hradec Králové   | 93                           | 27.0                     |
| Pardubice        | 90                           | 32.0                     |
| Zlín             | 75                           | 24.7                     |
| Chomutov-Jirkov  | 68                           | 20.9                     |
| Most             | 67                           | 18.5                     |
| Jihlava          | 51                           | 39.0                     |
| Karlovy Vary     | 49                           | 23.4                     |
| <b>Total</b>     | <b>3018</b>                  | <b>631.9</b>             |

**UA 2012** dataset features **21 classes** in the city of Olomouc, which are represented by a 5-digit code. Three of these classes contain 67 % of the area. These are 21000 – **Arable land** (28 %), 12100 – **Industrial, commercial, public, military and private units** (21 %) and 11100 – **Continuous urban fabric** (18 %). Nine of the classes are heavily under-represented, having **less than 1 %** of the total area. These classes are summarized as *other* in Figure 7.10 and visualised as **outlines** in 7.11. Even though they have a small size, some of them are still notable in **logical analysis**. Especially 12400 – Airports and 12210 – Fast transit roads cannot be excluded from the overall picture.

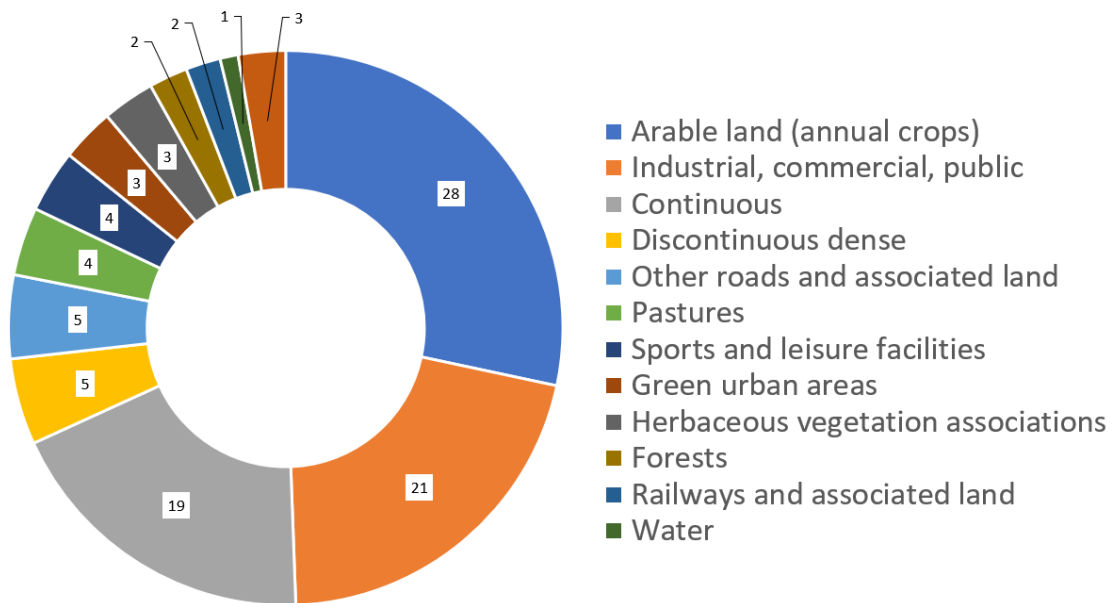


Figure 7.10 Percentage of class representation in UA 2012 for the city of Olomouc

The mean temperatures read from the afternoon and morning datasets are visualized in Figure 7.11. Morning average temperatures range approximately between 15 and 20 °C while afternoon means range from 23 to 35 °C. The **Land-use/Land-cover (LULC)** categories are sorted by the **ID number** and their respective super-categories. Water shows the typical behaviour of a material with high **thermal inertia** having the second highest morning temperature of 18.21 °C while having significantly lowest afternoon temperature of only 23 °C. There is a potential threshold between natural and artificial materials at 30 °C. Classes 1.4, 2, 3, and 5 have mean afternoon temperature under 30 °C while all artificial classes 1.1, 1.2, and 1.3 have mean over 30 °C.

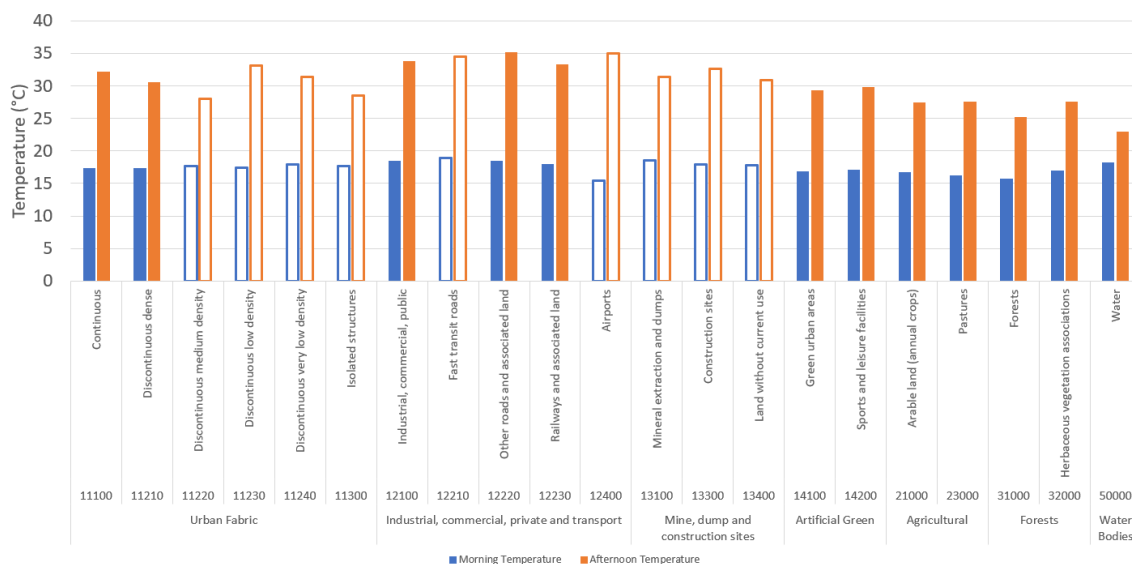


Figure 7.11 Morning and afternoon temperature of Urban Atlas 2012 classes in the city of Olomouc. Classes visualized as outlines are under-represented in the dataset. Their area is lower than 1 % of the total area.

### 7.3.2 CORINE Land Cover 2018

**CORINE Land Cover** (CLC; *CORINE Land Cover — Copernicus Land Monitoring Service*, 2019) is another great and ambitious source of data. The creation of this dataset was initiated in **1985** for the first reference year 1990. Since then, four more datasets (2000, 2006, 2012 and 2018) were created. CLC classification consists of **44 classes** with minimal mapping unit of **25 ha** for areal and **100 m** minimal width for **linear phenomena**. The dataset is produced by most countries by visual interpretation of high-resolution satellite imagery (*Home :: Corine Land Cover classes 2019*). The production time of the dataset was reduced from **10 years** (1990) to just about **1 year** (2018). The **number of countries** was also increased from the original 26 to 39 in the latest dataset. CLC 2018 has the same overlay and access for download as **Urban Atlas**, requiring only free registration. It is available for the whole **39 countries** as 100 m resolution GeoTiff (under 200 MB), SQLite Database (3.3 GB) or ESRI Geodatabase (1.7 GB). Along with the datasets from mentioned years, CLC contains also LULC change data labelled as “CHA” in the file structure. These **change datasets** are generated for every two following datasets, e.g. 2006-2012.

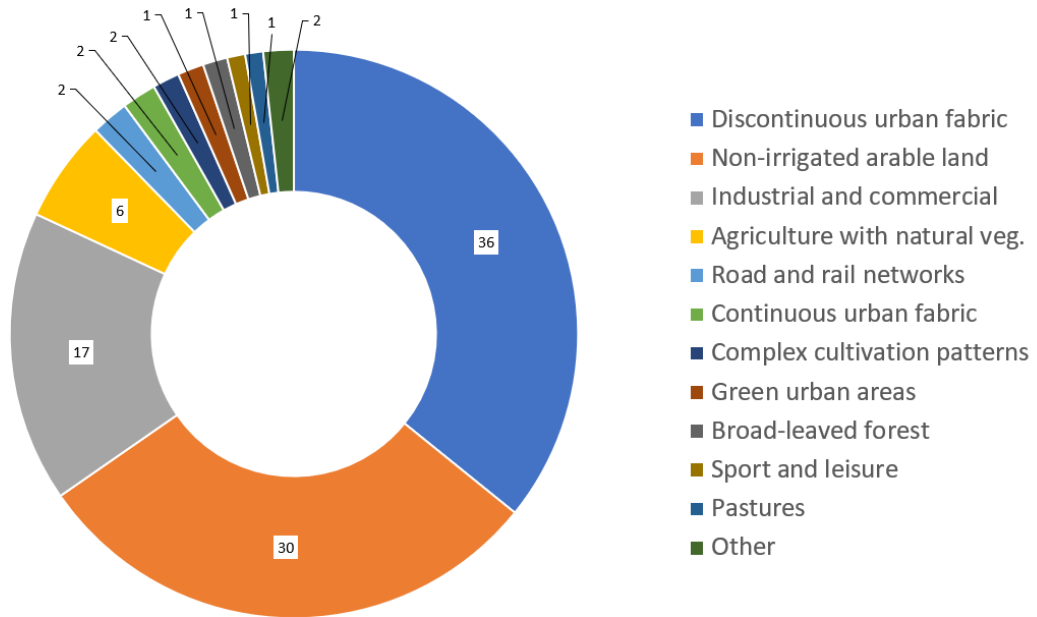


Figure 7.12 Percentage of class representation in CLC 2018 for the city of Olomouc

The CLC 2018 dataset for the city of Olomouc consists of **14 classes**. Three of the classes add up to **80 %** of the whole area (Figure 7.12). These are 112 – Discontinuous urban fabric (35 %), 211 – Non-irrigated arable land (29 %) and 121 – Industrial and commercial (16 %).

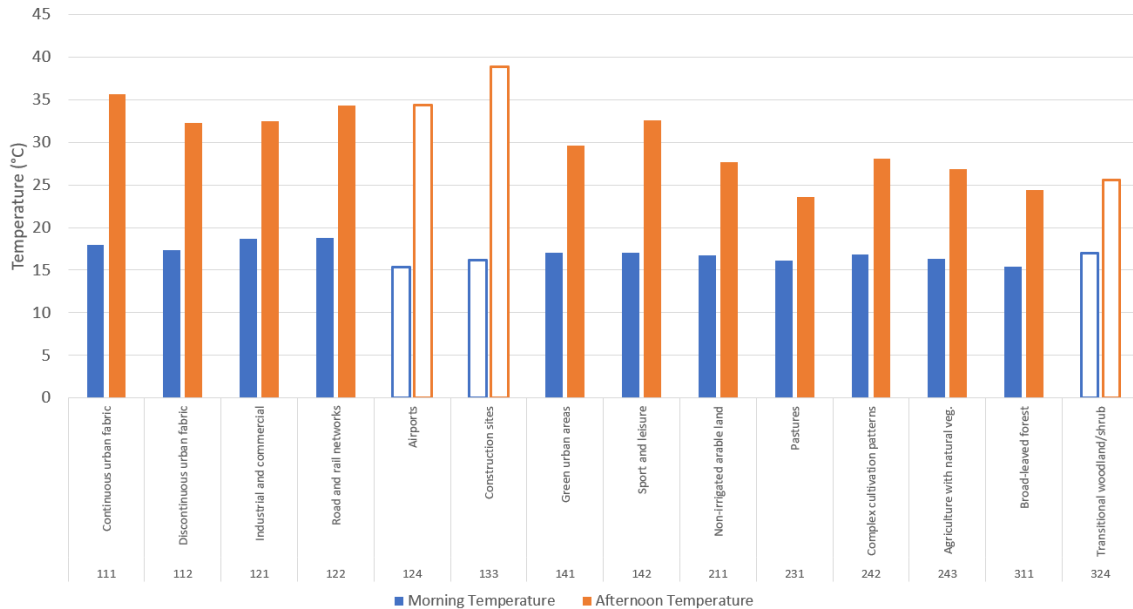


Figure 7.13 Morning and afternoon temperature of CORINE Land Cover 2018 classes in the city of Olomouc. Classes visualized as outlines are under-represented in the dataset. Their area is lower than 1 % of the total area.

Three of the classes were **under-represented**, specifically Airports (code 124), Construction sites (code 133) and Transitional woodland and shrub (code 324). These classes have under 1 % of the total area, are summed up into the class *other* in Figure 6.12 and are visualised only as an outline in Figure 7.13.

The highest afternoon surface temperature was measured on construction sites (class 133) followed by airports (124), continuous urban fabric (111) and road and railway networks (122). An interesting fact is that airport class is among the hottest in the afternoon but has very good **cooling capability** during the night resulting in low morning temperature. This is most probably caused by the **elevated position** of the airport combined with its open space providing great **ventilation**.

Traditionally, **natural surface** classes account for the lowest afternoon temperature, broad-leaved forest (311) and pastures (231) heating up to less than 25° C. Surprisingly high are the green urban areas (141) having average afternoon surface temperature of almost 30° C. The reason here is probably coarse spatial resolution of the CLC dataset, so the green urban area class consists also of surrounding streets and buildings neighbouring the actual parks.

## 8 RESULTS

The main objective of the thesis was to **investigate and improve airborne thermal remote sensing in urban climate research**. Based on the objective, three sub-objectives were defined.

### Airborne thermal data acquisition

The first sub-objective was to **acquire and process a series of thermal datasets of the city of Olomouc for urban environment research**. Based on this assignment, a flight campaign over the city of Olomouc was planned and carried out (described in Chapter 5.1). After that, the image processing (Chapter 5.2) including radiometric processing (Chapter 5.2.1), atmospheric corrections (Chapter 5.2.2) and emissivity corrections (Chapter 5.2.3) were performed. The set of corrected **single images** is attached as **Appendix 1**. In the final step, the photogrammetric processing (Chapter 5.3) including georeferencing, orthorectification and mosaicking was performed. This resulted in **two raster images** containing the information about the morning and the afternoon **radiant surface temperature** in Olomouc. The data are attached in **Appendix 2**.

### Descriptive analyses carried out on thermal mosaics of Olomouc

The second sub-objective was to investigate possibilities of **sampling, typology** and **classification** methods on the Olomouc thermal mosaics.

In the first study, a descriptive method of point sampling was carried out. The method is described in Chapter 6.1 and focuses primarily on the distinction between **natural** and **artificial** materials and their thermal regime, e.g. the **relationship** between the morning and the afternoon radiant surface temperatures. In the **preliminary study**, rooftop, street and natural materials, land-cover and land-use types were examined. The study was followed up by the **second sampling**, which focused more on specific material types. In the second sampling, only known road and natural materials were included as well as different water bodies in the city. The results of the analysis are shown in Figure 6.2. In the figure, the **dramatic difference** between **artificial** and **natural** material behaviour is visible. Moreover, the diagram shows very interesting properties of various **water bodies** that are described in Chapter 6.1. The data, as well as the full resolution graphs, are attached as **Appendix 3**.

In the second study, the **TURN** method was applied to investigate the spatial distribution of microclimatic influence on **asphalt concrete road material** temperature. (Chapter 6.2) The method was originally proposed to subtract the microclimatic effect

from the thermal mosaic but might serve as well as a stand-alone **microclimatic indicator**. The results of the method are visualised in Figures 6.3 and 6.4. Moreover, a **composite image** combining the morning and the afternoon datasets is shown in Figure 6.5. The source data are attached in **Appendix 4**.

The third study is based on quantile-based typology, specifically tertile-based and quartile-based typologies. In this method, firstly the breakpoints – the **tertiles** and the **quartiles** – were identified. After that, the classification was carried out according to Tables 6.1 and 6.2, respectively. The **proposed classes** are named according to the combination of quantiles used. The results of this method are shown in Figures 6.5 and 6.6 with **detailed comparison** in Figure 6.7. The layers are included in **Appendix 5**.

### Data fusion analyses carried out on thermal mosaics of Olomouc

The third sub-objective was to research possible methods of **data fusion** and sampling using **external datasets**. Three methods were carried out to meet this goal.

The first method, described in Chapter 7.1, combines the **buildings layer** from Czech governmental system **RÚIAN** and the **Digital Surface Model (DSM)**. Firstly, the data had to be manually adjusted because of slight spatial distortion caused by the mosaicking. After that, two vertical levels – **ground and rooftop** – were identified and evaluated. This analysis (Figure 7.2) confirmed an important factor that is often not considered; that the **rooftop level is heating up much more than the ground**, more than 5° C on average. This is very important when evaluating the heat comfort of the citizen who naturally spends more time near the ground than on elevated structures. Furthermore, there was a possibility of investigating the relationship between building height and its rooftop temperature. **Regression analysis** was performed but showed **no clear trend** regarding this topic. (Figures 7.3 and 7.4) The data regarding building height and building rooftop temperature are attached as **Appendix 6**. The original data, as well as the full resolution graphs, are attached as **Appendix 3**.

The second method was based on **Local Climate Zone (LCZ)** methodology. (Chapter 7.2) In the preliminary study, 24 LCZs were identified based on visual recognition and knowledge of the city structure. The results of the **pilot study** are shown in Figure 7.5. After that, a second LCZ identification was performed. Due to **unfitting auxiliary data**, it wasn't possible to identify the LCZs according to the official methodology and characteristics. Therefore, the second study was also based on manual recognition as well as **auxiliary information** about **building height** and **location**. 47 LCZs were identified, and eight were removed from the analysis as there was no certainty of their fitting class. The remaining **39 LCZs** were analysed for **vegetation fraction** (Figure 7.6), **building fraction** (Figure 7.7), their combination (Figure 7.8) and

**the temperature regime** (Figure 7.9). The data, as well as the full resolution graphs, are attached as **Appendix 3**. This study proved LCZs being a **valid option** for evaluation of the city's surface temperature and its regime.

The third method was focusing on **European-wide datasets** that can be beneficial for nation-wide or Europe-wide **comparison** (Chapter 7.3). The chosen datasets are **Urban Atlas** (UA), and **CORINE Land Cover** (CLC) analysed in Chapters 7.3.1 and 7.3.2, respectively. In the first step, the datasets were described, and the **class coverage** in the area of interest was investigated (Figures 7.10 and 7.12). The results for both the morning and the afternoon **radiant surface temperature** are visualised in Figure 7.11 and 7.13 and attached along with the full resolution graphs as **Appendix 3**. This method showed the thermal regime of classes found **all over Europe** with the possibility of **immediate comparison** to similar classes in different areas in Europe.



## 9 DISCUSSION

During the work, some **challenges** and problems were encountered. While most of them were **solved**, there are still some methods that should be improved for further and possibly **long-term research**. Recommendations for similar projects or follow-up research is also mentioned in this chapter. The topics discussed are mentioned in **chronological order**.

### Flight campaign and data processing

It was rather difficult to predict all possible issues during the thermal airborne campaign without previous experience. A laboratory testing prior to the flight was performed on both cameras, which resulted in **satisfactory results**. The flight was planned based on **previous experience** with optical sensors.

One of the greatest issues was the combination of **long image acquisition time** on the thermal sensor, low altitude and wind turbulences during the flight. The high image acquisition time resulted in **low vertical layover**, which was sufficient in the end, but very low aeroplane speed was required. The low altitude was required in order to get the best spatial resolution possible. However, this resulted in very low horizontal layover that was on the **edge of being viable**. The Cessna aeroplane is **very light**, and the time of exposure is relatively high on the thermal sensor, which resulted in many images being blurry due to several turbulences. In combination with a low horizontal layover, this caused some **gaps** in the final mosaic.

The used camera was relatively simple and **low-cost**, and there are other possible devices suitable for airborne thermal remote sensing. The most common sensor for airborne campaigns is probably **TASI-600** from company ITRES. TASI-600 is a push-broom scanner which produces whole flight lines as single images. This is tied to some specific problems such as **georeferencing** and **orthorectification** issues that were not present while using single camera images and mosaicking methods. The massive advantage of TASI-600 system comes from its **hyperspectral** sensor, which allows more **sophisticated atmospheric and emissivity corrections** based on multiple thermal bands. The Tau2 sensor used in this thesis is a **broadband camera** that is producing a one-band image, while TASI-600 produces a hyperspectral cube containing 32 spectral channels.

In terms of the final product, the closest comparison for the thermal mosaic of Olomouc is the project **UrbanAdapt** performed by Global Change Research Institute of the Czech Academy of Sciences. The final dataset over the city Brno is available online in the form of a web-map (*Thermal map of surfaces, Brno 2015*). Instead of day-time and night-time flights, both flights were carried out during the day — one dataset in the

**summer** and one in the **winter**. One of the main difficulties in this work is that there was a different altitude chosen for each flight. Therefore, the flight lines had different width, and each dataset also has a **different spatial resolution** etc. This further complicates any kind of analysis performed on such dataset. However, it is apparent that authors had fewer problems with objects of **extremely low emissivity** even though some are still identifiable in the image. For the atmospheric and emissivity correction process, **Temperature and Emissivity Separation** (TES) algorithm was used. The campaign took a considerably longer time of almost **4 hours**, which was unwisely spread throughout the day (from 9:43 to 13:22 CEST). Regarding the quality, a significant **blur** is visible throughout the whole mosaic. This was most probably caused by relatively **high aeroplane speed**. Even considering the higher altitude (meaning larger scan swath and fewer flight lines) and longer flight time, the aeroplane had to cover approximately **four times larger area** in the only slightly larger time frame. The interpretation was performed only on a very basic level in the form of a description of several interesting areas.

I would like to emphasise that even the 3 hours in Olomouc campaign is **extremely long** flight time for the thermal campaign. Thus, it is unclear if and how it would be possible to collect data from larger cities, even larger than Brno. One of the possible solutions would be **night-time campaign**, but the night-time data do not contain information about the heating ability of the surfaces. Another possible solution would be a series of shorter campaigns over specific areas or city districts. This would possibly require extensive auxiliary meteorological data to compensate for the changes in weather between different days.

Another topic worth noting is the general **auxiliary data collection** at the time of the flight campaign. It is very beneficial to secure not only high-quality ground truth data but also logs from the meteorological station, both private and governmental ones. Very important is also to get up to date datasets about any topic the operator wants to analyse and of course any free datasets. For example, **OpenStreetMap** historical data are not easily accessible after some time. The same principle applies to **municipal datasets** that are being updated constantly.

### Self-contained analysis

There are several ways of approaching methods based on data sampling. In this case, I've exploited our **long-term cooperation** with the local municipality and extensive knowledge of the area. Thanks to this, the data sampling was rather **quick** and possibly **very precise**. For any long-term analysis, it would be beneficial to keep the **same sample locations** or to use the same samples that were used in this thesis.

The **TURN method** was first proposed as a tool to remove the **microclimatic effect**, so the data from different parts of the city are comparable in terms of material temperature. In my humble opinion, this method is very smart and has tremendous **potential** in terms of intra-city comparison. Combined with some **field data** and further investigation, it might be potentially a **very strong tool** of TIR remote sensing. Of course, it has its limits such as sample collection and the error caused by the age and condition of the roads, but these effects can be **minimised** when approached correctly. The proper ways to analyse and visualise the data and information are still subject to research.

The third method not requiring any special external data source was **quantile-based typology**. This method is very strong when investigating unknown areas and for **immediate analysis** of extreme phenomena. The method is much stronger **in detail** when investigating smaller areas than for large scale statistical comparison or complex analysis.

### Analyses using external data sources

The first method using **data fusion** for advanced analysis is based on **building height** dataset. The first part of the analysis was trying to prove that rooftop layer heats up considerably more than the ground level, which was achieved **successfully**. In the second part, the relation between building height and the rooftop temperature was investigated without success. It would be possibly more beneficial to also take into account the roof material, its inclination, slope and other characteristics to perform more in-depth look into this topic.

The **Local Climate Zones** are a recent trend in urban climatology, and the methodology is successfully used in many studies since it was developed. As mentioned by the authors, it is still **improving**, and many related questions are being raised. Probably the most important one is about the actual process of automated classification. Even though some progress has been made, the heterogeneity of the urban environment is very complicated and affects any efforts in a negative way. Besides that, I would consider the **LCZ methodology** as one of the most potential and successful.

The use of the large European datasets was suggested by the reviewer during the thesis outline defence, and even though I was not certain about its practical use, it turned out to be **very interesting** and **effective**. The lower spatial resolution of **CORINE Land Cover** (CLC) looks slightly worse in the results, but the detail of **Urban Atlas** (UA) classification is very helpful at this spatial resolution. It would be certainly beneficial to **update** the thermal mosaic with every new CLC or UA version.

### Other remarks

One more analysis was prepared for evaluation. This method was investigating the relationship between the **age of a building** and the rooftop temperature. The hypothesis behind this was that **newer buildings** would have materials better **adapted** to modern climatic issues. While the method was performed successfully, the difference between buildings of different age was marginal and almost non-existent. Therefore, I have decided not to include this study in the final manuscript. However, the data and the results can be found in **Appendix 3**.

## 10 CONCLUSION

The main objective of this doctoral thesis was to **investigate and improve airborne thermal remote sensing in urban climate research**. With the increasing fraction of the world's population living in the cities, the **necessity of urban applications** increases accordingly in **remote sensing** as in many other fields such as **GIS, urban planning and architecture**. The recent **rapid increase** in Earth's ecosystem **temperature** and the increase of **severity of natural disasters** caused by **global change** makes the situation even more **alerting**. In this very moment, it is the **thermal infrared remote sensing** that comes with answers to many of the questions asked by the urban **climatologists**. How good is the **cooling effect** of the materials **during the night**? How severe is the **increase** in materials **temperature**? Are **citizens endangered** by the upwelling radiation coming from **artificial materials**? A **flight campaign** collecting extreme resolution data about radiant surface temperature was proposed to answer these questions. The **data processing** currently poses a difficult challenge and was carried out in the next step. After the **thermal mosaics of Olomouc** were created, the work continued with **self-reliant analyses** on the dataset. In the last part of the thesis, a set of analyses exploiting **external data sources** was carried out.

The main **empirical findings** are chapter specific and were summarized within the respective chapters. This section will **synthesize** the findings according to the sub-objectives.

- Airborne thermal remote sensing is a viable source of information about the surface temperature for urban climate research. This was proven by extensive data analysis.
- The data processing chain described in Chapter 5 is reliable and has consistent, detailed and high-quality results.
- An immediate and self-reliant analysis can be performed right after the data acquisition to identify crucial locations within the thermal mosaics, as described in Chapter 5.
- The TURN method described in Chapter 6.2 is a promising tool for assessing the spatial variability in urban microclimate. The results show great potential for further interpretation and future research.
- When investigating the heat stress on population, the different vertical levels need to be carefully distinguished. The difference between ground and rooftop height levels is described in Chapter 7.1
- Local Climate Zones are an important tool for the future of urban climate research, especially when combined with remote sensing methods.

- International cooperation and open Europe-wide datasets are beneficial for urban climate research.

The main **theoretical impact** of this thesis is undoubtedly the possibility of a relatively **low-cost high-accuracy thermal remote sensing** based on a single-image camera approach and mosaicking. This task can be performed in a **timely manner**, by a **small team** of specialists and with **interesting results**. Another large step forward is the **ability to analyse** such data. **Extreme resolution** thermal datasets are **very rare** and not many scientific papers are devoted to their analysis and interpretation. In this thesis, **several methods** were proposed and tested. Some offered **immediate results**, some were not fitting for this kind of data, and some showed **incredible potential** and possible **further improvements**.

Based on presented findings, **continuous monitoring** of city surface temperature should be considered as a viable option for a **scientific grant** and supported by **municipalities**. The **social benefits** of such research are unquestionable as well as the **positive impact** on the population. With the **global change progressing**, the local governments are responsible for the **aftermath of heat wave events** and the proper long-term investigation of the city structure may help the **population resilience and awareness**.

The possibilities of **future research** are many. The **improvements** to the data processing chain would increase the **accuracy** of the data and the **speed** of overall processing. The improvements to the analytical part can also be performed. **Auxiliary data** were proven to be almost **essential** to the future of such research. Most importantly, it would be very meaningful to provide **long-term monitoring** with additional **meteorological** and **climatological** data tied to **modelling** and the broader context of climatology.

To summarise, the thesis investigated **the possibilities of airborne thermal remote sensing in urban climate research**. The author performed the data processing chain leading to **thermal mosaic products** on which a series of analyses were performed. The improvements were made by proposing **new methods** of analysis and **improvements** within the data processing chain. The results of the **six analyses** were evaluated, and further recommendations were proposed.

## REFERENCES

CHRYSOULAKIS, Nektarios et al., 2016. A NOVEL APPROACH FOR ANTHROPOGENIC HEAT FLUX ESTIMATION FROM SPACE Foundation for Research and Technology Hellas ( FORTH ), Greece , 2 German Aerospace Center ( DLR ), Germany , 3 Centre d ' Etude Spatiale de la Biosphère ( CESBIO ), France , 4 University. . 2016. P. 6774–6777.

CIMBALISTA, Mario, 2014. Method for improving visualization of infrared images. [online]. 2014. Vol. 9105, p. 910504. DOI 10.1117/12.2063670. Available from: <http://proceedings.spiedigitallibrary.org/proceeding.aspx?doi=10.1117/12.2063670>

Copernicus Land Monitoring Service - Urban Atlas — European Environment Agency, 2018. [online]. [Accessed 28 May 2019]. Available from: <https://www.eea.europa.eu/data-and-maps/data/copernicus-land-monitoring-service-urban-atlas>

CORINE Land Cover — Copernicus Land Monitoring Service, 2019. [online]. [Accessed 28 May 2019]. Available from: <https://land.copernicus.eu/pan-european/corine-land-cover>

ČÚZK - RÚIAN, 2019. [online]. [Accessed 28 May 2019]. Available from: <https://www.cuzk.cz/Uvod/Produkty-a-sluzby/RUIAN/RUIAN.aspx>

DHAINAUT, Jean François, CLAESSENS, Yann Erick, GINSBURG, Christine and RIOU, Bruno, 2004. *Unprecedented heat-related deaths during the 2003 heat wave in Paris: Consequences on emergency departments*. 2004. ISBN 1466-609X (Electronic)r1364-8535 (Linking).

EISELE, Andreas et al., 2012. Applicability of the thermal infrared spectral region for the prediction of soil properties across semi-arid agricultural landscapes. *Remote Sensing*. 2012. Vol. 4, no. 11, p. 3265–3286. DOI 10.3390/rs4113265.

FOK, S C, NG, E Y K and TAI, K, 2002. Early Detection and Visualization of Breast Tumor With Thermogram and Neural Network. . 2002. Vol. 2, no. 2, p. 185–195.

FONSTAD, Mark A. et al., 2013. *Topographic structure from motion: A new development in photogrammetric measurement*. 2013. ISBN 0197-9337.

GELETIČ, Jan and LEHNERT, Michal, 2016. GIS-based delineation of local climate zones: The case of medium-sized Central European cities. *Moravian Geographical Reports*. 2016. DOI 10.1515/mgr-2016-0012.

GLENN J. TATTERSALL, 2018. *Thermimage: Thermal image analysis* [online]. 2018. 3.1.1. Available from: Glenn J. Tattersall

GUNAWARDENA, K. R., WELLS, M. J. and KERSHAW, T., 2017. Utilising green and

bluespace to mitigate urban heat island intensity. *Science of the Total Environment* [online]. 2017. Vol. 584–585, p. 1040–1055. DOI 10.1016/j.scitotenv.2017.01.158. Available from: <http://dx.doi.org/10.1016/j.scitotenv.2017.01.158>

HAY, Geoffrey J. et al., 2011. Geospatial technologies to improve urban energy efficiency. *Remote Sensing*. 2011. DOI 10.3390/rs3071380.

HAYHOE, Katharine, SHERIDAN, Scott, KALKSTEIN, Laurence and GREENE, Scott, 2010. Climate change, heat waves, and mortality projections for Chicago. *Journal of Great Lakes Research*. 2010. DOI 10.1016/j.jglr.2009.12.009.

Home :: Corine Land Cover classes, 2019. [online]. [Accessed 28 May 2019]. Available from: <https://land.copernicus.eu/user-corner/technical-library/corine-land-cover-nomenclature-guidelines/html>

IRANI RAHAGHI, Abolfazl, LEMMIN, Ulrich, SAGE, Daniel and BARRY, David Andrew, 2019. Achieving high-resolution thermal imagery in low-contrast lake surface waters by aerial remote sensing and image registration. *Remote Sensing of Environment* [online]. 2019. Vol. 221, no. November 2018, p. 773–783. DOI 10.1016/j.rse.2018.12.018. Available from: <https://doi.org/10.1016/j.rse.2018.12.018>

JIMÉNEZ-MUÑOZ, Juan C., MATTAR, Cristian, SOBRINO, José A. and MALHI, Yadvinder, 2016. Digital thermal monitoring of the Amazon forest: an intercomparison of satellite and reanalysis products. *International Journal of Digital Earth*. 2016. DOI 10.1080/17538947.2015.1056559.

JOVANOVIĆ, Dušan et al., 2015. Spatial analysis of high-resolution urban thermal patterns in Vojvodina, Serbia. *Geocarto International*. 2015. DOI 10.1080/10106049.2014.985747.

KNOWLTON, Kim et al., 2009. The 2006 California heat wave: Impacts on hospitalizations and emergency department visits. *Environmental Health Perspectives*. 2009. DOI 10.1289/ehp.11594.

KYSELÝ, Jan, KALVOVÁ, Jaroslava and KVĚTOŇ, Vít, 2000. Heat waves in the south Moravian region during the period 1961–1995. *Studia Geophysica et Geodaetica*. 2000. DOI 10.1023/A:1022009924435.

LEHNERT, Michal, GELETIČ, Jan, HUSÁK, Jan and VYSOUDIL, Miroslav, 2015. Urban field classification by “local climate zones” in a medium-sized Central European city: the case of Olomouc (Czech Republic). *Theoretical and Applied Climatology*. 2015. DOI 10.1007/s00704-014-1309-6.

LENG, Pei et al., 2019. First results of all-weather soil moisture retrieval from an optical/thermal infrared remote-sensing-based operational system in China. *International Journal of Remote Sensing* [online]. 2019. Vol. 40, no. 5–6, p. 2069–2086. DOI 10.1080/01431161.2018.1468119. Available from:



<https://doi.org/10.1080/01431161.2018.1468119>

LI, Haiyan and ZHU, Min, 2009. Simulation of vignetting effect in thermal imaging system. [online]. 2009. Vol. 7494, p. 749427. DOI 10.1117/12.831306. Available from: <http://proceedings.spiedigitallibrary.org/proceeding.aspx?doi=10.1117/12.831306>

MINKINA, Waldemar and DUDZIK, Sebastian, 2009. *Infrared Thermography, Errors and Uncertainties*. ISBN 9780470747186.

O'SULLIVAN, Antóin M., DEVITO, Kevin J. and CURRY, R. Allen, 2019. The influence of landscape characteristics on the spatial variability of river temperatures. *Catena* [online]. 2019. Vol. 177, no. February, p. 70–83. DOI 10.1016/j.catena.2019.02.006. Available from: <https://doi.org/10.1016/j.catena.2019.02.006>

OERKE, E. C., STEINER, U., DEHNE, H. W. and LINDENTHAL, M., 2006. Thermal imaging of cucumber leaves affected by downy mildew and environmental conditions. *Journal of Experimental Botany*. 2006. Vol. 57, no. 9, p. 2121–2132. DOI 10.1093/jxb/erj170.

OKE, Timothy R et al., 2017. *Urban Climates*. Cambridge University Press. ISBN 9780521849500.

OKE, Timothy R., 2002. *Boundary layer climates*. 2nd editio. Routledge. ISBN 0-203-40721-0.

LOUDIN ÅSTRÖM, Daniel, BERTIL, Forsberg and JOACIM, Rocklöv, 2011. *Heat wave impact on morbidity and mortality in the elderly population: A review of recent studies*. 2011. ISBN 03785122.

PARLOW, Eberhard, 2003. The urban heat budget derived from satellite data. *Geographica Helvetica*. 2003. Vol. 58, no. 2, p. 99–111.

PRAKASH, Anupma, 2000. Thermal remote sensing: concepts, issues and applications. ... *Archives of Photogrammetry and Remote Sensing* [online]. 2000. Vol. XXXIII, p. 239–243. Available from: [http://www.isprs.org/proceedings/XXXIII/congress/part1/239\\_XXXIII-part1.pdf](http://www.isprs.org/proceedings/XXXIII/congress/part1/239_XXXIII-part1.pdf)

RAHMAN, Mir Mustafizur, HAY, Geoffrey J., COULOIGNER, Isabelle and HEMACHANDRAN, Bharanidharan, 2014. Transforming image-objects into multiscale fields: A GEOBIA approach to mitigate urban microclimatic variability within H-Res thermal infrared airborne flight-lines. *Remote Sensing*. 2014. DOI 10.3390/rs6109435.

REISCHL, Christiane et al., 2017. Urban vulnerability and adaptation to heatwaves : a case study of Graz ( Austria ) a case study of Graz ( Austria ). *Climate Policy* [online]. 2017. Vol. 0, no. 0, p. 1–13. DOI 10.1080/14693062.2016.1227953. Available from: <http://dx.doi.org/10.1080/14693062.2016.1227953>

RIGO, G. and PARLOW, E., 2007. Modelling the ground heat flux of an urban area using

remote sensing data. *Theoretical and Applied Climatology*. 2007. DOI 10.1007/s00704-006-0279-8.

ROBINE, Jean Marie et al., 2008. Death toll exceeded 70,000 in Europe during the summer of 2003. *Comptes Rendus - Biologies*. 2008. DOI 10.1016/j.crv.2007.12.001.

ROBINSON, Peter J., 2001. On the Definition of a Heat Wave. *Journal of Applied Meteorology*. 2001. DOI 10.1175/1520-0450(2001)040<0762:OTDOAH>2.0.CO;2.

ROTH, M., OKE, T. R. and EMERY, W. J., 1989. Satellite-derived urban heat islands from three coastal cities and the utilization of such data in urban climatology. *International Journal of Remote Sensing*. 1989. DOI 10.1080/01431168908904002.

SCHLERF, Martin et al., 2012. A hyperspectral thermal infrared imaging instrument for natural resources applications. *Remote Sensing*. 2012. DOI 10.3390/rs4123995.

SEPULCRE-CANTÓ, G. et al., 2006. Detection of water stress in an olive orchard with thermal remote sensing imagery. *Agricultural and Forest Meteorology*. 2006. Vol. 136, no. 1–2, p. 31–44. DOI 10.1016/j.agrformet.2006.01.008.

SOLIMAN, Aiman, DUGUAY, Claude, SAUNDERS, William and HACHEM, Sonia, 2012. Pan-arctic land surface temperature from MODIS and AATSR: Product development and intercomparison. *Remote Sensing*. 2012. Vol. 4, no. 12, p. 3833–3856. DOI 10.3390/rs4123833.

STEWART, I. D. and OKE, T. R., 2012. Local climate zones for urban temperature studies. *Bulletin of the American Meteorological Society*. 2012. Vol. 93, no. 12, p. 1879–1900. DOI 10.1175/BAMS-D-11-00019.1.

SUNDBORG, Ake, 1952. Climatological studies in Uppsala with special regard to the temperature conditions in the urban area. *Geographica*. 1952. Vol. No. 22. DOI 10.1002/qj.49707833828.

TAN, Jen Hong and ACHARYA, U. Rajendra, 2015. Pseudocolours for thermography - Multi-segments colour scale. *Infrared Physics and Technology* [online]. 2015. Vol. 72, p. 140–147. DOI 10.1016/j.infrared.2015.07.018. Available from: <http://dx.doi.org/10.1016/j.infrared.2015.07.018>

Thermal Color Palettes | FLIR Delta - Episode 4 - YouTube, 2018. [online]. [Accessed 28 May 2019]. Available from: <https://www.youtube.com/watch?v=qZiMn0wuxdo>

Thermal map of surfaces, Brno, 2015. [online]. [Accessed 28 May 2019]. Available from: [http://gis6.brno.cz/mapa/teplotni-mapa/?c=-598156%3A-1160771&z=4&lb=of-brno\\_2015&ly=tepmap0&lbo=1&lyo=](http://gis6.brno.cz/mapa/teplotni-mapa/?c=-598156%3A-1160771&z=4&lb=of-brno_2015&ly=tepmap0&lbo=1&lyo=)

TORGERSEN, Christian E. et al., 2001. Airborne thermal remote sensing for water

temperature assessment in rivers and streams. *Remote Sensing of Environment*. 2001. Vol. 76, no. 3, p. 386–398. DOI 10.1016/S0034-4257(01)00186-9.

TUHÁČEK, Tomáš, 2017. *Floor area ratio of buildings in Olomouc*. Palacky University Olomouc.

UNITED NATIONS, 2016. The World's Cities in 2016: Data Booklet. *Economic and Social Affairs* [online]. 2016. P. 29. DOI 10.18356/8519891f-en. Available from: [http://www.un.org/en/development/desa/population/publications/pdf/urbanization/the\\_worlds\\_cities\\_in\\_2016\\_data\\_booklet.pdf](http://www.un.org/en/development/desa/population/publications/pdf/urbanization/the_worlds_cities_in_2016_data_booklet.pdf)

URBAN, Aleš et al., 2016. Spatial patterns of heat-related cardiovascular mortality in the Czech Republic. *International Journal of Environmental Research and Public Health*. 2016. Vol. 13, no. 3. DOI 10.3390/ijerph13030284.

Urban Atlas — Copernicus Land Monitoring Service, 2019. [online]. [Accessed 28 May 2019]. Available from: <https://land.copernicus.eu/local/urban-atlas>

VOELKEL, Jackson, HELLMAN, Dana, SAKUMA, Ryu and SHANDAS, Vivek, 2018. Assessing vulnerability to urban heat: A study of disproportionate heat exposure and access to refuge by socio-demographic status in Portland, Oregon. *International Journal of Environmental Research and Public Health*. 2018. Vol. 15, no. 4. DOI 10.3390/ijerph15040640.

VOOGT, J. A. and OKE, T. R., 2003. Thermal remote sensing of urban climates. *Remote Sensing of Environment*. 2003. Vol. 86, no. 3, p. 370–384. DOI 10.1016/S0034-4257(03)00079-8.

WENG, Qihao, 2009. Thermal infrared remote sensing for urban climate and environmental studies: Methods, applications, and trends. *ISPRS Journal of Photogrammetry and Remote Sensing* [online]. 2009. Vol. 64, no. 4, p. 335–344. DOI 10.1016/j.isprsjprs.2009.03.007. Available from: <http://dx.doi.org/10.1016/j.isprsjprs.2009.03.007>

Which is the Best Color Palette for Thermal Imaging? - YouTube, 2015. [online]. [Accessed 28 May 2019]. Available from: <https://www.youtube.com/watch?v=qX0mDXy2Sy4>

ZEMEK, F. et al., 2014. *Letecký dálkový průzkum Země: teorie a příklady hodnocení terestrických systémů*. ISBN 978-80-87902-07-3.

ZEMEK, František, 2014. *Airborne remote sensing: theory and practice in assessment of terrestrial ecosystems*. Brno: Global Change Research Centre AS CR. ISBN 978-80-87902-05-9.

ZHANG, Kai, CHEN, Tsun-Hsuan and BEGLEY, Charles E, 2015. Impact of the 2011 heat wave on mortality and emergency department visits in Houston, Texas. *Environmental Health*. 2015. DOI 10.1186/1476-069X-14-11.

## SHRNUTÍ

Tato doktorská práce pojednává o **leteckém snímkování v termálním infračerveném spektru** pro aplikaci v **městské klimatologii**. Práce si klade za cíl **vylepšit** možnosti pořizování dat o teplotě zemského povrchu, možnosti jejich dalšího zpracování a analýz. Prvním dílčím cílem práce je **plánování letecké kampaně**, samotný sběr dat a následný zpracovatelský řetězec. Výsledkem tohoto procesu je **termální mozaika** nebo také teplotní mapa povrchu. Druhým dílčím cílem je použít **analytické nástroje** pro vyhodnocení a interpretaci těchto dat bez použití dalších pomocných datových zdrojů. Třetím dílčím cílem je využití **externích datových zdrojů**, které poskytují další možnosti srovnání a interpretace dat.

**Letecká kampaň** byla provedena 10. července 2016 nad zájmovým územím pokrývajícím město Olomouc ve 4:55 CEST a 17:00 CEST. Toto území bylo snímkováno termální kamerou se senzorem **FLIR Tau2** a zároveň fotogrammetrickou kamerou **Phase One iXA-R 180**. Celkem bylo provedeno **22 letových** os z průměrné výšky **769 m** nad zemským povrchem, což ve výsledku znamenalo **prostorové rozlišení** kolem **1 m**. Během zpracovatelského procesu byla data **radiometricky** zpracována, byl odstraněn efekt **vinětace**, byly provedeny **atmosférické korekce** a korekce pro **emisivitu** snímkaných objektů. V posledním kroku této části byla provedena **ortorektifikace**, **georeferencování** a **mozaikování**. Výsledkem tohoto dílčího cíle je ranní a odpolední **termální mozaika** pokrývající území města Olomouce a okolí.

Ke splnění druhého dílčího cíle byly navrženy **tři analytické metody** pro hodnocení městského klimatu v Olomouci. První metoda je založena na **sběru vzorků** typů materiálu v prostředí GIS. Tato metoda se skládala ze dvou částí, kdy byla nejdříve provedena předběžná studie s omezeným množstvím vzorků a následně rozsáhlejší studie se zmenšeným počtem tří a větším počtem vzorků. Jako druhá metoda byla použita **metoda TURN**, která byla využita pro plošný výpočet vlivu **mikroklimatu** na teplotu asfaltových silnic na území města. Třetí metoda byla založena na statistickém zpracování dat, konkrétně na aplikování **kvantilů** a **typizaci** na nich založené. V této části byly vyzkoušeny **dvě typizace**, jedna založená na tercilech a druhá na kvartilech.

Třetí dílčí cíl se zaměřoval na **fúzi termálních mozaik s dalšími datovými zdroji**. V první metodě byla zkoumána závislost vlivu **výšky budovy** na teplotu povrchu. Bylo dokázáno, že teplota povrchů na zemi a v úrovni střech se velmi výrazně liší a je potřeba ji ve výzkumu městského klimatu zohledňovat; především na satelitních snímcích, kde tyto **dvě úrovně vertikality** často nejdou odlišit. Dále metoda neprokázala souvislost mezi výškou budovy a teplotou její střechy. Ve druhé studii byla aplikována metodika **Lokálních Klimatických Zón (LCZs)** pro klasifikaci a následnou analýzu takto vytyčených zón s uniformním klimatologických chováním. Poslední metoda se zaměřovala na

kombinaci termální mozaiky s daty z **evropských projektů** zaměřených na **využití krajiny** a **krajinného pokryvu**. Byly použity dvě datové sady, **Urban Atlas (UA)** a **CORINE Land Cover (CLC)**. Obě datové sady byly popsány jak z hlediska struktury, tak jejich dostupnosti a aktuálnosti. Dále bylo zkoumáno **pokrytí zájmového území** třídami využití krajiny u obou datových sad. V posledním kroku byly pro jednotlivé třídy vypočítány hodnoty ranní a odpolední teploty a popsány jejich základní trendy.

Hlavní výsledky práce se dají shrnout do několika poznatků:

- Letecké termální snímkování je jeden z možných zdrojů informací o teplotě povrchu, která je dále využitelná ve výzkumu městského klimatu.
- Zpracovatelský proces popsaný v této práci je spolehlivý a poskytuje konzistentní, podrobné a kvalitní výstupy.
- Okamžitá analýza nasbíraných dat může být provedena bez potřeby dalších vstupních dat. Takováto analýza dokáže v obraze identifikovat extrémní případy a základní trendy v daném území.
- Metoda TURN je velmi slibný nástroj pro výzkum prostorového rozložení vlivu mikroklimatu na městskou krajinu.
- Výškové stupně (u země a ve výši střech) hrají důležitou roli při posuzování negativního vlivu tepla na obyvatelstvo, zejména během letních náporů veder.
- Lokální Klimatické Zóny jsou užitečným nástrojem pro srovnání tepelných vlastností různých částí města jak v rámci jednoho regionu, tak i mezi městy, případně státy.
- Mezinárodní spolupráce při produkci celoevropských datových sad o využití krajiny je velmi užitečná při výzkumu tepelných vlastností městské krajiny.

Tato doktorská práce prozkoumala možnosti využití **leteckého termálního snímkování** ve výzkumu **městského klimatu**. Autor naplánoval **leteckou kampaň** a **zpracovatelský řetězec** na jehož konci vznikla datová sada dvou termálních mozaik zájmového území města Olomouce. Tato data autor zpracoval pomocí **šesti analýz** zaměřených nejen na vytvořenou datovou sadu, ale i na kombinaci s dalšími zdroji dat. Tato práce prezentuje **vylepšení zpracovatelského řetězce** a navrhuje **nové metody** pro hodnocení **městského klimatu**.

## LIST OF APPENDICES

All appendices are included in electronic form on the flash drive attached to the doctoral thesis.

Appendix 1 – Thermal images

Appendix 2 – Thermal mosaics

Appendix 3 – Graphs

Appendix 4 – Results of the TURN method

Appendix 5 – Results of the typology method

Appendix 6 – Buildings data



**KATEDRA GEOINFORMATIKY**

Univerzita Palackého v Olomouci | Přírodovědecká fakulta

## **LETECKÉ TERMÁLNÍ SNÍMKOVÁNÍ VE VÝZKUMU MĚSTSKÉHO KLIMATU**

### **AUTOREFERÁT DISERTAČNÍ PRÁCE**

Studijní program: P1301 Geografie

Obor studia: 1302V011 Geoinformatika a kartografie

Školitel: prof. RNDr. Vít Voženílek, CSc.

**Mgr. Tomáš Pour**

## **AIRBORNE THERMAL REMOTE SENSING IN URBAN CLIMATE RESEARCH**

### **Ph.D. THESIS SUMMARY**

Study Programme: Geography

Specialization: Geoinformatics and Cartography

Supervisor: prof. RNDr. Vít Voženílek, CSc.

**Department of Geoinformatics**

Faculty of Science, Palacký University Olomouc

**Olomouc 2019**

*Disertační práce byla vypracována v distanční formě doktorského studia na Katedře geoinformatiky Přírodovědecké fakulty Univerzity Palackého v Olomouci.*

*Dissertation thesis was compiled within Ph.D. study at the Department of Geoinformatics, Faculty of Science, Palacký University Olomouc.*

**Předkladatel / Submitter:**

Mgr. Tomáš Pour

**Školitel / Supervisor:**

prof. RNDr. Vít Voženílek, CSc.

Katedra geoinformatiky

Přírodovědecká fakulta Univerzity Palackého v Olomouci

17. listopadu 50

771 46 Olomouc

**Oponenti / Reviewers:**

doc. RNDr. Ján Feranec, DrSc. (Geografický ústav Slovenská akademie věd, Bratislava)

doc. RNDr. Přemysl Štych, PhD. (Univerzita Karlova, Praha)

doc. Mgr. Michal Gallay, Ph.D. (Univerzita Pavla Jozefa Šafárika v Košicích)

Autoreferát byl rozeslán dne / Summary was posted on: 10. května 2019

Obhajoba disertační práce se koná dne \_\_\_\_\_ před komisí pro obhajoby disertačních prací doktorského studia v oboru P1301 Geografie, studijním oboru 1302V011 Geoinformatika a kartografie, v prostorách Katedry geoinformatiky Přírodovědecké fakulty Univerzity Palackého v Olomouci, 17. listopadu 50, 771 46 Olomouc.

The defence of the dissertation thesis will be held on \_\_\_\_\_ at the commission for the defence of dissertation thesis of Ph.D. degree in study programme P1301 Geography, specialization Geoinformatics and cartography, in the premises of the Department of Geoinformatics, Faculty of Science, Palacký University Olomouc, 17. listopadu 50, 771 46 Olomouc.

*S disertační prací je možno se seznámit na studijním oddělení Přírodovědecké fakulty Univerzity Palackého v Olomouci, 17. listopadu 12, 77 46 Olomouc.*

*The dissertation thesis is available at the Study Department, Faculty of Science, Palacký University in Olomouc, 17. listopadu 12, 771 46 Olomouc.*

© Tomáš Pour, 2019

ISSN 1805-7500

ISBN .....



## Contents

|  |    |
|--|----|
| 1. Introduction.....   | 4  |
| 2. Objectives .....  | 5  |
| 3. State of art.....   | 6  |
| 4. Olomouc airborne thermal data acquisition.....                    | 11 |
| 5. Descriptive analyses carried out on Olomouc thermal mosaics ..... | 16 |
| 6. Data Fusion Analyses Carried Out on Olomouc Thermal Mosaics ..... | 22 |
| 7. Discussion .....  | 27 |
| 8. Conclusion .....  | 30 |
| 9. Literature .....  | 32 |
| 10. Shrnutí .....  | 38 |
| Overview of author's activity during his study .....                 | 41 |

# 1. Introduction

Remote sensing plays a strong role in both the Earth and other solar system objects observation. Both sensors and carriers have changed dramatically over the last years. What once started as a camera attached to a balloon in 1906, capturing a black and white image of the results of the San Francisco earthquake, is now recognised as a scientific field with growing popularity.

Thermal remote sensing helps in many disciplines such as medicine, earth observation and machine, construction and electrical engineering. Made possible only decades ago, the ability to measure the kinetic or radiant temperature of an object from a distance is fascinating by itself because it is not possible by any living creature. The key improvements implemented over the last years vastly improved the spatial and spectral resolution and reduced the sensors in size. Even with the improvements in the scientific community, thermal remote sensing for commercial and municipal purposes remains very rare due to its complexity.

Nowadays, half of the population of our planet already lives in the cities. There are natural phenomena connected to the urban environment which were not considered as important in the past as they are today. For example, powerful heat waves and heat stress inside the cities increased in intensity by vague city planning. The need for the research of urban environment, thus, becomes pivotal.

Thermal remote sensing has reached the point when the collected data become extremely relevant for urban environmental studies. Such possibilities enable us not only to compare the urban environment with its rural counterpart but also to differentiate different types of thermal behaviour within the city. The results of such research will play a crucial role in urban planning and population readiness in the time of crisis.

The thesis is motivated by the desire to improve this field of study in terms of technical quality and public enlightenment. It follows up the previous research in bachelor's and master's theses, both regarding urban environment using remote sensing methods. The bachelor's thesis explored the possibilities of inner urbanization using very high-resolution satellite data combined with Object-Based Image Analysis (OBIA) method. In the diploma thesis, five middle-European cities with mining and/or heavy industry history are compared based on their city structure. Based on the years of experience and the current socio-political pressure in climate adaptation strategies, it is vital to explore new possibilities of thermal remote sensing in an urban environment to improve the quality of life of the population and ensure sustainability to the future.

## 2. Objectives

The objective of the thesis is to investigate and improve airborne thermal remote sensing in urban climate research. Urban climate research is benefiting from thermal remote sensing data already, but satellite images have a too coarse resolution to explore for example the structure of surface urban heat island in detail or to learn heat conditions of Local Climate Zones (LCZ). With custom-made extreme resolution thermal imagery, it is possible to research new areas and create new scientific questions inside the urban climate topic. Fulfilling the objective of the thesis will improve the process of data acquisition, research and analysis of the urban climate.

### **SUB-OBJECTIVE 1 Olomouc Airborne Thermal Data Acquisition**

The first sub-objective is to acquire and process a series of thermal datasets of the city of Olomouc for urban environment research. Preparing the flight campaign means thoroughly considering the specifications such as the attributes of the carrier, the sensors, the time of the day and the day of the year. This process is very important and cannot be taken lightly since the campaign cannot be repeated most of the times. The planning reflected the aim of the thesis and the thermal regime of the urban ecosystem. After that, the campaign was carried out according to the plan, along with ground sample data collection. The collected dataset contains raw signal data from the sensor. Those need to be corrected to acquire brightness and, later in the process, radiant surface temperature. Digital number values were compensated for meteorological influences, the geometry of the sensor, the emissivity of the surface and then orthorectified and georeferenced into the mosaic. The resulting mosaic is a unique dataset representing early morning radiant surface temperature cooled after night and afternoon peak radiant surface temperature. Combination of these two flights is most beneficial for urban surface temperature regime and other urban climate studies.

### **SUB-OBJECTIVE 2 Descriptive Analyses Carried Out on Olomouc Thermal Mosaics**

The aim of the second sub-objective is to use the thermal mosaics dataset and self-sufficient methods of sampling, typology and classification to characterize the area of interest. Proposed methods of quantile-based typology, material sampling and Local Climate Zones (LCZs) are a viable option for any kind of thermal imagery and are providing some basic information about the researched area. Quantile-based typology is a method exploiting the statistical variance and the heterogeneity of the thermal image. It allows focusing on unique objects with extreme thermal behaviour. Material sampling was combined with some auxiliary data, but in its core, it would be enough to use another remote sensing dataset such as satellite or airborne imagery in the optical part of the electromagnetic spectrum. Local Climate Zones are unified basic structural units with uniform behaviour from urban climatology point of view. Their biggest strength is that they are transferable among cities and with some light tuning also in between different continents and cultural environments. Another strength is the ability to classify them using only remote sensing data as the classifying tree requires

mostly Sky View Factor (SVF) data that can be acquired from the Digital Surface Model (DSM), buildings and vegetation that can be both acquired from high-resolution satellite imagery. To summarize, the goal of this sub-objective is to introduce and test the possibility of use of various methods to evaluate the area of interest.

### **SUB-OBJECTIVE 3 Data Fusion Analyses Carried Out on Olomouc Thermal Mosaics**

The third sub-objective is to analyse the dataset and propose its fusion with other data sources to investigate the surface temperature patterns and trends among various land-cover and land-use types. The aim is to use external datasets acquired from cooperating departments such as the Department of Urban Planning and Architecture of the city of Olomouc. Another source of valuable data is regional European initiatives regarding the topic of land-use and land-cover. These datasets provide a solid baseline for the assessment of the thermal regime of various city structures, neighbourhoods, materials and public spaces. Proposed analyses include the use of CORINE Land Cover and Urban Atlas datasets and use of building height information for verticality analysis. The goal of this sub-objective is to use auxiliary data and Europe-wide datasets to analyse the city thermal behaviour. This might help to set up a trend of comparison among multiple cities.

## **3. State of art**

Thermal infrared (TIR) remote sensing (RS) is a challenging field that requires interdisciplinary knowledge from physics and optics. TIR remote sensing is mainly used on two types of carriers – aeroplanes and satellite. Drone TIR remote sensing usually plays a tactical role during fires, missing people cases, police chases, and so on. While satellite RS is well established, the applications of airborne thermal remote sensing are rather sparse in the literature. The urban applications of TIR are most commonly based on satellite imagery, which comes with many challenges and specifics that need to be considered. The last topic discussed in the following chapter is TIR data visualisation and the role of thermograms in the scientific literature.

### **Thermal infrared remote sensing**

Prakash (2000) sums up the thermal remote sensing as the branch of remote sensing that deals with the acquisition, processing and interpretation of data acquired primarily in the thermal infrared (TIR) region of the electromagnetic (EM) spectrum. In the thermal remote sensing, the radiation emitted from the surface of the target is measured, as opposed to optical remote sensing where we measure the radiations reflected by the target.

### **Thermal infrared wavelength emittance**

Every natural target reflects as well as emits radiation in various wavelengths. In the TIR region of the EM spectrum, the radiations emitted by the earth, due to its thermal state, are

far more intense than the solar reflected radiations and, therefore, sensors operating in this wavelength region primarily detect thermal radiative properties of the ground material. As thermal remote sensing deals with the measurement of emitted radiations, for high-temperature phenomenon, the realm of thermal remote sensing broadens to encompass not only the TIR but also the short-wave infrared (SWIR), near-infrared (NIR) and in extreme cases even the visible region of the EM spectrum, Zemek et al. (2014) report.

Prakash (2000) further describes thermal remote sensing, in principle, as different from remote sensing in the optical and microwave region. In practice, thermal data prove to be complementary to other remote sensing data. Thus, though still not fully explored, thermal remote sensing reserves potentials for a variety of applications.

An object, having the kinetic temperature higher than 0 °K, emits the electromagnetic (EM) radiation. The amount and the spectral distribution of the emitted energy depend on the temperature of the object and its emissivity. In the case of a pure blackbody, the spectral distribution is described in Planck's law. Most of the objects measured in remote sensing have the kinetic temperature between 270 and 330 °K. According to Planck's law, it means that we can measure the thermal radiation in two atmospheric windows, the first one being 3 to 5 micrometres and the second one being 8 to 14 micrometres. The first atmospheric window is not suitable for remote sensing because a part of the gathered data is also reflected in solar irradiation. The second atmospheric window is much more suitable because surface emittance is dominant in this wavelength.

An image taken in the thermal infrared part of EM spectrum can be in the form of thermogram or thermal hyperspectral cube. In the case of the thermogram, only one measured value is taken for each pixel. In the case of the hyperspectral cube, the spectral behaviour of the material over the whole range of the thermal infrared spectrum is measured.

Thermal data can be used for both qualitative and quantitative research. For qualitative comparison, there is no need for atmospheric corrections if interpreted correctly. For qualitative data, several corrections must be performed. These include (i) sensor calibrations, (ii) geometric corrections and (iii) atmospheric corrections.

The most important factor affecting the thermal characteristics of an object is emissivity ( $\epsilon$ ). (Minkina, Dudzik 2009) Emissivity is an ability to emit EM radiation in thermal wavelength compared to the radiation emitted by the black body of the same temperature. The emissivity depends on wavelength, temperature and the direction of emittance. If the sensor is perpendicular to the surface and the temperature is relatively stable between 270 and 330 °K, the emissivity depends only on the wavelength.

Besides emissivity, Zemek et al. (2014) describe the characteristics of the object that contribute to its temperature. These are:

- Thermal conductivity
- Thermal capacity
- Thermal inertia

Thermal conductivity describes the speed of the heat transfer within an object. Thermal capacity describes the amount of heat the material is able to contain. Thermal inertia is the ability of a material to change its temperature over time.

### **Vignetting, atmospheric and emissivity corrections**

Vignetting is a commonly known distortion in the visible region of the EM spectrum which affects TIR region as well. The consequence of this effect results in uneven distribution of the signal in a single image, where the central region is bright and regions towards the side of the image appears darker. According to Li and Zhu (2009), the effect is caused by gradually decreasing radiation illumination. The effect is stronger to the sides of the image while being strongest in the corners. Because TIR imaging works with low contrast between 1 and 2 %, compensating for vignetting effect is crucial for high-quality TIR image.

The atmosphere affects the measurement in three ways – it lowers the amount of emitted radiance that reaches the sensor, emits radiance itself and reflects radiance. Removal of the atmospheric effect is essential when retrieving high-quality TIR image. Atmospheric corrections differ based on sensor type. Zemek et al. (2014) define two basic categories of corrections – hyperspectral and broadband.

Hyperspectral atmospheric corrections rely mostly on complex models such as MODTRAN. They require accurate simulation of vertical atmospheric parameters such as CO<sub>2</sub> concentration, humidity and temperature profile aerosol model. These data are usually measured in-situ, obtained from local meteorological stations or can be simulated in the model.

Broadband sensors, on the other hand, do not require such a complex approach. Main variables influencing the measurements are relative humidity, object distance, above ground temperature, the temperature near the sensor and atmospheric temperature. Calibration of such sensor can be then calculated using general formulas.

### **Leading applications in TIR remote sensing**

TIR remote sensing has numerous applications in different geographical topics. In physical geography, the examples are natural resources detection using thermal spectroscopy (Schlerf et al. 2012), arctic region monitoring (Soliman et al. 2012), soil property research using thermal and visible spectral region data fusion (Eisele et al. 2012) or research in water quality and fisheries management (Torgersen et al. 2001) using stream temperature acquired by airborne remote sensing. Due to recent droughts in Amazon forest, Jiménez-Muñoz, Mattar, Sobrino and Malhi (2016) were investigating the possibilities of using MODIS and ERA-

Interim products to understand forest response and potential impact on carbon absorption. Sepulcre-Cantó et al. (2006) suggest water stress detection in non-homogeneous crop canopies as another possible application.

TIR remote sensing is also extremely beneficial in urban studies, especially regarding (surface) urban heat island, urban modelling and heat comfort. TIR remote sensing is beneficial in urban heat budget studies (Parlow 2003), which then overlap with urban heat flux modelling (Rigo, Parlow 2007). It can also help the property owners and communities regarding urban energy efficiency and insulation quality assessment (Hay et al. 2011) or help with spatial planning. (Jovanović et al. 2015) Most importantly, TIR remote sensing is used for detection, evaluation and monitoring of urban heat island (UHI) effect (Weng 2009), including assessment of surface urban heat island.

### **Thermal imaging for urban climatology**

The surface temperature plays a crucial role in the research of the urban climate (Figure 1). Air mass above the ground is highly affected by the surface temperature as well as energy balance and the internal climate inside buildings. Human interception and urbanization in the landscape led to a general trend of increasing temperature in the urban climate. This phenomenon is described as the Urban Heat Island (UHI). UHIs are most often monitored using ground stations. Recent advances in thermal imaging and remote sensing technology allowed the use of satellite and aircraft platforms (and recently drone platforms). Nowadays, UHI studies can combine thermal remote sensing data with urban micrometeorology. This approach brings new opportunities but also new challenges. Voogt and Oke (2003) state that the emphasis on proper and precise definitions of various phenomena is crucial in advancements of this field.

Thermal remote sensing measures emitted radiation by the surface which incorporates effects of the surface such as surface moisture, thermal admittance, emissivity, sun and atmospheric irradiance and the effects of the near-surface atmosphere. The term directional brightness temperature is commonly used to describe the temperature calculated using the inversion of Planck's law using a certain thermal sensor that operates at a certain wavelength. After the data are corrected for atmospheric effects and surface emissivity, it is called directional radiometric temperatures. Roth et al. (1989) formulated the four main questions regarding satellite-derived thermal remote sensing:

- What are the characteristics of the urban surface as viewed by thermal remote sensors?
- What is the relationship between remotely observed radiometric surface temperature and the actual temperature of the urban-atmosphere interface?
- How can surface urban heat islands be related to atmospheric urban heat islands?

- How can thermal remote sensing of urban surfaces provide input into models of urban climate?

The first question can be answered using sensor view models. These models simulate simplified surfaces viewed by a certain model taking into account a number of variables. At a lower scale, we can model certain buildings and urban structure using LIDAR data; at larger scales, we work with larger areas, especially using multispectral satellite imagery. Understanding the characteristics of surfaces is important for further work with local variability. Spatial phenomena such as roof or vegetation geometry, building height and others affect remotely sensed data in a major way.

According to Zemek et al. (2014), thermal remote sensing measurements are affected by two main sources: the atmosphere and the measured surface. While atmospheric corrections are rather well established due to other remote sensing applications, we cannot say the same about the thermodynamic properties and geometry of the surface. Emissivity corrections can be applied easily when the surface material is known to the researcher. On the other hand, the geometry of the object and the effect of thermal anisotropy are not that easy to remove. Various models are trying to predict this phenomenon and improve thermal images.

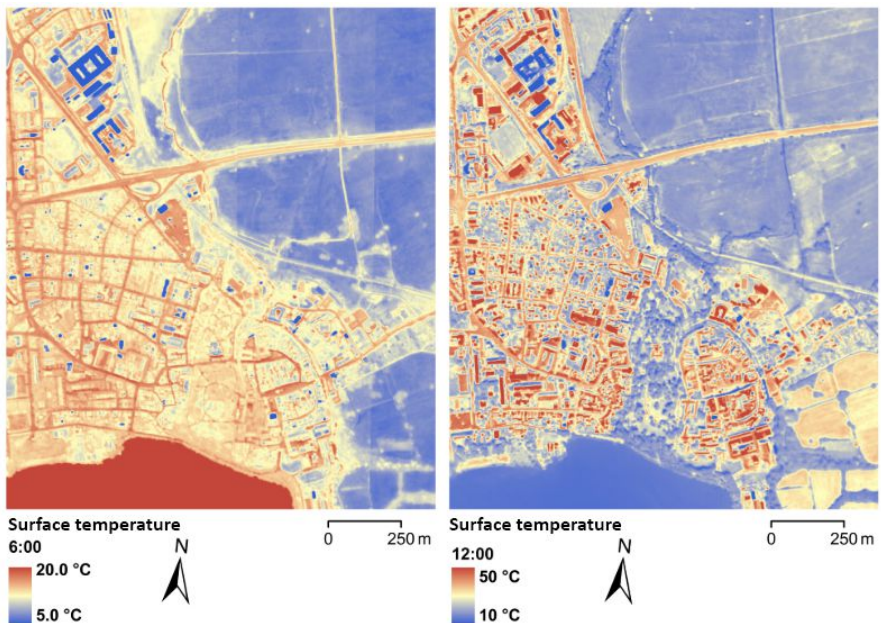


Figure 1 Thermal image of city Třeboň, the Czech Republic on 27th July 2008.  
Source: edited from Zemek (2014)



Oke et al. (2017) described the correlation between surface temperature and air temperature at UCL as a possible result of micro-advection caused by increased surface temperature. For the night-time case of the UHI, surface–air temperature differences are expected to be minimized as winds increase, due to mixing and disruption of any surface-based inversion layer. Under calm winds and clear skies, when the UHI has its best expression, micro-scale processes dependent on surface thermal properties, sky view factor and microscale advection will be most apparent thereby increasing differences between the UHI and SUHI.

As the main disadvantage of using thermal remote sensing data in urban climate models is according to Voogt and Oke (2003) the difference between surface temperature and the aerodynamic temperature needed for the calculation of the surface sensible heat flux.

### **Surface urban heat island**

Urban heat island and its uniqueness for the urban environment is known since Sundborg (1952) articulated the theory about urban energy balance based on the incoming and outgoing energy flux balance. He further elaborated, that the energy absorbed by the urban surface system from solar radiation and generated by anthropogenic activity is physically balanced by warming the air above the surface, the evaporation of moisture, and storage of heat in surface materials.

Oke (2002) pointed out that UHI can be observed on two different levels. Urban Canopy Layer (UCL) describes the air mass between the surface and approximate mean building height, while Urban Boundary Level (UBL) lays above the canopy layer and is affected by the upward urban effect. For UCL measuring, regular measurement in meteorological height or vehicle-mounted sensors is sufficient to model this phenomenon. However, Chrysoulakis et al. (2016) suggest UBL specialized sensor platforms for proper measurements at UBL. A special case of UHI called Surface Urban Heat Island (SUHI) is observed by remote sensing platforms. However, analysis of this phenomenon must be carried out with caution because of the specific regime of various materials.

While anthropogenic heat flux, along with anthropogenic materials contributes the most to the urban heat island effect, Gunawardena et al. (2017) suggest greenspaces and bluespaces as the natural countermeasure. In their meta-analysis, they suggest careful urban planning heavily based on urban modelling to mitigate the UHI effect.

## **4. Olomouc airborne thermal data acquisition**

The process of the production of a high-quality extreme resolution thermal mosaic of the city of Olomouc is described in the following chapter. The mosaic contains the radiometric temperature of the surface at two different times during the day. The process includes flight planning, data acquisition, data correction, and photogrammetry processing.

## Olomouc flight campaign, 10th July 2016

The aeroplane Cessna 172 was mounted with a photogrammetric sensor Phase One iXA-R 180 and a thermal camera Workswell Thermal Vision Pro (based on a FLIR Tau2 core). This version of Tau2 is mounted with 13 mm,  $f/1,25$  optics which allows a field of view (FoV) of  $45^\circ \times 37^\circ$  with an iFoV of 1,308 mrad. The flight campaign consisted of thermal and visible spectrum imaging. The flight height and spectral resolution were chosen primarily considering the thermal sensor because of its smaller iFoV. Different scenarios were created to satisfy the need for overlap and fine spatial resolution. After spatial resolutions from 30 cm to 130 cm were considered, the final decision was to aim for a 100 cm spatial resolution per pixel edge. Based on this decision, the rest of the variables were calculated. The size of the scene was 512 m  $\times$  640 m, and the average flight height was set to 769 m above sea level.



Figure 2 Flight lines and ground control locations over the Olomouc city. The flight was carried out from the west towards the east. In red, the planned flight lines are visualised. Blue dots symbolise the ground truth data locations.

The area of interest is about 10 km × 8 km in size (Figure 2), which required 22 flight lines. The flight was carried out on July 10, 2016. Because the closest airport does not allow night take-offs and landings, the early flight started as soon as possible; that is, right after civil dawn, which was at 4:55 CEST for that day. The second flight time was aimed at the highest possible stored temperature, which in this case took place at about 17:00 CEST. Both flights took about 180 minutes and consisted of approximately 2135 thermal images.

### **Image processing**

Thermal imaging requires similar corrections as other conventional remote sensing methods do. According to Zemek (2014), the corrections can be divided into four main groups: geometric, radiometric, atmospheric, and emissivity corrections.

#### **Radiometric correction**

Radiometric correction originates from a camera calibration based on imaging a black body object of known temperature. In our case, this calibration was performed by the manufacturer. The camera is always calibrated to specific measured surface temperature, and the error increases farther away from this point. The FLIR Tau2 sensor used for the campaign was calibrated to temperatures between 40 °C and 50 °C.

Off-axis vignetting compensation had to be performed, which is, according to Li and Zhu (2009), a phenomenon commonly present in thermal imaging. Vignetting appears on all images, be it optical or from a near-infrared sensor. In thermal imaging, this effect is usually very strong due to the low contrast of imaging systems (Li and Zhu 2009). The further the object is away from the system's axis and the larger the field of view, the more serious the vignetting becomes.

The off-axis vignetting effect not only distorts the real kinetic temperature data but also corrupts the images for mosaicking. The digital values towards the sides of the images suffer from heavy error, not allowing the mosaicking algorithm proper tying of neighbouring images. In general, the off-axis vignetting results in a gradient of declining temperature from the image nadir to the image sides.

Four images were acquired to compensate for the vignetting effect. An object with a smooth, unpolished surface with constant emissivity and temperature was used. The images were taken from a strictly orthogonal position from approximately 40 cm away. However, in this thermal measurement, the off-axis vignetting effect does not seem to increase with distance from the emitting object; it maintains the same pattern and same difference on airborne images as on close-range images. Another fact is that it does not represent a linear gradient from the nadir to the sides but rather shows an irregular pattern. Although the temperature appears lower especially in corners in what corresponds to the off-axis effect described previously, in the lower-right corner, the effect is much stronger than in the rest of the corners, and the effect is stronger in the lower part of the picture, in general. Another

inconsistency appears in the upper-central area. According to the theory, there is no possibility that the digital values near the upper edge of the image are like those in nadir, due to the conditions mentioned above. The true reason for the vignetting-like effect in these images was not identified. However, the error was treated and solved the same way as the casual vignetting without any problems.

Images were to be exported to raw numbers because the camera produces images already recalculated to temperatures. At the raw number level, the largest pixel value was subtracted from each pixel value in the entire image to obtain the vignetting mask. This was performed on four images. A low-pass filter was applied afterwards to smoothen the differences in the mask. In the next step, the masks of the four images were averaged to secure the most suitable outcome. The final mask was added to all images. The results are satisfactory, regarding visual comparison and value comparison. After applying the vignetting mask, the same objects show highly similar values as many other images in different parts of the image.

### **Atmospheric corrections**

Atmospheric corrections are based on modelling the atmospheric signal loss and atmospheric emission. Main atmospheric characteristics affecting thermal imaging are air temperature and air humidity. Two meteorological data sources were available as the auxiliary data source. One is a GNSS reference station operated by the Department of Geoinformatics, Palacký University Olomouc. The station provides reference GNSS data for VESOG and CzechGeo projects. Moreover, it provides basic information about the atmosphere every five minutes. The basic variables are air temperature, air pressure, and air humidity. The other source comes from an amateur meteorological station located near the city borders. The station provides information about air temperature, air pressure, and air humidity as well as solar irradiation.

In the study, we used an algorithm developed specifically for FLIR cameras integrated as an R package called Thermimage (Glenn J. Tattersall, 2018). This package recalculates data from raw values to temperature based on calibration constants acquired during the calibration, applies corrections for atmospheric transmission loss based on distance from the object, compensates for radiance emitted from surrounding objects (reflected temperature), and compensates for emissivity. The algorithm uses equations from Minkina and Dudzik (2009) to simulate the signal passing through the atmosphere using atmospheric constants and humidity recalculated to water vapour pressure.

### **Emissivity corrections**

Emissivity is a characteristic of the viewed object which affects the resulting temperature in a major way. Emissivity is defined as the ratio of emitted thermal radiation of the object to the thermal radiation of a blackbody. Emissivity is unique for each material and wavelength.

Emissivity corrections are of special importance in thermal remote sensing because they may cause the highest amount of error in the data (Minkina and Dudzik 2009). Low emissivity objects such as metal rooftops appear as very low-temperature objects, which is not the case in reality. Even though most objects have a similar emissivity of about 0.95, the remaining objects must be corrected to analyse the data further.

The emissivity of every object in the image for a certain wavelength must be known for proper emissivity corrections. At the satellite image level, this issue is solved by estimating emissivity from NDVI with which it correlates. At the fine scale level, however, low emissivity objects are very significant, especially for analysis following the imaging, and are not recognised in the NDVI image. Therefore, at a finer scale, emissivity must be compensated for each object separately. This problem has no easy solution and is still quite new because there were not many thermal campaigns solving this issue.

The proposed approach combines the use of auxiliary GIS and satellite imaging data to access the land cover. The national system RUIAN which manages certain land cover classes was used. After some minor corrections, it shows buildings, roads, and sidewalks accurately. A simple threshold for NDVI based on QuickBird satellite imagery was created to separate vegetation and non-vegetation classes. When combining the data, we created an easy hierarchy rule saying that vegetation can overlap roads, pavements, and buildings and that buildings can overlap roads and pavements. After this mash-up was created, we semi-manually tied these objects with their respective material emissivity number. This approach allowed us to partially eliminate the cold spots that might corrupt further analysis results.

### **Photogrammetric processing**

The biggest challenge of the mosaicking part of the study was the fact that plenty of images were corrupted due to blurring caused by the slow shutter speed of the camera and high aeroplane speed. Moreover, the aeroplane was considerably light. Therefore, it suffered from heavy wind and was unsteady in general.

AgiSoft Photoscan Professional (currently called Metashape) and Trimble INPHO software were used for the photogrammetric process (Figure 3). The basic method for image orientation and calculation of the exterior orientation parameters is Structure from Motion (SfM). This approach includes a few methods like “Stereo matching” or “Multi-view stereo – MVS”. Stereo methods can be global or local. Semi-global matching methods are implemented in Agisoft Photoscan Pro. The main fundamental difference between SfM and classic photogrammetry is the use of a new generation of image matching algorithms, which allow for unstructured image acquisition. While classic photogrammetric methods typically rely on strips of overlapping images acquired in parallel flight lines, MVS was designed to reconstitute the three-dimensional geometry of buildings and objects from randomly acquired images (Fonstad et al. 2013). The multi-view matching method performs very well for oblique images as well as for classic aerial images with forward-overlap and side-overlap.

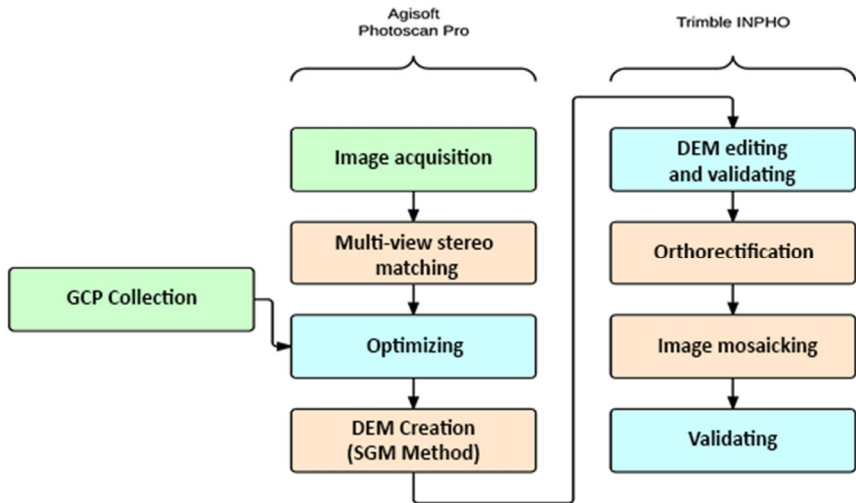


Figure 3 Workflow of photogrammetric image processing for the flight campaign over Olomouc city. Green colour shows data inputs, in light brown, are the main methods described in the text, and the light blue steps are auxiliary processes in the workflow.

Moreover, different settings and digital elevation models were tried. Namely, we used an automatically generated elevation model created by Agisoft with the semi-global matching method (SGM), digital surface model, and digital elevation model. The low overlap of the images in combination with corrupted images caused serious damage to the mosaic. The algorithm could not identify a large number of images and created gaps in the mosaic or, in the worst case, tried to distort images to fill the gaps. This process was unsatisfying, but most of the corrupted images were located outside the city or in the suburbs. Therefore, it was decided to reduce the area of interest to only the city centre, which was of high quality in the images in general. The final mosaic was created from only 117 images in the case of the morning flight and 115 in the case of the afternoon flight.

## 5. Descriptive analyses carried out on Olomouc thermal mosaics

The first group of analyses is based on self-reliant methods requiring no or minimal auxiliary data to perform. The first method consists of manual sampling from optical imagery and then analysis performed on the collected values. The second method exploits the sample dataset as it is based on the spatial distribution of asphalt-concrete material temperature. The third method is based on a statistical analysis of the datasets investigating extreme values in the thermograms.

### **Thermal regime of materials in an urban environment**

For the first analysis, a simple approach to data sampling was performed. More than any functional class, land-cover or land-use type, the temperature regime depends on the specific material type. Meaning that asphalt rooftop is very similar on TIR imagery as the asphalt road, although it is completely different land-use and functional class.

The sampling was based on auxiliary data from the city's municipality. The data contained information about specific road material type, so a more accurate typology and sampling could have been performed. The road material class was further divided into the five most common material types. Road material classes are asphalt concrete, macadam, cobblestone, gravel, and concrete. The asphalt concrete class is covering the majority of the roads in Olomouc and represents more than 90 % of the area. Macadam is used mainly for parking lots, cobblestone in the historical centre of the city, gravel was found in the suburbs used for utility roads and pure concrete was located in several industrial areas. The class of natural materials was divided into several subclasses as well. These were grass, bare soil, tree crowns, and agricultural crops. The grass was sampled based on another auxiliary dataset containing information for Technical Services of the city of Olomouc, helping them with effective watering. Tree crowns were identified based on optical imagery combined with the Digital Surface Model (DSM). Agricultural crops were differentiated from bare soil based on the Normalized Difference Vegetation Index (NDVI).

Water bodies were distinguished based on topographic maps of the area. There are two small lakes close to the city, Hamrýs and Morava's oxbow lake which does not have an official name. Two main rivers, Morava and Bystřice, were identified, and more samples were gathered. The Trusovický brook is a very small stream flowing into the Morava river before reaching the city. Morava arm is a part of the river that separates from the main river before it reaches the city and connects with it in the city. A large number of samples taken for asphalt concrete was due to its use in the next analysis as the main input. The other numbers of samples were chosen based on the sampled material type with respect to their appearance in the image.

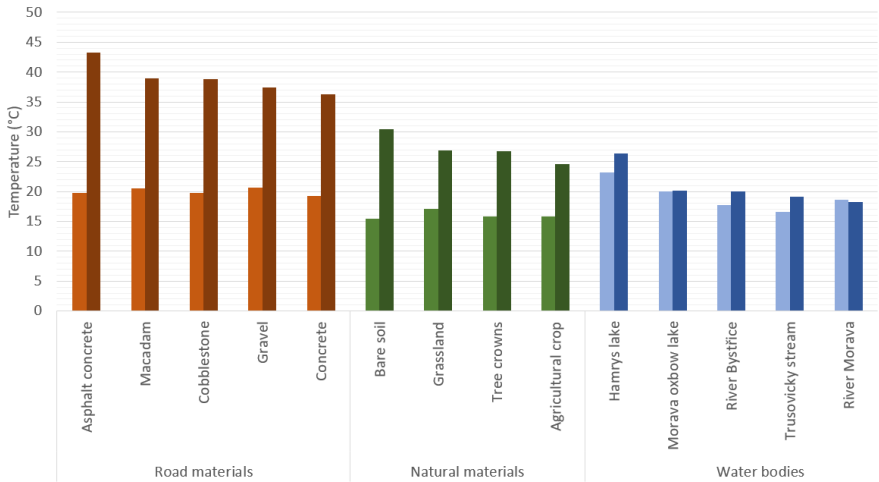


Figure 4 Thermal material regime in the city of Olomouc. Light colours are the morning temperature; darker colours are the afternoon temperature.

The results of the analysis are visualized in Figure 4. The materials within their respective groups are sorted descending based on their afternoon temperature. The asphalt concrete material is easily recognized as the one with the largest afternoon temperature as well as the temperature difference between the morning and the afternoon. The same class heats about 10 % more than other road materials. The difference between asphalt concrete and cobblestone is even more striking than in the preliminary dataset due to the larger number of samples.

All the natural materials have very low morning temperature and tend not to heat up as much as the artificial ones. For example, in the afternoon, the grass material class is about 40 % cooler than the asphalt concrete. Within the natural materials, the bare soil is approximately 5 °C hotter than the other materials due to bare soil absorbing a large portion of the incoming EM radiation.

The water bodies group shows some very interesting information as well. The most significant is the Hammys lake, which is still water prone to incoming EM radiation. The difference between rivers Morava and Bystřice is the same as described in the preliminary results section. Morava's oxbow lake is a very interesting phenomenon as it does not change its temperature at all throughout the day. The Trusovický brook is a very shallow and fast stream which thermal behaviour compares to the Bystřice river.

### Investigation of microclimate using TURN method

This analysis is heavily inspired by Thermal Urban Road Normalization (TURN) method published by Rahman et al. (2014). TURN is based on the premise that roads as objects are



pseudo-invariant features and can be used to model the microclimatic variability. Based on the premise, all differences from median road temperature can be considered as the effect of the microclimate. In the mentioned paper, Rahman et al. (2014) subtracted the resulting microclimatic influence from the image to correct the thermal imagery for it. However, quantifying the microclimatic effect over the whole city are is very interesting as is and thus it is calculated in this thesis.

In the original paper, Rahman et al. (2014) identified the roads based on local GIS data, specifically, from linear objects. For this study, the polygon layer with road material types was available. Therefore, more accurate sampling based on the actual material type, could have been performed.

The process of sample generation is very problematic. The original TURN study performed by Rahman et al. (2014) simply took auxiliary GIS data, namely linear roads, and created point geometry along the lines. After that, some postprocessing was performed to, for example, remove points covered by vegetation. While this approach is practically true GIS and very correct, in Olomouc dataset, there were issues forbidding this approach. The basic layer that was provided for this study was road material polygon layer provided by the Institute of Urban Planning of the city of Olomouc. The dataset is very detailed, including tram lines, tram stations, distinguishing more than 30 types of road materials and containing a layer of sidewalks. One downside of the dataset is that some of the roads are not owned and operated by the municipality and thus do not have all the attributes, and their material type is 'unknown' or 'unspecified'.

The results of this method are shown in Figure 5. In the left side of the image, the morning dataset is visualised, to the right, there is the afternoon dataset. The values represent the difference from mean asphalt concrete temperature in the mosaics. In both images, a west-east gradient is clearly visible. In the morning, the western part of the city is heated up much more. In the afternoon this situation changes. The central part of the city in the river meander is relatively hotter in the both images.

The TURN method shows one of the possibilities of microclimate analysis from extreme resolution thermal mosaics.

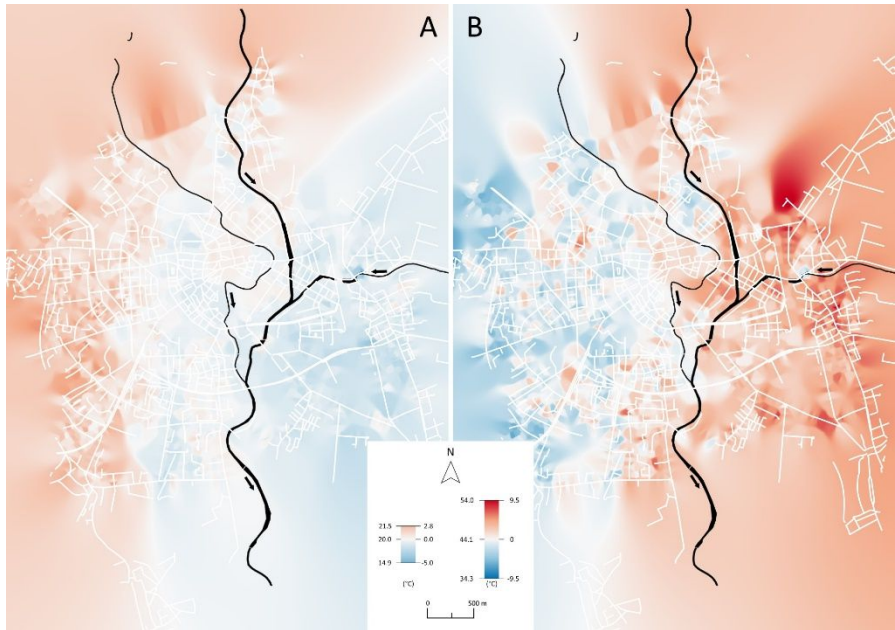


Figure 5 Microclimatic map of Olomouc in the morning (A) and in the afternoon (B). Auxiliary data used are street network (white) and water bodies (black). The Legend shows relative differences of temperature from the mean as well as their absolute values.

### A typology based on temperature change

For immediate classification of the thermal data, an approach based on relative change was carried out. The method exploits an easy principle that most of the objects can be identified based on their typical behaviour, i.e. the change in temperature between the two times of the day. The typology always has 4 unspecified classes. The first class consists of objects having a relatively low temperature in the morning and relatively low temperature in the afternoon (LL). The second class are objects with a relatively low temperature in the morning and relatively high in the afternoon (LH). Third and fourth classes are created similarly (HL, HH). Having relatively low temperature means having a temperature below a specific threshold. These thresholds were calculated based on tertiles in the first case and based on quartiles in the second. This means that the first class in the first study contains objects that were among 33 % coldest objects in the morning as well as among 33 % coldest objects in the afternoon. Other classes are defined in a similar way. The second study works with quartiles, meaning that it considers 25 % coldest and hottest objects. It is also possible to use this method for different types of quantiles. However, having fewer quantiles (medians) results in very chaotic

image and having more quantiles (quintiles) on the other hand, results in an empty image, which is hard to interpret.

This method has many limits and inaccuracies as it depends on the value distribution within the dataset. However, it is not meant as a classification method that provides a perfect delineation of given phenomena. It is quite the opposite, a rather quick and universal tool for investigation of unknown territory. As described in the following chapter, it is a suitable tool for pinpointing areas of interest and quickly recognizing the situation in the image.

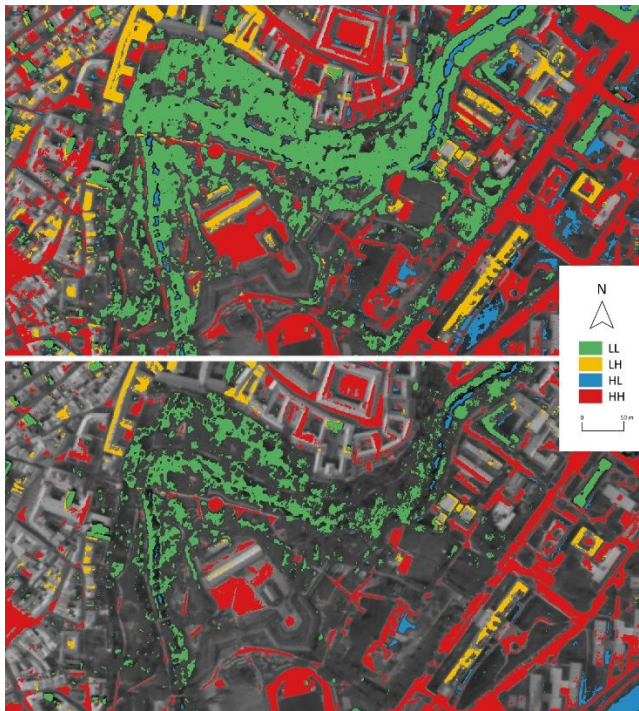


Figure 6 Visual comparison of Tertile typology (top) and Quartile typology (bottom).

In Figure 6, the difference between Tertile and Quartile typologies is shown. The key is to understand that these typologies are not supposed to serve as precise classifications but merely as an indicator of interesting phenomena in the city. Therefore, dense or sparse classification is not necessarily a downside. The user needs to choose what serves the purpose better. For visualisation, the sparse Quartile typology may be easy to read and thus better. On the other hand, if the image is read by an operator or analyst in detail, the dense Tertile typology will serve the purpose better.

## 6. Data Fusion Analyses Carried Out on Olomouc Thermal Mosaics

The second chapter regarding analyses is focusing on the external data source. In this section, data from municipal government and open Europe-wide initiatives data are used to evaluate the surface temperature and the thermal regime. Moreover, Local Climate Zones are tested as a concept of comparison in both inter-city and intra-city approaches.

### **Investigation of temperatures on different vertical levels**

Verticality is a very important factor in urban climate research. One of the crucial paradigms regarding the quality of life within the city and the effect of long-wave irradiation on humans is that people live in the streets, not on the rooftops. Having a small to medium resolution thermal satellite images provides us with information about the temperature of the city surface. However, these data tell us only a little about the inner structure of the city. In fact, the denser the city is, the stronger the UHI effect might appear in comparison to a rural area. This is caused mainly by materials used for rooftops. Another example of factors contributing to the temperature difference between the rooftop and ground level are shadows and vegetation. On the contrary, the rooftop level should not be affected by city canyons, upwelling radiation and should be ventilated much more effectively. In this chapter, GIS tools are used to investigate the various possible hypothesis.

### **Description of buildings dataset and its corrections**

The building dataset comes from the governmental Registry of Territorial Identification, Addresses and Real Estate (ČÚZK - RÚIAN, 2019). The system was fully established on 1st July 2012 and is since then serviced by State Administration of Land Surveying and Cadastre (ČÚZK). It is a Czech national system collecting data originally stored in multiple systems. The initial data that filled the system came from Information System of the Cadastre of Real Estate (ISKN), Register of Census Districts and Buildings (RSO), Territorial Identification Registry of Addresses (UIR-ADR), Database of Deliver Sites of Czech Post (DDM) and Registry of Municipal Symbols (REKOS). The system is freely accessible through various means such as Public Remote Access (VDP), Information System of Territorial Identification (ISÚI) or service Atom operated by ČÚZK. In this thesis, data were downloaded using ArcGIS plugin named VFR Import. The plugin was created by company ARCDATA PRAHA, and its basic version is available free of charge. The RÚIAN dataset consists of many different layers in many vector types. For example, the layer of built-up objects used in this thesis is available as both point and multi-polygon layer. The dataset was significantly enhanced by Tuháček (2017). The database was corrected for some errors and filled with missing features resulting in a total of 18 627 building objects. The height of the buildings was calculated based on the 5th Generation Digital Terrain Model of the Czech

Republic (DMR 5G) and 1st Generation Digital Surface Model of the Czech Republic (DMP 1G). The difference of the models was added to the polygon layer attribute table.

There were multiple errors that forbid the immediate use of the data. These obstacles come from the specifics of the airborne campaign and the RŮIAN data. The data contain information only about the building footprint; therefore, in some cases, it does not precisely represent the rooftop layer. Another problem was the quality of the mosaic. The spatial accuracy of the mosaicking process was very bad in certain parts of the image due to multiple issues within the processing chain. This caused significant offset, especially in the western part of the image. Furthermore, the image suffers heavily from the skewing effect of tall buildings, which creates offset increasing with building height. For these reasons, the dataset was manually edited, and the offset was adjusted to the afternoon thermal mosaic. Additionally, some buildings had to be manually added because they were either still missing from RŮIAN dataset due to outdated information or are not supposed to be part of it all.

### Ground-rooftop and verticality analyse results

Regarding the difference between ground and rooftop height levels, the results show a very significant difference (Figure 7). In the morning, most of the materials share similar temperature around 17.5 °C because of the night cooling effect. In the afternoon, however, the rooftop level shows a drastic increase of 18.44 °C in comparison to ground level 12.62 °C.

To summarize, within the observed timeframe, rooftop materials heated up on average 46 % more than ground level materials. These results prove the high importance of very high-resolution or down-scaled data providing context for city surface temperature.

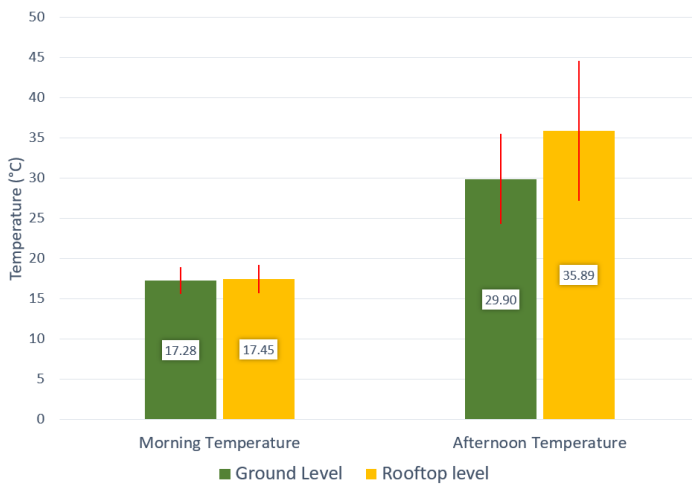


Figure 7 Comparison of temperature means on different vertical levels. Red line shows the standard deviation of the datasets.

### **Local Climate Zones as the basis for zonal analysis**

The principle of Local Climate Zones (LCZ) was firstly presented by Stewart, Oke (2012). LCZs are supposed to be the answer for urban statistical analysis as they set a basic unit of comparison. From the point of climatology, LCZs are relatively homogeneous areas (neighbourhoods) about 4 km<sup>2</sup> large. They are classified based on their structural characteristics, which are discussed later in this section. The main strength of LCZs is the possibility of comparing similar data from different regions and creating metadata information for climate data.

Classification of LCZs is based on several characteristics as described by Stewart, Oke (2012). The key characteristics are Sky View Factor (SVF), Built-up area fraction, Vegetation fraction, and Impervious surface fraction.

The sampling was collected manually. Large patches of the surface were digitised covering nearly the entire area of the city. Total of 47 LCZs was identified of which eight were classified as other as they had very specific land-use/land-cover mixture and could not be classified easily. One of the examples is the area around football stadium which contains an outdoor swimming pool, three football fields with tribunes, several tennis courts, some low-rise and mid-rise buildings as well as multiple high-rise hotels. Following the LCZ methodology, the climatic characteristic of this area is unclear.

The final Figure 8 regarding vegetation and building fractions combines these two characteristics and complements them with the other category, which is calculated only for visualisation purposes. The main purpose of this diagram is to put emphasis on the relationship between vegetation and built-up areas. For example, in LCZ6 (open low-rise) it is clearly identifiable that most of the areas do have twice as much vegetation as buildings. Even though the large open high-rise areas from the socialist area do usually have a playground for kids and smaller patches of grass or parks, in the statistics, these are clearly underrepresented within the class. Only LCZ4 areas #4 and #5 show better vegetation to building ratio.

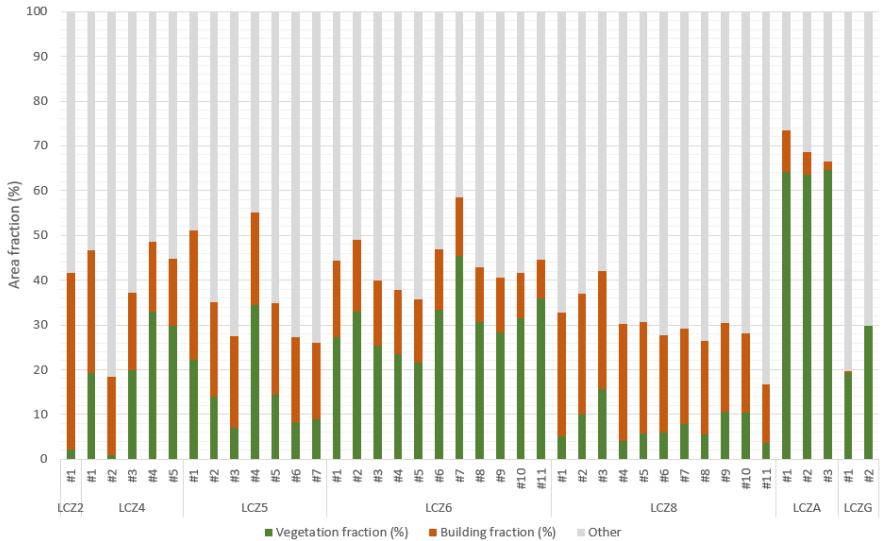


Figure 8 LCZs characteristics based on the vegetation and building fractions complemented to 100 % by the class other.

The most important part of this analysis is its relation to the surface temperature (Figure 9). For easier interpretation, vertical lines visualising temperature change between the morning and the afternoon temperatures are used. Moreover, horizontal blue dashed lines are representing the mean morning (light blue) and afternoon (dark blue) temperature within certain LCZ type for easier visual comparison of the LCZ types as they have large variability. Open low-rise (LCZ6) seems to be the best area in terms of temperature regime among residential areas. It is important to emphasise that the average surface temperature of the other residential zones (LCZ2, LCZ4, and LCZ5) is the same or higher than the temperature of industrial areas (LCZ8).

To summarise, the LCZ methodology is a viable and interesting option in urban climatology research. It is important to improve semi-automatic and automatic approaches of their classification as well as carefully choosing the input data. It might be beneficial to connect the methodology with object-based image analysis (OBIA), segmentation and other technologies.

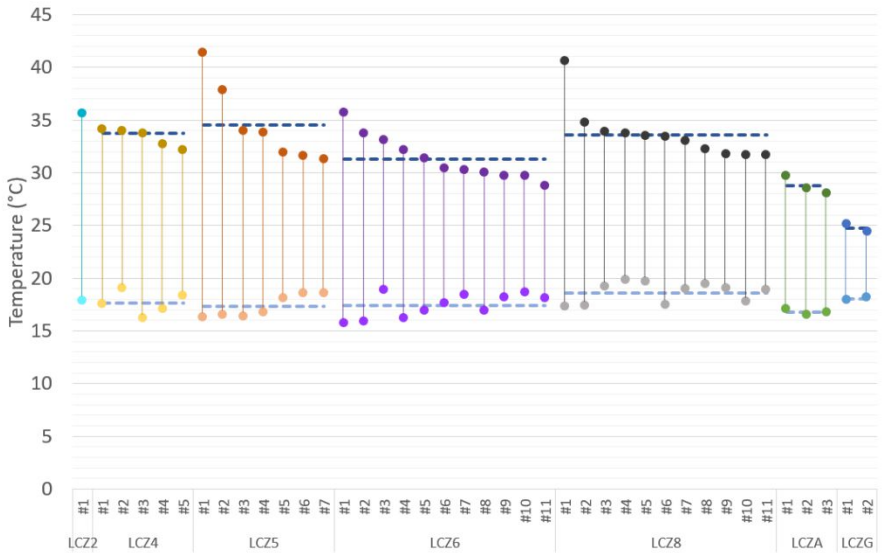


Figure 9 Temperature regime of various LCZs. The lighter colours implicate the morning temperature; the darker colours stand for the afternoon temperature. The dashed line shows averages of the LCZ classes for both morning and afternoon temperatures.

### Temperature evaluation based on open data

European programme Copernicus offers several products that are very valuable to urban research. Copernicus services can be divided based on the website into three categories.

#### Urban Atlas 2012

Urban Atlas (UA; Urban Atlas — Copernicus Land Monitoring Service, 2019) is a tremendously unique dataset. It is a Europe-wide mapping service under European Space Agency Copernicus programme monitoring the land-use and land-cover changes over Large Urban Zones (LUZ). For the year 2006, there were 319 LUZs defined for the analysis, including cities with more than 100 000 inhabitants. In the year 2012, the number grew to 785 cities including EU28, EFTA and West Balkans countries and Turkey. The dataset is limited by minimal mapping unit (MMU). The MMU for 17 urban classes is 0.25 ha, while for 10 rural classes the MMU is 1 ha. The methodology consists of Earth Observation (EO) data interpretation enhanced by topographic maps and auxiliary information, including local expertise.

Morning average temperatures range approximately between 15 and 20 °C while afternoon means range from 23 to 35 °C. The Land-use/Land-cover (LULC) categories are sorted by the ID number and their respective super-categories. Water shows the typical behaviour of



a material with high thermal inertia having the second highest morning temperature of 18.21 °C while having significantly lowest afternoon temperature of only 23 °C. There is a potential threshold between natural and artificial materials at 30 °C. Classes 1.4, 2, 3, and 5 have mean afternoon temperature under 30 °C while all artificial classes 1.1, 1.2, and 1.3 have mean over 30 °C.

### **CORINE Land Cover 2018**

CORINE Land Cover (CLC; CORINE Land Cover — Copernicus Land Monitoring Service, 2019) is another great and ambitious source of data. The creation of this dataset was initiated in 1985 for the first reference year 1990. Since then, four more datasets (2000, 2006, 2012 and 2018) were created. CLC classification consists of 44 classes with minimal mapping unit of 25 ha for areal and 100 m minimal width for linear phenomena. The dataset is produced by most countries by visual interpretation of high-resolution satellite imagery (Home :: Corine Land Cover classes, 2019). The production time of the dataset was reduced from 10 years (1990) to just about 1 year (2018). The number of countries was also increased from the original 26 to 39 in the latest dataset. CLC 2018 has the same overlay and access for download as Urban Atlas, requiring only free registration. It is available for the whole 39 countries as 100 m resolution GeoTiff (under 200 MB), SQLite Database (3.3 GB) or ESRI Geodatabase (1.7 GB). Along with the datasets from mentioned years, CLC contains also LULC change data labelled as “CHA” in the file structure. These change datasets are generated for every two following datasets, e.g. 2006-2012.

The highest afternoon surface temperature was measured on construction sites (class 133) followed by airports (124), continuous urban fabric (111) and road and railway networks (122). An interesting fact is that airport class is among the hottest in the afternoon but has very good cooling capability during the night resulting in low morning temperature. This is most probably caused by the elevated position of the airport combined with its open space providing great ventilation.

Traditionally, natural surface classes account for the lowest afternoon temperature, broad-leaved forest (311) and pastures (231) heating up to less than 25° C. Surprisingly high are the green urban areas (141) having average afternoon surface temperature of almost 30° C. The reason here is probably coarse spatial resolution of the CLC dataset, so the green urban area class consists also of surrounding streets and buildings neighbouring the actual parks.

## **7. Discussion**

During the work, some **challenges** and problems were encountered. While most of them were **solved**, there are still some methods that should be improved for further and possibly **long-term research**. Recommendations for similar projects or follow-up research is also mentioned in this chapter. The topics discussed are mentioned in **chronological order**.

## Flight campaign and data processing

It was rather difficult to predict all possible issues during the thermal airborne campaign without previous experience. A laboratory testing prior to the flight was performed on both cameras, which resulted in **satisfactory results**. The flight was planned based on **previous experience** with optical sensors.

One of the largest issues was the combination of **long image acquisition time** on the thermal sensor, low altitude and wind turbulences during the flight. The high image acquisition time resulted in **low vertical layover**, which was sufficient in the end, but very low aeroplane speed was required. The low altitude was required in order to get the best spatial resolution possible. However, this resulted in very low horizontal layover that was on the **edge of being viable**. The Cessna aeroplane is **very light**, and the time of exposure is relatively high on the thermal sensor, which resulted in many images being blurry due to several turbulences. In combination with a low horizontal layover, this caused some **gaps** in the final mosaic.

The used camera was relatively simple and **low-cost**, and there are other possible devices suitable for airborne thermal remote sensing. The most common sensor for airborne campaigns is probably **TASI-600** from company ITRES. TASI-600 is a push-broom scanner which produces whole flight lines as single images. This is tied to some specific problems such as **georeferencing** and **orthorectification** issues that were not present while using single camera images and mosaicking methods. The massive advantage of TASI-600 system come from its **hyperspectral** sensor, which allows more **sophisticated atmospheric and emissivity corrections** based on multiple thermal bands. The Tau2 sensor used in this thesis is a **broadband camera** that is producing a one-band image, while TASI-600 produces a hyperspectral cube containing 32 spectral channels.

In terms of the final product, the closest comparison for the thermal mosaic of Olomouc is the project **UrbanAdapt** performed by Global Change Research Institute of the Czech Academy of Sciences. The final dataset over the city Brno is available online in the form of a web-map (*Thermal map of surfaces, Brno*, 2015). Instead of day-time and night-time flights, both flights were carried out during the day — one dataset in the **summer** and one in the **winter**. One of the main difficulties in this work is that there was a different altitude chosen for each flight. Thus, the flight lines had different width; each dataset has **different spatial resolution** etc. This further complicates any kind of analysis performed on such dataset. However, it is apparent that the authors had fewer problems with objects of **extremely low emissivity** even though some are still identifiable in the image. For the atmospheric and emissivity correction process, **Temperature and Emissivity Separation** (TES) algorithm were used. The campaign took a considerably longer time of almost **4 hours**, which was unwisely spread throughout the day (from 9:43 to 13:22 CEST). Regarding the quality, a significant **blur** is visible throughout the whole mosaic. This was most probably caused by relatively **high aeroplane speed**. Even considering the higher altitude (meaning larger scan

swath and fewer flight lines) and longer flight time, the aeroplane had to cover approximately **four times larger area** in the only slightly larger time frame. The interpretation was performed only on a very basic level in the form of a description of several interesting areas.

I would like to emphasise that even the 3 hours in Olomouc campaign is **extremely long** flight time for the thermal campaign. Thus, it is unclear if and how it would be possible to collect data from larger cities, even larger than Brno. One of the possible solutions would be **night-time campaign**, but the night-time data do not contain information about the heating ability of the surfaces. Another possible solution would be a series of shorter campaigns over specific areas or city districts. This would possibly require extensive auxiliary meteorological data to somehow approach the changes in weather between different days.

Another topic worth noting is the general **auxiliary data collection** at the time of the flight campaign. It is very beneficial to secure not only high-quality ground truth data but also logs from the meteorological station, both private and governmental ones. Very important is also to get up to date datasets about any topic the operator wants to analyse and of course any free datasets. For example, **OpenStreetMap** historical data are not easily accessible after some time. The same principle applies to **municipal datasets** that are being updated constantly.

### **Self-contained analysis**

There are several ways of approaching methods based on data sampling. In this case, I've exploited our **long-term cooperation** with the local municipality and extensive knowledge of the area. Thanks to this, the data sampling was rather **quick** and possibly **very precise**. For any long-term analysis, it would be beneficial to keep the **same sample locations** or to use the same that was used in this thesis.

The **TURN method** was first proposed as a tool to remove the **microclimatic effect**, so the data from different parts of the city are comparable in terms of material temperature. In my humble opinion, this method is very smart and has tremendous **potential** in terms of intra-city comparison. Combined with some **field data** and further investigation, it might be potentially a **very strong tool** of TIR remote sensing. Of course, it has its limits such as sample collection and the error caused by the age and condition of the roads, but these effects can be **minimised** when approached correctly. The proper ways to analyse and visualise the data and information are still subject to research.

The third method not requiring any special external data source was **quantile-based typology**. This method is very strong when investigating unknown areas and for **immediate analysis** of extreme phenomena. The method is much stronger **in detail** when investigating smaller areas than for large scale statistical comparison or complex analysis.

### **Analyses using external data sources**

The first method using **data fusion** for advanced analysis is based on **building height** dataset. The first part of the analysis was trying to prove that rooftop layer heats up considerably more than the ground level, which was achieved **successfully**. In the second part, the relation between building height and the rooftop temperature was investigated without success. It would be possibly more beneficial to also take into account the roof material, its inclination, slope and other characteristics to perform more in-depth look into this topic.

The **Local Climate Zones** are a recent trend in urban climatology, and the methodology is successfully used in many studies since it was developed. As mentioned by the authors, it is still **improving**, and many related questions are being raised. Probably the most important one is about the actual process of automated classification. Even though some progress has been made, the heterogeneity of the urban environment is very complicated and affects any efforts in a negative way. Besides that, I would consider the **LCZ methodology** as one of the most potential and successful.

The use of the large European datasets was suggested by the reviewer during the thesis outline defence, and even though I was not certain about its practical use, it turned out to be **very interesting** and **effective**. The lower spatial resolution of **CORINE Land Cover** (CLC) looks slightly worse in the results, but the detail of **Urban Atlas** (UA) classification is very helpful at this spatial resolution. It would be certainly beneficial to **update** the thermal mosaic with every new CLC or UA version.

## 8. Conclusion

The main objective of this doctoral thesis was to **investigate and improve airborne thermal remote sensing in urban climate research**. With the increasing fraction of the world's population living in the cities, the **necessity of urban applications** increases accordingly in **remote sensing** as in many other fields such as **GIS, urban planning** and **architecture**. The recent **rapid increase** in Earth's ecosystem **temperature** and the increase of **severity of natural disasters** caused by **global change** makes the situation even more **alerting**. In this very moment, it is the **thermal infrared remote sensing** that comes with answers to many of the questions asked by the urban **climatologists**. How good is the **cooling effect** of the materials **during the night**? How severe is the **increase** in materials **temperature**? Are **citizens endangered** by the upwelling radiation coming from **artificial materials**? A **flight campaign** collecting extreme resolution data about radiant surface temperature was proposed to answer these questions. The **data processing** currently poses a difficult challenge and was carried out in the next step. After the **thermal mosaics of Olomouc** were created, the work continued with **self-reliant analyses** on the dataset. In the last part of the thesis, a set of analyses exploiting **external data sources** was carried out.

The main **empirical findings** are chapter specific and were summarized within the respective chapters. This section will **synthesize** the findings according to the sub-objectives.

- Airborne thermal remote sensing is a viable source of information about the surface temperature for urban climate research. This was proven by extensive data analysis.
- The data processing chain described in Chapter 5 is reliable and has consistent, detailed and high-quality results.
- An immediate and self-reliant analysis can be performed right after the data acquisition to identify crucial locations within the thermal mosaics, as described in Chapter 5.
- The TURN method described in Chapter 6.2 is a promising tool for assessing the spatial variability in urban microclimate. The results show the most potential for interpretation and future research.
- When investigating the heat stress on population, the different vertical levels need to be carefully distinguished. The difference between ground and rooftop height levels is described in Chapter 7.1
- Local Climate Zones are an important tool for the future of urban climate research, especially when combined with remote sensing methods.
- International cooperation and open Europe-wide datasets are beneficial for urban climate research.

The main **theoretical impact** of this thesis is undoubtedly the possibility of a relatively **low-cost high-accuracy thermal remote sensing** based on a single-image camera approach and mosaicking. This task can be performed in a **timely manner**, by a **small team** of specialists and with **interesting results**. Another large step forward is the **ability to analyse** such data. **Extreme resolution** thermal datasets are **very rare** and not many scientific papers are devoted to their analysis and interpretation. In this thesis, **several methods** were proposed and tested. Some offered **immediate results**, some were not fitting for this kind of data, and some that showed **incredible potential** and possible **further improvements**.

Based on presented findings, **continuous monitoring** of city surface temperature should be considered as a viable option for a **scientific grant** and supported by **municipalities**. The **social benefits** of such research are unquestionable as well as the **positive impact** on the population. With the **global change progressing**, the local governments are responsible for the **aftermath of heat wave events** and the proper long-term investigation of the city structure may help the **population resilience and awareness**.

The possibilities of **future research** are many. The **improvements** to the data processing chain would increase the **accuracy** of the data and the **speed** of overall processing. The improvements to the analytical part can also be performed. **Auxiliary data** were proven to be almost **essential** to the future of such research. Most importantly, it would be very meaningful to provide **long-term monitoring** with additional **meteorological** and **climatological** data tied to **modelling** and the broader context of climatology.

To summarise, the thesis investigated **the possibilities of airborne thermal remote sensing in urban climate research**. The author performed the data processing chain leading to **thermal mosaic products** on which a series of analyses were performed. The improvements were made by proposing **new methods** of analysis and **improvements** within the data processing chain. The results of the **six analyses** were evaluated, and further recommendations were proposed.

## 9. Literature

CHRYSOULAKIS, Nektarios et al., 2016. A NOVEL APPROACH FOR ANTHROPOGENIC HEAT FLUX ESTIMATION FROM SPACE Foundation for Research and Technology Hellas ( FORTH ), Greece , 2 German Aerospace Center ( DLR ), Germany , 3 Centre d ' Etude Spatiale de la Biosphère ( CESBIO ), France , 4 University. . 2016. P. 6774–6777.

CIMBALISTA, Mario, 2014. Method for improving visualization of infrared images. [online]. 2014. Vol. 9105, p. 910504. DOI 10.1117/12.2063670. Available from: <http://proceedings.spiedigitallibrary.org/proceeding.aspx?doi=10.1117/12.2063670>

Copernicus Land Monitoring Service - Urban Atlas — European Environment Agency, 2018. [online]. [Accessed 28 May 2019]. Available from: <https://www.eea.europa.eu/data-and-maps/data/copernicus-land-monitoring-service-urban-atlas>

CORINE Land Cover — Copernicus Land Monitoring Service, 2019. [online]. [Accessed 28 May 2019]. Available from: <https://land.copernicus.eu/pan-european/corine-land-cover>

ČÚZK - RÚIAN, 2019. [online]. [Accessed 28 May 2019]. Available from: <https://www.cuzk.cz/Uvod/Produkty-a-sluzby/RUIAN/RUIAN.aspx>

DHAINAUT, Jean François, CLAESSENS, Yann Erick, GINSBURG, Christine and RIOU, Bruno, 2004. Unprecedented heat-related deaths during the 2003 heat wave in Paris: Consequences on emergency departments. 2004. ISBN 1466-609X (Electronic)r1364-8535 (Linking).

EISELE, Andreas et al., 2012. Applicability of the thermal infrared spectral region for the prediction of soil properties across semi-arid agricultural landscapes. *Remote Sensing*. 2012. Vol. 4, no. 11, p. 3265–3286. DOI 10.3390/rs4113265.

FOK, S C, NG, E Y K and TAI, K, 2002. Early Detection and Visualization of Breast Tumor With Thermogram and Neural Network. . 2002. Vol. 2, no. 2, p. 185–195.

FONSTAD, Mark A. et al., 2013. Topographic structure from motion: A new development in photogrammetric measurement. 2013. ISBN 0197-9337.

GELETIČ, Jan and LEHNERT, Michal, 2016. GIS-based delineation of local climate zones: The case of medium-sized Central European cities. *Moravian Geographical Reports*. 2016. DOI 10.1515/mgr-2016-0012.

GLENN J. TATTERSALL, 2018. Thermimage: Thermal image analysis [online]. 2018. 3.1.1. Available from: Glenn J. Tattersall

GUNAWARDENA, K. R., WELLS, M. J. and KERSHAW, T., 2017. Utilising green and bluespace to mitigate urban heat island intensity. *Science of the Total Environment* [online]. 2017. Vol. 584–585, p. 1040–1055. DOI 10.1016/j.scitotenv.2017.01.158. Available from: <http://dx.doi.org/10.1016/j.scitotenv.2017.01.158>

HAY, Geoffrey J. et al., 2011. Geospatial technologies to improve urban energy efficiency. *Remote Sensing*. 2011. DOI 10.3390/rs3071380.

HAYHOE, Katharine, SHERIDAN, Scott, KALKSTEIN, Laurence and GREENE, Scott, 2010. Climate change, heat waves, and mortality projections for Chicago. *Journal of Great Lakes Research*. 2010. DOI 10.1016/j.jglr.2009.12.009.

Home :: Corine Land Cover classes, 2019. [online]. [Accessed 28 May 2019]. Available from: <https://land.copernicus.eu/user-corner/technical-library/corine-land-cover-nomenclature-guidelines/html>

IRANI RAHAGHI, Abolfazl, LEMMIN, Ulrich, SAGE, Daniel and BARRY, David Andrew, 2019. Achieving high-resolution thermal imagery in low-contrast lake surface waters by aerial remote sensing and image registration. *Remote Sensing of Environment* [online]. 2019. Vol. 221, no. November 2018, p. 773–783. DOI 10.1016/j.rse.2018.12.018. Available from: <https://doi.org/10.1016/j.rse.2018.12.018>

JIMÉNEZ-MUÑOZ, Juan C., MATTAR, Cristian, SOBRINO, José A. and MALHI, Yadvinder, 2016. Digital thermal monitoring of the Amazon forest: an intercomparison of satellite and reanalysis products. *International Journal of Digital Earth*. 2016. DOI 10.1080/17538947.2015.1056559.

JOVANOVIĆ, Dušan et al., 2015. Spatial analysis of high-resolution urban thermal patterns in Vojvodina, Serbia. *Geocarto International*. 2015. DOI 10.1080/10106049.2014.985747.

KNOWLTON, Kim et al., 2009. The 2006 California heat wave: Impacts on hospitalizations and emergency department visits. *Environmental Health Perspectives*. 2009. DOI 10.1289/ehp.11594.

KYSELÝ, Jan, KALVOVA, Jaroslava and KVĚTOŇ, Vít, 2000. Heat waves in the south Moravian region during the period 1961-1995. *Studia Geophysica et Geodaetica*. 2000. DOI 10.1023/A:1022009924435.

LEHNERT, Michal, GELETIČ, Jan, HUSÁK, Jan and VYSOUDIL, Miroslav, 2015. Urban field classification by “local climate zones” in a medium-sized Central European city: the case of Olomouc (Czech Republic). *Theoretical and Applied Climatology*. 2015. DOI 10.1007/s00704-014-1309-6.

LENG, Pei et al., 2019. First results of all-weather soil moisture retrieval from an optical/thermal infrared remote-sensing-based operational system in China. *International Journal of Remote Sensing* [online]. 2019. Vol. 40, no. 5–6, p. 2069–2086. DOI 10.1080/01431161.2018.1468119. Available from: <https://doi.org/10.1080/01431161.2018.1468119>

LI, Haiyan and ZHU, Min, 2009. Simulation of vignetting effect in thermal imaging system. [online]. 2009. Vol. 7494, p. 749427. DOI 10.1117/12.831306. Available from: <http://proceedings.spiedigitallibrary.org/proceeding.aspx?doi=10.1117/12.831306>

MINKINA, Waldemar and DUDZIK, Sebastian, 2009. *Infrared Thermography, Errors and Uncertainties*. ISBN 9780470747186.

O’SULLIVAN, Antóin M., DEVITO, Kevin J. and CURRY, R. Allen, 2019. The influence of landscape characteristics on the spatial variability of river temperatures. *Catena* [online]. 2019. Vol. 177, no. February, p. 70–83. DOI 10.1016/j.catena.2019.02.006. Available from: <https://doi.org/10.1016/j.catena.2019.02.006>

OERKE, E. C., STEINER, U., DEHNE, H. W. and LINDENTHAL, M., 2006. Thermal imaging of cucumber leaves affected by downy mildew and environmental conditions. *Journal of Experimental Botany*. 2006. Vol. 57, no. 9, p. 2121–2132. DOI 10.1093/jxb/erj170.

OKE, Timothy R et al., 2017. *Urban Climates*. Cambridge University Press. ISBN 9780521849500.

OKE, Timothy R., 2002. *Boundary layer climates*. 2nd editio. Routledge. ISBN 0-203-40721-0.



LOUDIN ÅSTRÖM, Daniel, BERTIL, Forsberg and JOACIM, Rocklöv, 2011. Heat wave impact on morbidity and mortality in the elderly population: A review of recent studies. 2011. ISBN 03785122.

PARLOW, Eberhard, 2003. The urban heat budget derived from satellite data. *Geographica Helvetica*. 2003. Vol. 58, no. 2, p. 99–111.

PRAKASH, Anupma, 2000. Thermal remote sensing: concepts, issues and applications. ... *Archives of Photogrammetry and Remote Sensing* [online]. 2000. Vol. XXXIII, p. 239–243. Available from: [http://www.isprs.org/proceedings/XXXIII/congress/part1/239\\_XXXIII-part1.pdf](http://www.isprs.org/proceedings/XXXIII/congress/part1/239_XXXIII-part1.pdf)

RAHMAN, Mir Mustafizur, HAY, Geoffrey J., COULOIGNER, Isabelle and HEMACHANDRAN, Bharanidharan, 2014. Transforming image-objects into multiscale fields: A GEOBIA approach to mitigate urban microclimatic variability within H-Res thermal infrared airborne flight-lines. *Remote Sensing*. 2014. DOI 10.3390/rs6109435.

REISCHL, Christiane et al., 2017. Urban vulnerability and adaptation to heatwaves : a case study of Graz ( Austria ) a case study of Graz ( Austria ). *Climate Policy* [online]. 2017. Vol. 0, no. 0, p. 1–13. DOI 10.1080/14693062.2016.1227953. Available from: <http://dx.doi.org/10.1080/14693062.2016.1227953>

RIGO, G. and PARLOW, E., 2007. Modelling the ground heat flux of an urban area using remote sensing data. *Theoretical and Applied Climatology*. 2007. DOI 10.1007/s00704-006-0279-8.

ROBINE, Jean Marie et al., 2008. Death toll exceeded 70,000 in Europe during the summer of 2003. *Comptes Rendus - Biologies*. 2008. DOI 10.1016/j.crv.2007.12.001.

ROBINSON, Peter J., 2001. On the Definition of a Heat Wave. *Journal of Applied Meteorology*. 2001. DOI 10.1175/1520-0450(2001)040<0762:OTDOAH>2.0.CO;2.

ROTH, M., OKE, T. R. and EMERY, W. J., 1989. Satellite-derived urban heat islands from three coastal cities and the utilization of such data in urban climatology. *International Journal of Remote Sensing*. 1989. DOI 10.1080/01431168908904002.

SCHLERF, Martin et al., 2012. A hyperspectral thermal infrared imaging instrument for natural resources applications. *Remote Sensing*. 2012. DOI 10.3390/rs4123995.

SEPULCRE-CANTÓ, G. et al., 2006. Detection of water stress in an olive orchard with thermal remote sensing imagery. *Agricultural and Forest Meteorology*. 2006. Vol. 136, no. 1–2, p. 31–44. DOI 10.1016/j.agrformet.2006.01.008.

SOLIMAN, Aiman, DUGUAY, Claude, SAUNDERS, William and HACHEM, Sonia, 2012. Pan-arctic land surface temperature from MODIS and AATSR: Product development

and intercomparison. *Remote Sensing*. 2012. Vol. 4, no. 12, p. 3833–3856. DOI 10.3390/rs4123833.

STEWART, I. D. and OKE, T. R., 2012. Local climate zones for urban temperature studies. *Bulletin of the American Meteorological Society*. 2012. Vol. 93, no. 12, p. 1879–1900. DOI 10.1175/BAMS-D-11-00019.1.

SUNDBORG, Ake, 1952. Climatological studies in Uppsala with special regard to the temperature conditions in the urban area. *Geographica*. 1952. Vol. No. 22. DOI 10.1002/qj.49707833828.

TAN, Jen Hong and ACHARYA, U. Rajendra, 2015. Pseudocolours for thermography - Multi-segments colour scale. *Infrared Physics and Technology* [online]. 2015. Vol. 72, p. 140–147. DOI 10.1016/j.infrared.2015.07.018. Available from: <http://dx.doi.org/10.1016/j.infrared.2015.07.018>

Thermal Color Palettes | FLIR Delta - Episode 4 - YouTube, 2018. [online]. [Accessed 28 May 2019]. Available from: <https://www.youtube.com/watch?v=qZiMn0wuxdo>

Thermal map of surfaces, Brno, 2015. [online]. [Accessed 28 May 2019]. Available from: [http://gis6.brno.cz/mapa/teplotni-mapa/?c=-598156%3A-1160771&z=4&lb=of-brno\\_2015&ly=tepmap0&lbo=1&lyo=](http://gis6.brno.cz/mapa/teplotni-mapa/?c=-598156%3A-1160771&z=4&lb=of-brno_2015&ly=tepmap0&lbo=1&lyo=)

TORGERSEN, Christian E. et al., 2001. Airborne thermal remote sensing for water temperature assessment in rivers and streams. *Remote Sensing of Environment*. 2001. Vol. 76, no. 3, p. 386–398. DOI 10.1016/S0034-4257(01)00186-9.

TUHÁČEK, Tomáš, 2017. Floor area ratio of buildings in Olomouc. Palacky University Olomouc.

UNITED NATIONS, 2016. The World's Cities in 2016: Data Booklet. Economic and Social Affairs [online]. 2016. P. 29. DOI 10.18356/8519891f-en. Available from: [http://www.un.org/en/development/desa/population/publications/pdf/urbanization/the\\_worlds\\_cities\\_in\\_2016\\_data\\_booklet.pdf](http://www.un.org/en/development/desa/population/publications/pdf/urbanization/the_worlds_cities_in_2016_data_booklet.pdf)

URBAN, Aleš et al., 2016. Spatial patterns of heat-related cardiovascular mortality in the Czech Republic. *International Journal of Environmental Research and Public Health*. 2016. Vol. 13, no. 3. DOI 10.3390/ijerph13030284.

Urban Atlas — Copernicus Land Monitoring Service, 2019. [online]. [Accessed 28 May 2019]. Available from: <https://land.copernicus.eu/local/urban-atlas>

VOELKEL, Jackson, HELLMAN, Dana, SAKUMA, Ryu and SHANDAS, Vivek, 2018. Assessing vulnerability to urban heat: A study of disproportionate heat exposure and access to refuge by socio-demographic status in Portland, Oregon. *International Journal of*

Environmental Research and Public Health. 2018. Vol. 15, no. 4. DOI 10.3390/ijerph15040640.

VOOGT, J. A. and OKE, T. R., 2003. Thermal remote sensing of urban climates. Remote Sensing of Environment. 2003. Vol. 86, no. 3, p. 370–384. DOI 10.1016/S0034-4257(03)00079-8.

WENG, Qihao, 2009. Thermal infrared remote sensing for urban climate and environmental studies: Methods, applications, and trends. ISPRS Journal of Photogrammetry and Remote Sensing [online]. 2009. Vol. 64, no. 4, p. 335–344. DOI 10.1016/j.isprsjprs.2009.03.007. Available from:

<http://dx.doi.org/10.1016/j.isprsjprs.2009.03.007>

Which is the Best Color Palette for Thermal Imaging? - YouTube, 2015. [online]. [Accessed 28 May 2019]. Available from:

<https://www.youtube.com/watch?v=qX0mDXy2Sy4>

ZEMEK, F. et al., 2014. Letecký dálkový průzkum Země: teorie a příklady hodnocení terestrických systémů. ISBN 978-80-87902-07-3.

ZEMEK, František, 2014. Airborne remote sensing: theory and practice in assessment of terrestrial ecosystems. Brno: Global Change Research Centre AS CR. ISBN 978-80-87902-05-9.

ZHANG, Kai, CHEN, Tsun-Hsuan and BEGLEY, Charles E, 2015. Impact of the 2011 heat wave on mortality and emergency department visits in Houston, Texas. Environmental Health. 2015. DOI 10.1186/1476-069X-14-11.

## 10. Shrnutí

Tato doktorská práce pojednává o leteckém snímkování v termálním infračerveném spektru pro aplikaci v městské klimatologii. Práce si klade za cíl vylepšit možnosti pořizování dat o teplotě zemského povrchu, možnosti jejich dalšího zpracování a analýz. Prvním dílčím cílem práce je plánování letecké kampaně, samotný sběr dat a následný zpracovatelský řetězec. Výsledkem tohoto procesu je termální mozaika nebo také teplotní mapa povrchu. Druhým dílčím cílem je použít analytické nástroje pro vyhodnocení a interpretaci těchto dat bez použití dalších pomocných datových zdrojů. Třetím dílčím cílem je využití externích datových zdrojů, které poskytují další možnosti srovnání a interpretace dat.

Letecká kampaň byla provedena 10. července 2016 nad zájmovým územím pokrývajícím město Olomouc ve 4:55 CEST a 17:00 CEST. Toto území bylo snímkováno termální kamerou se senzorem FLIR Tau2 a zároveň fotogrammetrickou kamerou Phase One iXA-R 180. Celkem bylo provedeno 22 letových os z průměrné výšky 769 m nad zemským povrchem, což ve výsledku znamenalo prostorové rozlišení kolem 1 m. Během zpracovatelského procesu byla data radiometricky zpracována, byl odstraněn efekt vinětace, byly provedeny atmosférické korekce a korekce pro emisivitu snímkaných objektů. V posledním kroku této části byla provedena ortorektifikace, georeferencování a mozaikování. Výsledkem tohoto dílčího cíle je ranní a odpolední termální mozaika pokrývající území města Olomouce a okolí.

Ke splnění druhého dílčího cíle byly navrženy tři analytické metody pro hodnocení městského klimatu v Olomouci. První metoda je založena na sběru vzorků typů materiálu v prostředí GIS. Tato metoda se skládala ze dvou částí, kdy byla nejdříve provedena předběžná studie s omezeným množstvím vzorků a následně rozsáhlejší studie se zmenšeným počtem tří a větším počtem vzorků. Jako druhá metoda byla použita metoda TURN, která byla využita pro plošný výpočet vlivu mikroklimatu na teplota asfaltových silnic na území města. Třetí metoda byla založena na statistickém zpracování dat, konkrétně na aplikování kvantilů a typizaci na nich založené. V této části byly vyzkoušeny dvě typizace, jedna založená na tercilech a druhá na kvartilech.

Třetí dílčí cíl se zaměřoval na fúzi termálních mozaik s dalšími datovými zdroji. V první metodě byla zkoumána závislost vlivu výšky budovy na teplotu povrchu. Bylo dokázáno, že teplota povrchů na zemi a v úrovni střech se drasticky liší a je potřeba ji ve výzkumu městského klimatu zohledňovat; především na satelitních snímcích, kde tyto dvě úrovně vertikality často nejdou odlišit. Dále metoda neprokázala souvislost mezi výškou budovy a teplotou její střechy. Ve druhé studii byla aplikována metodika Lokálních Klimatických Zón (LCZs) pro klasifikaci a následnou analýzu takto vymezených zón s uniformním klimatologickým chováním. Poslední metoda se zaměřovala na kombinaci termální mozaiky s daty z evropských projektů zaměřených na využití krajiny a krajinného pokryvu. Byly použity dvě datové sady, Urban Atlas (UA) a CORINE Land Cover (CLC). Obě datové sady byly popsány jak z hlediska struktury, tak jejich dostupnosti a aktuálnosti. Dále bylo

zkoumáno pokrytí zájmového území třídami využití krajiny u obou datových sad. V posledním kroku byly pro jednotlivé třídy vypočítány hodnoty ranní a odpolední teploty a popsány jejich základní trendy.

Hlavní výsledky práce se dají shrnout do několika poznatků:

- Letecké termální snímkování je jeden z možných zdrojů informací o teplotě povrchu, která je dále využitelná ve výzkumu městského klimatu.
- Zpracovatelský proces popsaný v této práci je spolehlivý a poskytuje konzistentní, podrobné a kvalitní výstupy.
- Okamžitá analýza nasbíraných dat může být provedena bez potřeby dalších vstupních dat. Takováto analýza dokáže v obraze identifikovat extrémní případy a základní trendy v daném území.
- Metoda TURN je velmi slibný nástroj pro výzkum prostorového rozložení vlivu mikroklimatu na městskou krajinu.
- Výškové stupně (u země a ve výši střech) hrají důležitou roli při posuzování negativního vlivu tepla na obyvatelstvo, zejména během letních náporů veder.
- Lokální Klimatické Zóny jsou užitečným nástrojem pro srovnání tepelných vlastností různých částí města jak v rámci jednoho regionu, tak i mezi městy, případně státy.
- Mezinárodní spolupráce při produkci celoevropských datových sad o využití krajiny je velmi užitečná při výzkumu tepelných vlastností městské krajiny.

Tato doktorská práce prozkoumala možnosti využití leteckého termálního snímkování ve výzkumu městského klimatu. Autor naplánoval leteckou kampaň a zpracovatelský řetězec na jehož konci vznikla datová sada dvou termálních mozaik zájmového území města Olomouce. Tato data autor zpracoval pomocí šesti analýz zaměřených nejen na vytvořenou datovou sadu, ale i na kombinaci s dalšími zdroji dat. Tato práce prezentuje vylepšení zpracovatelského řetězce a navrhuje nové metody pro hodnocení městského klimatu.

EUROPEAN  
CURRICULUM VITAE  
FORMAT



PERSONAL INFORMATION

Name

**POUR, TOMÁŠ**

E-mail

**[pour.tomas@gmail.com](mailto:pour.tomas@gmail.com)**

Nationality

Czech

Date of birth

31. 12. 1990

EDUCATION

- Date
- University
- Degree, field
- Dissertation topic

since 2015

**Department of Geoinformatics at Palacký University in Olomouc, Czech Republic**

Doctorate, Geoinformatics and Cartography

Object analysis of thermal data: algorithmization and application for urban environment

- Graduation year, university
- Degree, field, specialization

**2015 Department of Geoinformatics at Palacký University in Olomouc, Czech Republic**

Master's degree, Geoinformatics, Applied Geoinformatics

- Graduation year, university
- Degree, field

**2013 Department of Geoinformatics at Palacký University in Olomouc, Czech Republic**

Bachelor's degree, Geography and Geoinformatics

TRAINING AND EXPERIENCE

- Year, programme, university
  - Topic
- Year, name
  - Topic
- Year, name
  - Topic
- Year, name, organisation
  - Topic
- Year, programme, university
  - Topic
- Year, name
  - Topic
- Year, programme, university
  - Topic
- Year, name, organisation
  - Topic
- Year, programme, university
  - Principal subjects

**2018 DAAD Research Stay, Ruhr-Universität Bochum, Germany (1 month)**

Urban heat island, Urban climate research, Spatial analytics

**2017 ESA Land Training Course, SZIU Gödöllő, Hungary (1 week)**

Land remote sensing

**2017 Research Stay at CzechGlobe, Czech Academy of Sciences (2 weeks)**

Soil samples collection and preparation for analysis for carbon sequestration research

**2017 GeoS4S Summer School, Bangkok, Thailand (2 weeks)**

Climate change, Advanced remote sensing

**2017 CEEPUS Research Stay, Jagiellonian University in Krakow, Poland (1 month)**

Urban climate, Urban heat island

**2016 ESA Earth Observation Summer School, Frascati, Italy (2 weeks)**

Earth observation, Remote sensing, GIS

**2016 CEEPUS Research Stay, Universität Salzburg, Austria (1 month)**

Remote sensing, Python scripting

**2013 Geocomputation Summer School, Palacký University in Olomouc (1 week)**

Advanced mathematical methods in GIS, urban planning

**2012 ERASMUS Programme, Ruhr-Universität Bochum, Germany (6 months)**

Remote sensing, object-oriented classification, GIS

## Overview of author's activity during his study

Tomáš Pour's publishing and all presented activities reflect the content of the PhD study programme and research activities at the Department of Geoinformatics, Faculty of Science, Palacký University

in Olomouc. In addition to the mandatory requirements, the student attended multiple workshops

and summer schools. Namely:

- **2016 ESA Earth Observation Summer School, Frascati, Italy** (2 weeks)
- **2017 GeoS4S Summer School, Bangkok, Thailand** (2 weeks)
- **2017 ESA Land Training Course, SZIU Gödöllő, Hungary** (1 week)

Additionally, the student supervised two bachelor theses. First one, regarding Sentinel-2 application possibilities in agriculture, was successfully defended in June 2018. The second one, exploring possibilities of thermal drone imagery in hydrology, is still in progress – to be defended in 2019.

Beginning in September 2018, the student is cooperating with CzechGlobe - Global Change Research Institute of the Czech Academy of Sciences. The work regards thermal hyperspectral data processing.

Since the second half of the year 2017, the author is cooperating with ESA Business Incubation Centre in Prague. The cooperation consisted so far in two hackathons tutoring (IBM in Brno, ActInSpace in Prague, Q-Ton 2.0 in Prague), and review process for the ESA BIC competitions.

A team lead by the student has won the 2nd place at Farming by Satellite prize 2016 finals which took place in Berlin, Germany. The first sub-objective of the thesis was also presented at Dean's prize competition (Faculty of Science, Palacký University in Olomouc) resulting in the 1st place in PhD category in Earth Sciences.

During the studies, the author got proficient with several specialised devices including thermal cameras, robotic total station, drones and differential GPS receiver.

### *Study duties*

As a part of study duties, the student passed seven mandatory doctoral exams, completed three months of research abroad and participated in teaching lectures.

### **Passed exams**

Over the three years of doctoral study, three common mandatory subjects and four obligatory specialized subjects were completed. The specialized subjects were chosen regarding the thesis topic.

| Ac. year  | Subject   | Date       |
|-----------|---|------------|
| 2015/2016 | PRF/PGS00 Scientific and research management                | 24.11.2015 |
| 2015/2016 | VCJ/PGSAJ English for PhD students (C1)                     | 20.6.2016  |
| 2016/2017 | KGI/PGSVM Geoinf. methods in remote sensing                 | 12.7.2017  |
| 2016/2017 | KGI/PGSKP Mapping of land cover and its changes             | 18.8.2017  |
| 2017/2018 | PRF/PGSRD Theory, analysis and interpretation of radar data | 31.10.2017 |
| 2017/2018 | KGI/PGSGV Geovisualization in geoinformation technology     | 30.6.2018  |
| 2017/2018 | PRF/PGS01 Research internship abroad                        | 4.9.2018   |

### Completed research internships

Mandatory research stay was carried out during the first three years of study consisting of research stays at the University of Salzburg, Jagiellonian University in Krakow and Ruhr-Universität Bochum.

| Ac. year  | Institution                               | Date (duration)           |
|-----------|---|---------------------------|
| 2015/2016 | Z_GIS, University in Salzburg, Austria    | 15.4.-16.5.2016 (4 weeks) |
| 2016/2017 | Jagiellonian University in Krakow, Poland | 17.3.-18.4.2017 (4 weeks) |
| 2017/2018 | Ruhr-Universität Bochum, Germany          | 3.6.-30.6.2018 (4 weeks)  |

### Teaching overview

During the doctoral study, the student contributed to teaching in several subjects:

| Code      | Full name                   | Teaching years | Amount (h) |
|-----------|-----------------------------|----------------|------------|
| KGI/DAPRZ | Remote sensing              | 2015-2018      | 46         |
| KGI/GEOIN | Geoinformatics              | 2015-2018      | 24         |
| KGI/PODPZ | Advanced remote sensing     | 2015-2018      | 39         |
| KGI/PROPL | Spatial planning            | 2016, 2017     | 9          |
| KGI/GIPRO | Geoinformatics propaedeutic | 2015-2018      | 7          |
| OPB/ZZB05 | IT for paramedics           | 2018           | 16         |

### *Publications related to the thesis*

#### Articles in a research journal in an international database (WoS, Scopus)

POUR, T., MIRJOVSKY, J. and PURKET, TOMAS, 2018, Airborne thermal remote sensing: the case study of the city of Olomouc. In: European Journal of Remote Sensing. **IF:**

1.1



### **Conference proceedings (WoS)**

VOZENILEK, VIT and **POUR**, TOMAS, 2017, Visualization and processing of images in nano-resolution. Eighth International Conference on Graphic and Image Processing (ICGIP 2016). 2017. DOI 10.1117/12.2266888. SPIE

### **Conference presentations**

Airborne thermal remote sensing: the case study of the city of Olomouc, *EARSel conference 2017* (Prague, Czech Republic)

Geo-visualization of heterogeneous urban thermal data, *EARSel WS on Urban RS 2018* (Bochum, Germany)

### *Other published work*

### **Articles in a research journal in an international database (WoS, Scopus)**

NETEK, ROSTISLAV, **POUR**, TOMAS and SLEZAKOVA, RENATA, 2018, Implementation of Heat Maps in Geographical Information System – Exploratory Study on Traffic Accident Data. *Open Geosciences*. 2018. Vol. 10, no. 1, p. 367-384. DOI 10.1515/geo-2018-0029. Walter de Gruyter GmbH. **IF: 0.7**

### **Conference proceedings (WoS)**

**POUR**, TOMAS, BURIAN, JAROSLAV and MIRIJOVSKY, JAKUB, 2016, APPLICATION OF SEATH ALGORITHM ON HIGH RESOLUTION DATA SETS OF SELECTED CITIES. 16th International Multidisciplinary Scientific GeoConference SGEM2016, Informatics, Geoinformatics and Remote Sensing. 2016. DOI 10.5593/sgem2016/b21/s08.073. Stef92 Technology

**POUR**, T., BURIAN, J. and MIŘIJOVSKÝ, J., 2016, ADVANCED EXTRACTION OF SPATIAL INFORMATION FROM HIGH RESOLUTION SATELLITE DATA. *ISPRS - International Archives of the Photogrammetry, Remote Sensing and Spatial Information Sciences*. 2016. Vol. XLI-B3, p. 905-907. DOI 10.5194/isprsarchives-xli-b3-905-2016. Copernicus GmbH

VONDRAKOVA, A., NETEK, R., POHANKA, T., **POUR**, T. and MALACKA, M., 2017, LEGISLATIVE ASPECTS OF SPATIAL DATA PUBLICATION. 17th International Multidisciplinary Scientific GeoConference SGEM 2017. 2017. Vol. Vol. 17, no. Issue 21, p. 967-974. DOI 10.5593/sgem2017/21/S08.122.

### **Conference presentations**

Advanced Extraction of Spatial Information from High-Resolution Satellite Data, *Workshop for photogrammetry, RS and laser scanning 2015* (Telč, Czech Republic)

### *Project work overview*

Over the course of study, the author was a member of the following projects at the Department of Geoinformatics:

- IGA (2016), Advanced Monitoring, Spatial Analysis and Visualization of Urban Landscape
- IGA (2017), Cloud-based Platform for Integration and Visualisation of a Different Kind of Geodata
- IGA (2018), Innovative Methods of Evaluation and Advanced Analysis of Spatial-Based Systems

---

Mgr. Tomáš Pour

## **LETECKÉ TERMÁLNÍ SNÍMKOVÁNÍ VE VÝZKUMU MĚSTSKÉHO KLIMATU AIRBORNE THERMAL REMOTE SENSING IN URBAN CLIMATE RESEARCH**

Určeno pro studenty, partnerská akademická pracoviště a odbornou veřejnost.

Výkonný redaktor: prof. RNDr. Karel Lemr, Ph.D.

Odpovědná redaktorka: Mgr. Lucie Loutocká

Technická redakce: Mgr. Tomáš Pour

Publikace neprošla redakční jazykovou úpravou.

Vydala a vytiskla Univerzita Palackého v Olomouci

Křížkovského 8, 771 47 Olomouc

[www.vydavatelstvi.upol.cz](http://www.vydavatelstvi.upol.cz)

[www.e-shop.upol.cz](http://www.e-shop.upol.cz)

[vup@upol.cz](mailto:vup@upol.cz)

1. vydání

Olomouc 2019

Edice GEOINFO-CARTO-THESIS, svazek XVI.

ISSN 1805-7500

ISBN 978-80-244-XXXX-X

Neprodejná publikace